Theses, Dissertations and Capstones

2019

Characterizing the effects of environmental stressors on the photosynthetic capacity of Chlorella vulgaris

Amanda Louise Smythers

CHARACTERIZING THE EFFECTS OF ENVIRONMENTAL STRESSORS ON THE PHOTOSYNTHETIC CAPACITY OF *CHLORELLA VULGARIS*

A thesis submitted to
the Graduate College of
Marshall University
In partial fulfillment of
the requirements for the degree of
Master of Science
In
Chemistry
by
Amanda Louise Smythers
Approved by
Dr. Derrick R.J. Kolling, Committee Chairperson
Dr. B. Scott Day
Dr. Brian Antonsen

Marshall University
May 2019

APPROVAL OF THESIS

We, the faculty supervising the work of Amanda Louise Smythers, affirm that the thesis, *Characterizing the Effects of Environmental Stressors on the Photosynthetic Capacity of Chlorella vulgaris*, meets the high academic standards for original scholarship and creative work established by the Master of Science in Chemistry and the College of Science. This work also conforms to the editorial standards of our discipline and the Graduate College of Marshall University. With our signatures, we approve the manuscript for publication.

Dr. Derrick R.J. Kolling, Department of Chemistry   Committee Chairperson   5/2/19
                                                          Date

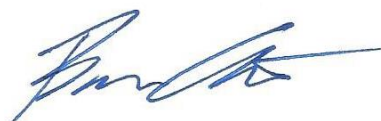Dr. B. Scott Day, Department of Chemistry   Committee Member   5/2/19
                                                          Date

Dr. Brian Antonsen, Department of Biology   Committee Member   5/2/19
                                                          Date

DEDICATION

For Abigail and Derek, the loves of my life.

For small creatures such as we the vastness is bearable only through love.

- Carl Sagan

ACKNOWLEDGEMENTS

My last four years of research at Marshall University has taught me that research cannot be conducted in a bubble. While there have been a host of contributors to my academic and personal success, for brevity, I've included only a few broad categories below.

TABLE OF CONTENTS

LIST OF TABLES

LIST OF FIGURES

ABSTRACT

Chlorella vulgaris is a unicellular green algae grown throughout the world. Due to its multiple

trophic modes as well as its ability to maintain high rates of growth under adverse conditions, it

has been of global interest for use in ecological contamination studies, biofuel feedstock

optimization, and studies of photosynthetic electron transfer. Using a wide-range of methods for

physiological and photosynthetic characterization, the studies within seek to further extend the

usefulness of *C. vulgaris* in a variety of environmentally important studies. Once the protocols

were optimized specifically for this alga, they could be applied in both ecologically relevant and

biodiesel optimization scenarios. Additionally, the reliance on the photosynthetic reactions for a

large portion of their energy production enables further investigation into photosynthetic

mechanisms under stress.

CHAPTER 1

MICROALGAE: MICROSCOPIC ORGANISMS WITH MANY USES

Microalgae are aquatic microbial oxygenic phototrophs (AMOPs) that evolved from cyanobacteria between 2.7 and 3.4 billion years ago and are of increasing ecological and economic importance.[1-2] Microalgae are robust eukaryotic organisms capable of withstanding a wide range of temperatures, salinities, pH and light intensities and can be found in nature growing in somewhat solitary cultures or in large symbiotic communities.[3] Microalgae provide food and oxygen to nearly all aquatic species as they are capable of reducing atmospheric carbon dioxide to generate high energy molecules. They do this by harnessing the sun's energy for oxygen production using the only known biocatalyst for water oxidation, the oxygen evolution complex (OEC).[4] Microalgae have growth rates nearly mirroring those of their prokaryotic ancestors. However, they also have the cellular machinery and abilities of more complex eukaryotic organisms, such as those needed for post-translational modifications and cellular sublocalization. This has caused increased interest in using microalgae for a variety of biotechnological applications, including sustainable food sources, cosmetics, pharmaceuticals, and biofuels. While the use of microalgae for agricultural purposes dates back over 2000 years to the Chinese, cultivation of microalgae for modern industrial purposes is only a few decades old.[5] While microalgae research has steadily increased since renewed interest in the 1950s, the sheer magnitude of worldwide algal species means that the research has barely scratched the surface of possible applications toward improving human health and increasing quality of life.[6]

Despite their longevity on earth and their role as the ancestors to all photosynthetic eukaryotes, the morphology of unicellular green algae has remained mostly unchanged.[7] For this reason, researchers have taken advantage of the genetic similarities between modern algae and

modern plants to use microalgae as a convenient, fast growing model for phototrophic function. This has been of increasing benefit to biotechnology as researchers have taken advantage of known photosynthetic processes for the engineering of more successful algal strains as well as a biological litmus test for the monitoring of ecosystem viability. Likewise, research has focused on determining the abilities of microalgae culture to enhance various agricultural and industrial processes, such as those needed for waste removal, phytoremediation, and protein bioengineering.[8]

Anthropogenic causes of environmental contaminants

Worldwide large-scale agricultural and industrial processing—often conducted irresponsibly and without regard for the potential environmental detriment—has generated widespread waste and environmental contamination, much of which is persistent in the environment and difficult to remedy. In agriculture, fertilizers often contain high levels of phosphate and heavy metals such as zinc, cadmium, iron, copper, manganese, and boron, which lead to increases in surrounding soil metal content and accumulation in nearby waterways.[9] The ubiquitous use of nitrate fertilizers extends the effect even further, as the end product nitrate ion has high mobility and easily mixes with groundwater sources following irrigation-related water application (Figure 1).[4, 10] The accumulation of various agrochemicals in waterways contributes to eutrophication that causes oxygen deficiency and aquatic dead zones, such as the one that occurred in the Gulf of Mexico (which was scrutinized widely in the media).[11] This is observed through the rise of harmful algal blooms, whose excessive growth and release of toxins kills aquatic organisms and can cause a sustained decrease in the biodiversity of aquatic ecosystems.[12]
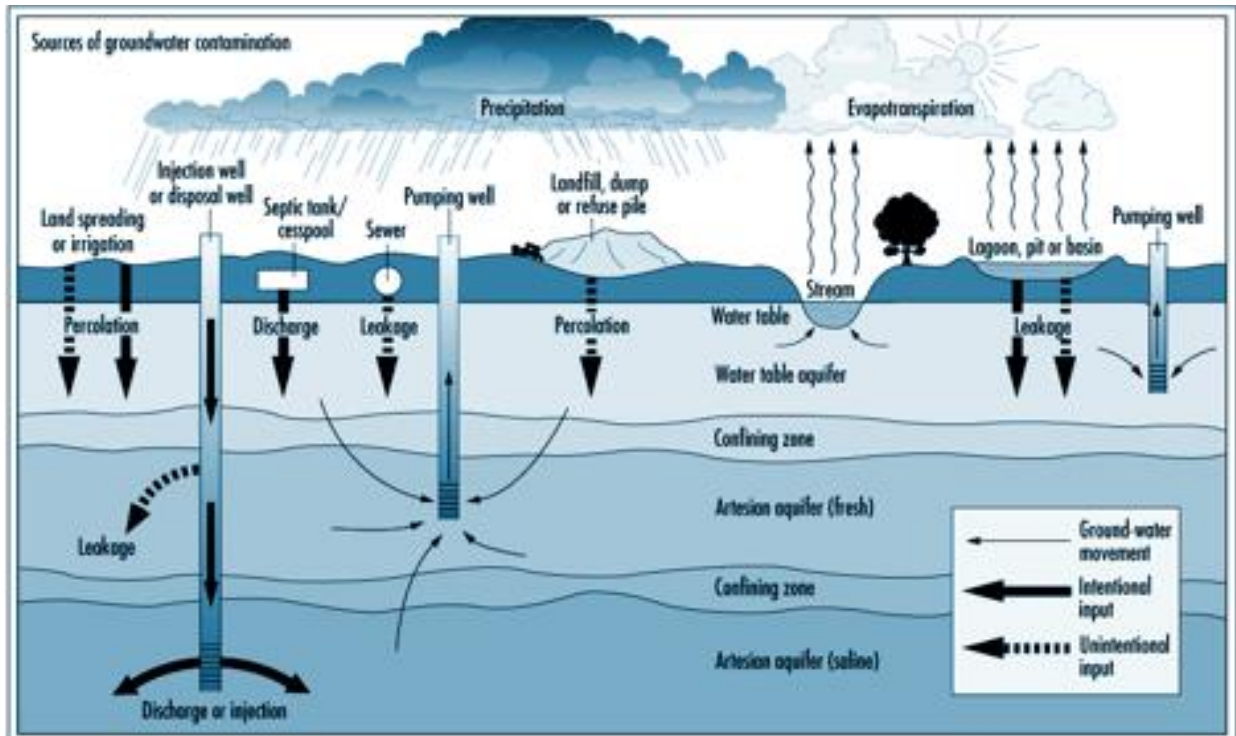
Figure 1. Modes of anthropogenic contamination of water sources. Once contaminants are introduced into the water, it can be challenging to remove them.

Despite outcry among environmental scientists, the input of inorganic nutrients into croplands is unlikely to drop any time soon, especially as newly developing nations increase the acreage of their croplands to keep up with rising agricultural demands. In fact, it is expected that phosphorus input will increase between 51-86% by the year 2050.[13]

Outside of agricultural sources, the growing manufacturing, pharmaceutical, and petrochemical industries, paired with negligent governmental policies governing waste removal, have led to an abundance of contaminants in water sources around the world. Phenolic compounds and their derivatives, designated high priority pollutants by the U.S. Environmental Protection Agency, are used for paints, surfactants, explosives, textiles, rubber, plastics, and pharmaceutical antioxidants and antibacterials, and are spread throughout the environment through waste effluents.[14] Since phenolic compounds can readily react in water, often via

oxidation or halogenation, they form a complex array of derivatives that can be chemically challenging to remedy.[15] In addition to organic compounds, many industrial processes release various heavy metals into the surrounding environment, including zinc, nickel, copper, chromium, lead, manganese, and arsenic. These non-biodegradable contaminants can be retained in soil long-term via adsorption to mineral particles as well as accumulation in organisms and passed up the food chain, magnifying their effect.[16]

Microalgae for phytoremediation

Phytoremediation is defined as the use of green plants and microorganisms to decrease the toxic effects of environmental contaminants. This technique has been used successfully for the remediation of heavy metals, metalloids, and organic contaminants from soil and water sources, and has been shown to be a more economic and efficient remediation option when compared to other engineering and chemical techniques.[9] AMOPs have developed natural mechanisms for metal sequestration, including non-ribosomal polypeptides known as phytochelatins, as well as gene-encoded class II metallothioneins, both of which are short-chain
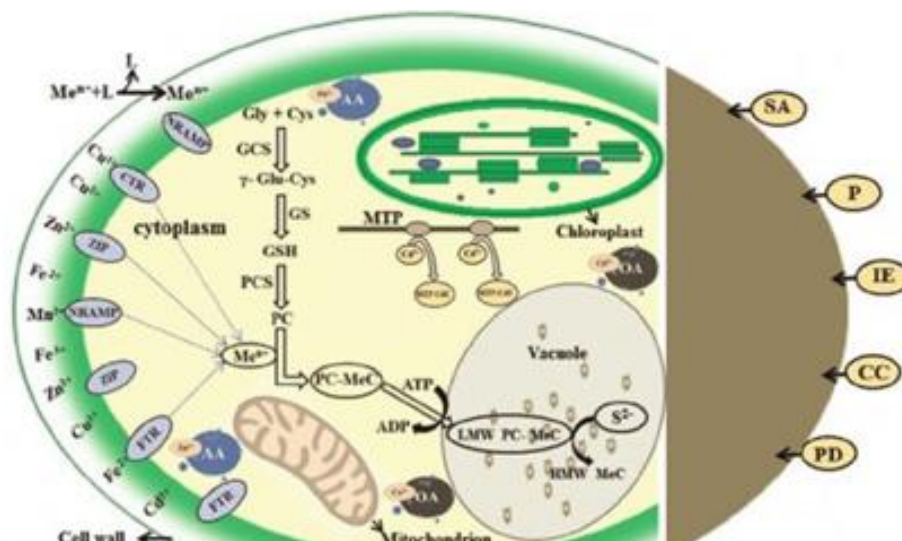
Figure 2. A schematic representation of heavy metal translocation, sequestration, and uptake in living (left-hand side) and non-living (shaded brown) microalgae. Manganese is of particular interest in this study due to its role in PSII.

4

polypeptides that bind heavy metals (Figure 2).[17-18] By binding the metals into organometallic

complexes and then further partitioning them into membrane-bound organelles, the organisms

prevent the potential toxic effect of high cytoplasmic metal concentrations, allowing them to

continue to freely engage in necessary biochemical processes.[19] Thus, microalgae are of

particular interest to phytoremediation strategies as they can grow successfully in waste water,

removing both organic carbon and inorganic nutrients such as nitrogen and phosphorus, while

simultaneously producing valuable biomass from which value-added products can be extracted.[20]

Microalgae are also able to rapidly respond to changing environmental conditions using a

versatile metabolism that includes both phototrophic and heterotrophic modes, allowing them to

decompose many organic contaminants into simpler, non-toxic byproducts. This has included the

decomposition of tributyltin (*Chlorella vulgaris*),[21] phenanthrene (*Selanastrum*

capricornutum),[22] napthalene (*C. vulgaris*),[23] and bisphenol (*Chlorella fuscai*),[24] among other

organic compounds.[25] While many microalgal species are capable of achieving high rates of

degradation without outside influence, genetic approaches can increase their capacities even

further.

Microalgae as biological environmental sensors

    While physical and chemical measurements of water sources can provide needed

information regarding levels of aquatic pollution, these measurements do not reflect the extent of

which these pollutants cause environmental stress nor the subsequent organismal effects of this

stress.[26] Microalgae are quick growing, easily cultured, and do not require expensive methods for

sampling and assessment. This allows them to be easily monitored at the laboratory scale for

studies of short-term contaminant effect as well as in their natural ecosystems to determine the

effect of long-term contaminant exposures.[27] Because they are primary producers they are

directly impacted by physical and chemical factors from water sources, which is easily monitored due to their naturally sensitive metabolism that rapidly reacts to changing environmental conditions. Additionally, by monitoring their biochemical composition, predictions can be made as to the effect of anthropogenic stressors on the greater food web of algal-based ecosystems.[28] Due to the sensitivity of the photosynthetic apparatus, various rapid, low-cost measurements including chlorophyll fluorescence and oxygen evolution can provide sensitive indication of contaminants, even at low concentrations.

Microalgae for value added products

Microalgae generate a variety of value-added products with industrial and human health applications, including high levels of proteins, polysaccharides, pigments, and lipids, most of which can be increased through the application of environmental stressors.[29] In addition to macromolecules, they are rich sources of essential micronutrients, including many vitamins and minerals such as vitamin A, C, B_1, B_2, B_6, iodine, potassium, iron, and magnesium. Due to their nutritional benefits, several algae and photosynthetic prokaryotes, notably *Chlorella vulgaris*, *Dunaliella salina*, and *Arthrospira ("Spirulina") maxima*, are commonly marketed and used for both human nutritional supplements as well as animal feed additives.[30]

Protein

Microalgae synthesize both essential and non-essential amino acids and can accumulate concentrations up to 60% of their biomass (m/m) under ideal conditions, allowing algal biomass to generate high-quality protein feedstocks for animal use, including chickenries and fisheries.[30] Under stress conditions, AMOPs can outproduce some of the best agricultural crops; *D. salina*, for example, can produce up to 100x the protein yield of terrestrial harvests when grown in an industrial scale under stress.[8] Furthermore, algae cultures are high in antioxidant-related proteins

and studies show that various algal extracts have the potential to reduce brain damage, decrease inflammatory activity and reduce allergy symptoms, increase antioxidant activity, and protect against cellular damage.[31]

Outside of agricultural and health-related supplements, eukaryotic microalgae are promising production platforms for the generation of recombinant proteins, as their protein synthesis machinery allows for more complex structures with a larger variety of post-translational modifications than those capable of being produced by prokaryotic organisms.[32] Additionally, the availability of a chloroplastic genome that can be modified and manipulated enables increased accumulation of transgenic proteins when compared to bacterial systems, as plastids lack gene silencing mechanisms that can reduce recombinant protein production from nuclear-encoded genes.[33] Additionally, the chloroplastic genome has multiple gene insertion sites, allowing microalgae to be transformed with multiple genes in a single event, decreasing cost and increasing the industrial feasibility of using microalgae for the generation of recombinant proteins.[34] A variety of therapeutic proteins have been produced using algal systems including bovine mammary-associated serum amyloid,[35] swine fever virus E2 viral protein,[36] diabetes-associated anutoantigen human glutamic acid decarboxylase 65,[37] and human vascular endothelial growth factor isoform 121,[38] among others.[32] The future of algae for biotechnology will likely contain the generation of more vaccine antigens, industrial relevant enzymes, and immunotoxins for use in chemotherapy treatments, as well as increasing libraries of bioactive peptides with novel antibacterial mechanisms.[32]

Polysaccharides

Microalgae contain anywhere from 2 – 60% carbohydrates per dry weight of various compositions, including glucose, starch, galactose, rhamnose, *N*-acetylglucosamide, among

others.[8, 30] Carbohydrates serve two primary purposes in algae: to increase structural integrity of the cell and to store excess energy, and are therefore easily manipulated under various stress conditions.[39] Due to the lack of hemicellulose and lignin found in terrestrial plants, structural microalgal carbohydrates are more accessed and degraded. However, this property is rarely used for the purpose of food additives as seen with algal proteins, and instead is taken advantage of for the production of bioethanol, as the cost of digestion on the industrial scale is much less than the cost to digest terrestrial plants.[40] Additionally, carbohydrates may be produced simultaneously with other useful co-products to increase the economic feasibility of bioethanol.[41] However, bioethanol is not drop-in ready and will require a significant carbon investment in order to be used as a large-scale transportation fuel.[42] For this reason, large scale impacts on the transportation industry are more likely to be achieved through the use of lipid production for the generation of biodiesel.[43]

Pigments

Microalgae accumulate large concentrations of a variety of pigments with health or industrial purposes, including β-carotene, lutein, zeaxanthin, and chlorophyll, among others.[30] Fat soluble β-carotene is used as a food coloring (most notably for margarine and fish) and as a dietary supplement for cattle, as well as used as an anticarcinogen and cardiovascular anti-inflammatory agent due to its antioxidant properties.[44] Lutein and zeaxanthin are both essential for ocular function and must be acquired through the diet. Nutritional interventions against macular degeneration and other diseases often involve dietary supplements containing high concentrations of lutein, zeazanthin and other xanthophylls, all readily available from microalgal biofeedstocks.[45] Similar to carotenoids, chlorophyll is used on an industrial scale as a coloring agent as well as a bioactive antioxidant and antimutagen, and is used widely in pharmaceuticals,

including those for wound healing, antibacterials, and proctological therapeutics.[46] These high-value compounds can be produced simultaneously with other macromolecules, increasing the economic feasibility of industrially scaled microalgal production.

Lipids

Microalgae can achieve up to 30-70% lipids per dry mass under stress conditions with the lipid composition mostly consisting of saturated and monounsaturated C14-C20 fatty acids, making them promising candidates for increasing the industrial feasibility of lipid-based biodiesel (see Chapter 2).[47] AMOPs are also able to synthesize polyunsaturated fatty acids needed for human health, including eicosapentenaoic acid, docosahexaenoic acid, and ω-3 fatty acids with anti-inflammatory properties.[48] Various microalgal species including *Nannochloropsis oceanica, Phaeodactylum tricornutum,* and *Mortierella alpine* have been genetically modified to increase concentrations of polyunsaturated fatty acids, with increases of up to 75% for arachidonic and eicosapentenaoic acid.[49-51] While these essential fatty acids are often added to diets via the use of fish oil, supplementation in this manner can also result in toxin accumulation, odor, unpleasant taste, and poor oxidative stability, making microalgae more advantageous for use in nutritional additives.[8, 52] Algal biofeedstocks are also able to accumulate high concentrations of sterols, triterpenes similar in structure and function to cholesterol, which have been shown to lower low-density-lipoprotein cholesterol levels *in vivo* as well as stimulate anti-inflammatory and anti-oxidant activities.[53] Phytosterols have been used in pharmaceuticals through the production of therapeutic steroids, nutrition, and various cosmetics.

Chlorella vulgaris: **an ideal AMOP for industrial and environmental purposes**

Chlorella vulgaris is a unicellular, spherical microalga averaging between 2-10 μm in diameter.[54] It is non-motile and reproduces asexually, with every cell autosporulating into four

daughter cells at least once every 24 hours under optimal conditions.[55] *C. vulgaris* has a single,

large chloroplast that can take up to 80% of the volume of the cell. The chloroplast is both home

to the photosynthetic machinery as well as many macromolecules including starch granules and

lipid globules, each accumulated in high concentrations under stress conditions. Despite the size

and significance of the chloroplast, *C. vulgaris* is capable of growing heterotrophically in

addition to phototrophically. However, despite its ability to thrive in a variety of culture

environments, including those with limited nutrient availability and using non-arable lands, *C.

vulgaris* has had a limited role as a model organism in algal research, likely because of the lack

of a full genetic sequence until quite recently. As the sequence was fully published, it is now

likely that it will take a larger role in future phototrophic research and applications.[56]

The ideal photosynthetic microalga for biofuel production would be able to produce high

yields on high light intensity, be stable and resistant to infections, form flocs, and be insensitive

to high oxygen concentrations (Figure 3).[57] These qualities are equally applicable to other
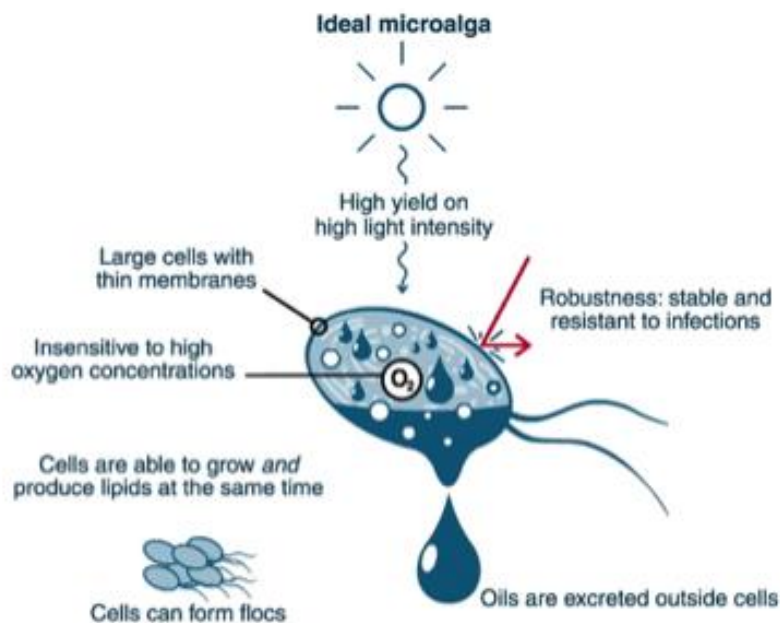
Figure 3. The ideal photosynthetic microalgae for biofuel production. More fundamental information is needed to engineer a microalga with the needed characteristics.

biotechnological applications, including both phytoremediation and environmental monitoring, as it is important to be able to easily harvest and monitor the algae for biochemical and metabolic changes following contaminant exposure. Depending on the growth phase, the cell wall of *C. vulgaris* is about 17–21 nm thick and is surrounded by a chitosan-like layer of glucosamine, generating a rigid structure that protects against microbial invaders and harsh environmental changes.[58] In fact, the rigid outer wall, while being a benefit for environmental monitoring and remediation, is one of the disadvantages of using *C. vulgaris* for biofuels, as harvesting the internal lipids requires a significant energy investment or expensive enzymatic methods.

Photosynthesis

Photosynthesis is the process through which phototrophs convert solar energy to biochemical energy through a series of conversion steps. Since algae are powered primarily through photosynthesis, their energy-containing byproducts, including triacylglycerols used for biofuel production, can be thought of as stored solar energy. For this reason, a rudimentary understanding of photosynthesis is necessary in order to evaluate the efficiency of algal-based biofuel feedstocks as well as to understand metabolic changes following the introduction of
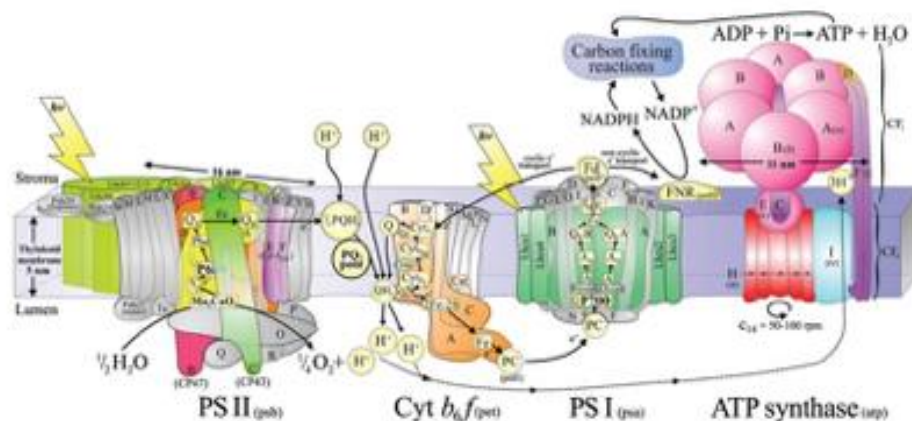
Figure 4. The oxygenic photosynthetic electron transport chain. Despite decades of research into photosynthesis, several mechanisms remain misunderstood.

environmental stressors. While photosynthesis can be both an oxygenic and anoxygenic process,

for brevity, this overview will only include the aerobic mechanism observed in unicellular algae. The photosynthetic apparatus is located in the thylakoid membranes of the chloroplast, which is divided into two distinct volumes, the stroma and the lumen. This compartmentalization provides the ability to generate electrochemical gradients, which is necessary in order to power ATP synthase, the terminal point of the electron transport chain. Photons start by exciting the reaction center of photosystem II (PSII) that releases an electron o travel down the electron transport chain. The electron travels out of PSII, through the membrane to cytochrome b_6f, and through the membrane again to PSI, at which point it is re-excited by another photon (Figure 4).[59] The electron is then used to either form NADPH, a high energy reducing molecule, or sent back to cyt b_6f by way of cyclic electron transfer. A more detailed summary is provided below.

Photosynthesis starts with the absorption of a photon between 400 and 700 nm at PSII. PSII is a heterodimer protein complex consisting of two main subunits, D1 and D2, six chlorophyll a (Chl *a*), two pheophytin *a*, two plastoquinone binding sites (Q_A and Q_B), a non-heme Fe^{2+}, and two carotenoids.[60] Surrounding the structure is chlorophyll protein 43 and chlorophyll protein 47, each of which bind approximately 15 chlorophyll molecules and together form the core of the light harvesting antenna, and cytochrome b_{559}, a heme-containing heterodimeric protein that helps protect PSII from photoinhibition.[59] When a photon between 400–700 nm enters the chloroplast, it is absorbed by a light harvesting antenna complex, that undergoes exciton transfer between chlorophyll molecules from the outer antenna to the inner antenna. At this point it can be used to excite the P680 reaction center, a pair of chlorophyll molecules near the lumen side of PSII. This excitation generates a charge separation between P680 and pheophytin, creating $P680^+$/Pheo a^-, the latter of which has a low reduction potential
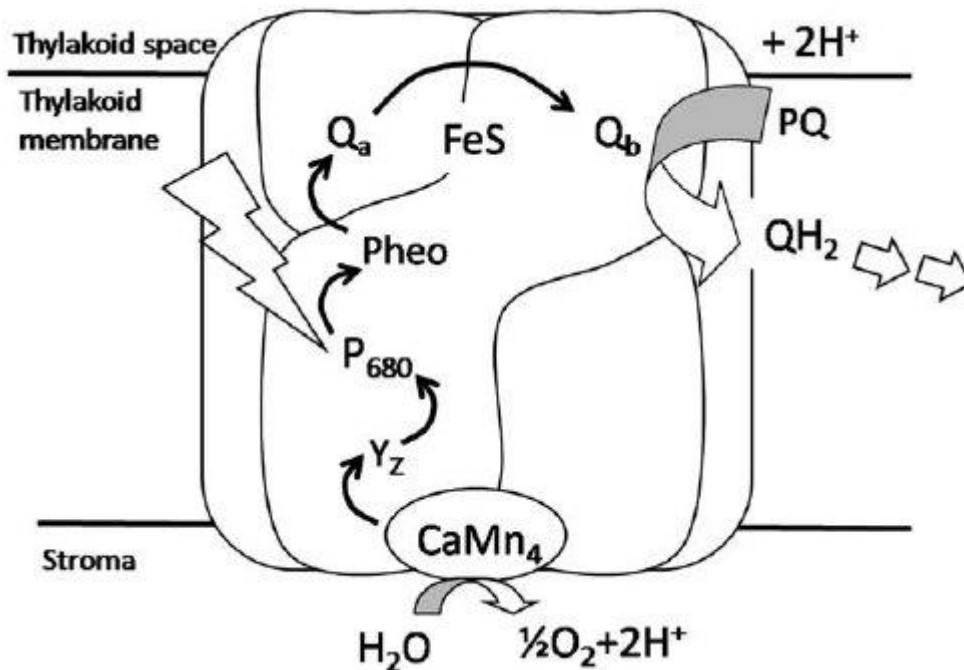
Figure 5. Electron transfer pathway of photosystem II. PSII is a homodimer consisting of matching D1 and D2 subunits, but only one pathway is active in electron transport.

that results in electron transfer from pheophytin to the plastoquinone permanently bound at Q_A, reducing it to a semiquinone (Figure 5).[61] This electron is then transferred to the Q_B site by way of a non-heme Fe^{2+} located equidistant between the two sites, which reduces a bound plastoquinone to a semiquinone. The semiquinone is reduced again by way of Q_A to form plastoquinol, which is released from PSII and travels through the membrane to the cytochrome b_6f complex.[59]

To re-reduce P680$^+$ to P680, PSII relies on the oxygen-evolution complex, a distorted-cubane Mn_4O_5Ca cofactor arranged peripherally to PSII in the lumen of the thylakoid and protected by three peripheral proteins (PsbO, PsbQ, and PsbP). Following the transfer of an electron from P680* to Q_A, P680$^+$ oxidizes a tyrosine residue, known as Y_Z, on the D1 protein to generate a tyrosine radical that in turn oxidizes the OEC.[62] After four sequential oxidations of the
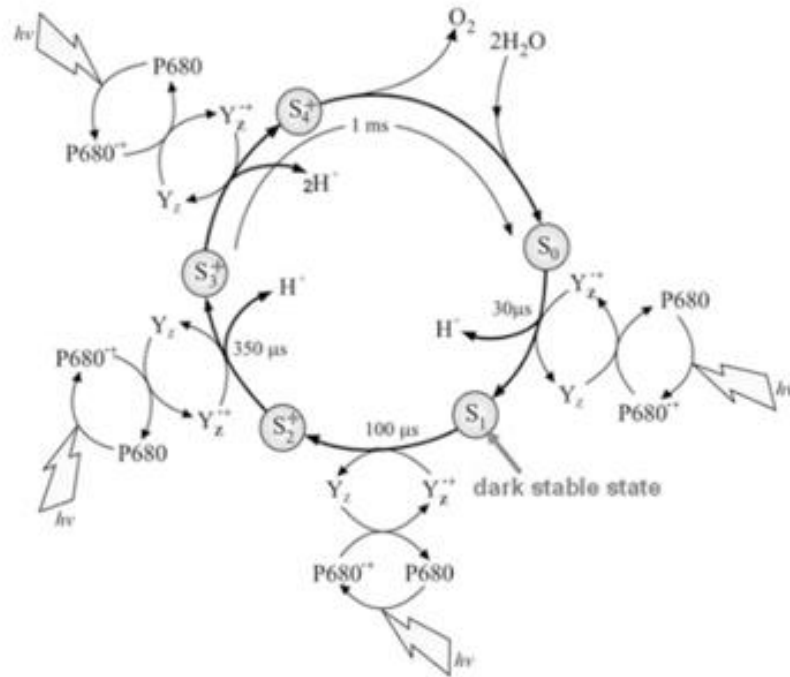
Figure 6. The S-state cycle of the oxygen evolving complex. The OEC generates electron holes through four sequential reductions before it has the energy needed to split water.

OEC (known as the S-state cycle), it possesses the redox potential needed to extract electrons from water and splits two molecules of water into molecular oxygen and four protons that are released into the lumen and contribute to the electrochemical gradient that powers ATP synthase (Figure 6).[63-64] The mechanism of the OEC, the only biological catalyst capable of oxidizing water, is still not completely understood.

Plastoquinol is a hydrophobic molecule that has a hydrocarbon tail that anchors it within the thylakoid membrane. It travels to the Q_0 site of cytochrome b_6f, a heterodimeric protein complex that facilitates electron transfer through a Rieske Fe-S protein.[65] After the initial oxidation of plastoquinol to a semiquinone, the Rieske protein shifts to transfer the electron to the heme-containing cytochrome f, which then reduces plastocyanin, a copper-containing water-soluble protein that is free to cross the lumen and travel toward photosystem I (PSI).[59] However,
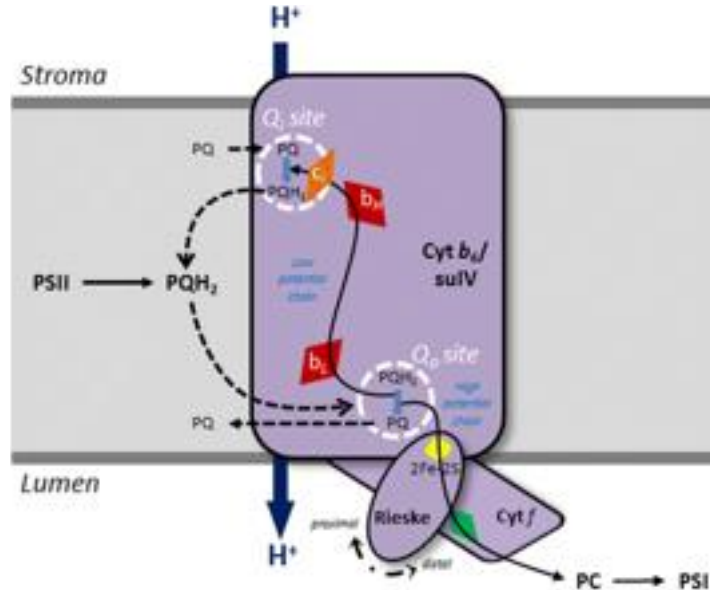
Figure 7. The electron transfers of cytochrome b6f. The modified Q-cycle, first described in the cyt bc1 complex, generates a net increase in oxidized plastoquinones, which increases the efficiency of photosynthesis.

the semiquinone bound to Q_0 must be oxidized again before plastoquinone is released; since the Rieske protein has temporarily moved approximately 20 Å out of position. This second oxidation occurs through an electron transfer to an internal heme, b_L, after which it is transferred to heme b_H; this entire process is known as the modified-Q cycle (Figure 7).[66-67] The electron at b_H then reduces a plastoquinone bound at Q_i. This process then repeats and the semiquinone at Q_i is reduced to a plastoquinol. In total, the modified Q-cycle oxidizes two plastoquinol for every one plastoquinone reduced, releasing four protons to the lumen. This process is important for re-oxidizing the plastoquinone pool, which provides substrates for reduction at the Q_B site of PSII. Without this oxidation, photosynthesis would be much more inefficient.

When plastocyanin binds to PSI, a heterodimeric protein, it is oxidized by $P700^+$, the PSI reaction center in its excited state following photon capture.[59] Following excitation of P700 to P700*, the electron is transferred through two chlorophylls before reducing a bound phylloquinone, after which it is transferred through three Fe_4S_4 clusters before reducing

15

ferredoxin, a soluble protein found within the stroma and contains a 2Fe-2S cluster .[68] Ferredoxin then reduces ferredoxin-NADP$^+$ reductase or travels back to cyt b$_6$f, where it can pass the electron back to cytochrome c in a process known as cyclic electron transport. While ferredoxin-NADP$^+$ reductase is used to catalyze the formation of NADPH, cyclic electron transport results in increased ATP synthesis with no net NADPH production.[59] The cell balances cyclic and linear electron transport based on the energy needs of the cell.

Specific Aims

This work used *C. vulgaris* to characterize the effects of environmental stressors for three primary goals: 1) to use it as a model system to determine the effects of various environmental contaminants, 2) to optimize its capacity to be a feedstock for biodiesel production, and 3) to use the photosynthetic data gathered from these two goals to learn more about the response of photosynthesis under stress conditions. These goals were achieved by mapping the physiological response to environmental stressors, both through measuring changing intracellular macromolecule composition and by measuring the flux of photosynthesis over time.

Specific Aim 1 was to characterize the effect of low concentrations of Poast, a commonly used agricultural herbicide formulation, on *C. vulgaris*, a non-target organism. Poast was introduced to *C. vulgaris* in mid-exponential phase and the physiological effects were monitored by measuring changing biochemical composition and photosynthetic productivity. Despite using concentrations about 16x less than the manufacturer's recommendations, Poast was determined to have a near-immediate toxic effect on the cells, with 80% of the cells becoming non-viable after 30 min of exposure. Using chlorophyll fluorescence and oximetry, it was determined that the Poast formulation interfered with the OEC of PSII, and resulted in a total loss of linear photosynthesis within 30 min. Additionally, tests on subcellular prepartions of PSII-enriched

membranes using sethoxydim, the active ingredient of the formulation, showed no effect on oxygen production, indicating that an unknown agent or some combination of agents caused the detrimental effects.

Specific Aim 2 was to determine the capacity of *C. vulgaris* to bioaccumulate manganese, a common mining contaminant, for use in phycoremediation. Using inductively coupled plasma optical emission spectroscopy, the intracellular and membrane-bound manganese was monitored over the course of the growth period. Simultaneously, cell density, pigment concentration, and photosynthetic capacity was monitored to determine the effect of manganese stress on the metabolism of the algae. *C. vulgaris* was able to accumulate manganese up to 55x the external media concentration and did so without significant biochemical detriment. Additionally, photosynthetic capacity increased with increasing manganese concentrations, despite the damaging effect similar metals have shown in the literature. The findings suggest that not only can *C. vulgaris* be used for bioremediation of manganese-contaminated waterways, but that manganese itself can be used to make algae more productive for the generation of value-added products.

Specific Aim 3 was to follow the use of glycerol in algal metabolism for the production of triacylglycerols needed for biofuel production. Glycerol is a byproduct of biodiesel production that has shown to be a useful carbon source for the upregulation of lipid synthesis in algal cultures. However, previous research has only utilized glycerol in purely heterotrophic cultures, negating the positive impact mixotrophic culturing has on lipid production. This study utilized a mixotrophic two-step fed batch system, in which cells were provided with dextrose upon initial inoculation and supplemented with glycerol once they reached stationary phase. Unlike the studies found in the literature, glycerol introduction did not significantly increase lipid

production in cells. However, using isotopically labeled glycerol and gas chromatography mass spectrometry, it was determined that glycerol is incorporated directly into the triacylglycerol backbone. Using chlorophyll fluorescence and oximetry, the photosynthetic output was observed to be less in cultures exposed to glycerol, suggesting that although carbon input is increased, contributions from photosynthesis are limited by glycerol addition. This study therefore highlights the need to further characterize the pathway of glycerol incorporation in order to better optimize *C. vulgaris* for biofuel production.

Specific Aim 4 is to determine the plasticity of PSII – both in the terms of antenna size and reducing ability of reaction centers – following exposure to increasing manganese concentrations. C. *vulgaris* was grown to exponential phase in concentrations of manganese up to 1000x the control and probed via *in vivo* fluorescence techniques to measure the relative amounts of active reducing centers and changing reliance on PSIIα and PSIIβ light harvesting antenna complexes. Additionally, the photosynthetic efficiency was monitored through the quantification of non-photochemical quenching, the process through which PSII dissipates unused photons and protects itself from photoinhibition. This study highlights ways in which algae can be engineered to be more photosynthetically productive for use in biofuel applications.

CHAPTER 2

ORGANISMAL OPTIMIZATION OF *CHLORELLA VULGARIS* FOR USE IN BIOFUEL

PRODUCTION: A REVIEW

Introduction

Amid diminishing fuel reserves and increasing global concern over climate change, it has

never been more important to develop renewable petroleum replacements. The most realistic

biological petroleum replacement is microalgae, as its ability to grow rapidly in adverse

environments using a variety of water sources makes it a promising source of energy that will not

compete with agricultural resources.[69] Microalgae surpass terrestrial biofuel feedstocks when

metabolizing solar energy; with a solar energy conversion efficiency of 3 – 9%, microalgae

outcompete the theoretical maximum of both C3 and C4 plants that have a solar energy

conversion efficiency of 2.4 and 3.7% efficiency, respectively.[43] Due to this increased efficiency,

current theoretical yields estimate that microalgae can be up to 20x more productive per unit area

than the most productive terrestrial crops.[70] If microalgae could be optimized to produce 70% oil

by biomass, it could satisfy 50% of the United States' transport fuel needs while using less than

2% of the existing 13.9 million acres used for corn-based ethanol production.[47]

Unlike agricultural crops, which have been subjected to a millennium of crop

domestication and optimization for human uses, the optimization of microalgae is in its infancy,

and with it, the knowledge needed to breed strains that are biochemically productive and

economically feasible. While investigations of photosynthesis and other topics in plant science

have laid the fundamental framework needed to strategically manipulate algal species, the

genetic diversity across microalgae, some of the most ancient organisms on earth with an

estimated 40,000 – 70,000 species over nine phyla, lends itself to unique challenges for plant

19

scientists and phycologists.[71] With diversity of species, comes diversity in biochemical

composition. While selecting species with high lipid production is important, it is equally

important to select species that have been screened on the basis of lipid yield, lipid class

composition, and fatty acid profile, as not all lipids are useful or efficient for biodiesel

production. Generally speaking, cetane number, heat of combustion, melting point, and viscosity

increase with chain length and decrease with increasing unsaturation, with polyunsaturated fatty

acids also being more prone to oxidation.[72] An ideal biofuel feedstock would be genetically

engineered to produce a higher than usual abundance of long chain saturated fatty acids, but the

diversity of algal species, enhanced by their evolved adaptations to a wide range of environments

and chemical stressors, has generated challenges for genetic manipulation. While the

chloroplastic, nuclear, and mitochondrial genomes can all be manipulated, electroporation and

biolistic methods of transformation have been most frequently used, causing inconsistencies as

the genes of interest can be subject to random integration.[73] Furthermore, due to diversity in both

genomes as well as physiology, it is likely that an appropriate DNA delivery system and

optimized transformation conditions will need to be developed for each microalgal species.[74]

 Chlorella vulgaris is a unicellular green alga that is capable of withstanding harsh

conditions and multiplies via auto sporulation at a rate of four daughter cells per mother cell per

day.[75] This rapid growth rate, combined with its ability to auto-flocculate under basic conditions

as well as thrive in both heterotrophic and photoautotrophic conditions, has made it a target for

biofuel research. Although *C. vulgaris* has an average accumulation of 25% lipids by biomass

under nutrient replete conditions, far from the target of 70%, significant increases have been

achieved through a variety of research and development initiatives.[70] In addition to physiological

characterizations, researchers recently sequenced and annotated the genome of *C. vulgaris*,

opening up the possibility for large-scale proteomic studies and genetic manipulations that were impossible only two years ago.[56] If these developments can be paired with the increased efficiency seen with advancements in biofuel engineering, *C. vulgaris* can provide an optimal feedstock for biodiesel and help to circumvent the use of petroleum worldwide. This review details the developments in growth conditions and genetic manipulation of *C. vulgaris* and its potential contribution to the global fuel industry. While the properties of the organism have already been extensively reviewed by Safi *et al*., this review details the research and development work that has significantly increased its viability as a biodiesel feedstock.

Carbon Sources for Increased Lipid Production

      Chlorella vulgaris is able to switch between photoautotrophic, heterotrophic, and mixotrophic growth modes in order to quickly adapt to environmental conditions. While heterotrophic cultures have been the standard for increasing lipid and biomass for many years, recent research has shown that *C. vulgaris* requires the photosynthetic light reactions to enhance its potential as a biodiesel feedstock, with mixotrophic cultures producing four times the amount of lipids of heterotrophic cultures after five days and over twice as much lipids after eight days, despite reaching the same biomass.[76] However, introducing light, specifically artificial light, will introduce yet another energy and financial investment, once again reducing the economic feasibility of algal biofuel feedstocks.

      In order to minimize the energy investments of artificial lighting and/or exogenous carbon sources, researchers have attempted to increase the lipid yield of *C. vulgaris* through different regimens of photoautotrophic growth. However, some investment is necessary: room air, which contains about 0.04% CO_2, is simply not concentrated enough to efficiently sustain the needs of *C. vulgaris'* photosynthetic output when used as the sole carbon source.[77] Increasing

concentration of CO_2 to 1% yielded higher biomass concentrations with 0.78 g/L and 20% lipids

per biomass, but further increases in concentration did not have a significant increase over room

Table 1. Summary of exogenous carbon sources used for increasing lipid production in *C. vulgaris*.

Waste source	Lipid rate (g · L^{-1} ·d^{-1})	Lipid %	Biomass (g · L^{-1})	Source(s)
Artificial wastewater	0.044 – 0.147	20 – 42	0.28 – 0.89	[78]
Cheese whey	0.253	30	3.58	[79]
Cyperus esculentus	0.381	34.44	4.43	[80]
Dairy waste	0.044	14.38	0.25 – 1.87	[81-84]
Ethanol thin stillage	1.1	43	5.8 – 9.8	[85]
Food waste	0.064	8.58 - 31	0.37 – 3.8	[86-88]
Glycerol waste	0.163	39	2.92	[89]
MSG effluent	0.005 – 0.013	13.47 – 25.40	0.35 – 1.02	[90]
Municipal wastewater	0.021 – 0.575	8.73 – 33.49	0.12 – 2.0	[82, 91-96]
Orange peel extract	0.022	12.27	2.2	[97]
Organic fertilizer	0.001	18.1	—	[98]
Piggery waste	0.093 – 0.28	16.9 - 28	0.75 – 1.68	[99-101]
Pine wood	0.072 – 0.319	21 - 32	0.69 – 4.94	[102]
Saline effluent	0.020 – 0.054	12 - 41	0.059 – 1.13	[103-105]
Sewage sludge	0.066 – 0.20	20.01	0.5 – 4.23	[82, 106]
Soy whey	0.2	11	2.5 – 6.3	[85]

air for biomass or lipid percent. Additionally, chlorophyll concentration was highest with the 1%

CO_2 cultures, indicating that photosynthesis was most active using this regimen. Like

Woodworth *et al*., this suggests that lipid productivity is tied to photosynthetic productivity, as the optimal CO_2 concentration for lipid and biomass productivity is also the best for photosynthesis.[76] This could show an enhancement of acetyl-CoA carboxylase (ACCase) functionality, as its catalytic activity is partially modified by changes in pH, Mg^{2+} concentration, and redox changes within the stroma of the chloroplast.[107] Increases in photosynthetic activity lead to increases in protons released into the thylakoid lumen, increasing the pH of the stroma. Since ACCase is more active in alkaline conditions, this could increase its activity, increasing the overall lipid percent of the organism.[108] It is possible to significantly increase lipid and biomass production with higher concentrations of CO_2, but only through the use of nutrition starvation conditions, such as when one group paired using 3% CO_2 with nitrogen limitation.[109] While they were able to achieve a biomass of 1.4 g/L and a lipid content of 23.3%, this method is expensive due to the need for centrifugation-mediated media exchange and for CO_2 concentration.

Supplying cells with exogenous carbon sources has greatly increased biomass and lipid production, even without incorporating the photosynthetic reactions. However, small differences in carbon sources leads to significant differences in both biomass production as well as lipid productivity. Gim *et al*. evaluated the effect that six different carbohydrates had on the growth productivities of *C. vulgaris* grown heterotrophically and mixotrophically, with glucose, a simple hexose monosaccharide, producing the best mixotrophic and heterotrophic growth, with a lipid content of 0.5, 1.7, and 1.8 g/L in photoautotrophic, heterotrophic, and mixotrophic cultures, respectively.[110] While the other carbon sources—galactose, rhamnose, xylose, fructose, and sucrose, listed in order of decreasing efficacy—all increased productivities beyond those seen under photoautotrophic growth, none could compete with the enhanced growth generated through glucose availability. This is because glucose can be catabolized directly into glucose-6-

phosphate before conversion to pyruvate via anaerobic glycolysis, after which it is entered into the citric acid cycle and used for ATP production through oxidative phosphorylation.[111] Thus the introduction of glucose can directly increase ATP production, generating excess energy in addition to what is needed for protein synthesis, allowing for increases in reproductive rate, biomass productivity, and lipid content. Other carbon sources need more complex and energy intensive inter-conversions before they can be used for metabolic processes. While glucose and fructose contain the same number of carbons, fructose cannot be directly converted into glucose-6-phosphate, requiring an energy investment to prepare it for the TCA cycle. Sucrose, a non-reducing sugar, requires hydrolysis to separate the molecules of fructose and glucose, as well as further conversion of the fructose, which explains why the cells had the lowest levels of biomass productivity when supplemented with sucrose.

Combining glucose availability with light exposure generated the most promising results, likely because this combination generates excess ATP and NAD(P)H, allowing for accelerated cell growth due to high availability of reducing equivalents.[76, 110, 112-115] However, while this increases the efficiency on the organismal level, it hurts economic feasibility as glucose is the most expensive carbohydrate available for use in growth media and can account for up to 80% of the total medium cost.[113, 116] In order to cut costs, researchers have used glycerol, a byproduct of the transesterification process that converts triacylglycerols into the fatty acid esters needed for biodiesel, as an exogenous carbon source. In one study, using 5 g/L glycerol medium, *C. vulgaris* reached a maximum biomass of 1.91 g/L, compared to just 1.37 g/L in photoautotrophic medium. When cultured with 5 g/L glycerol, the culture reached a TAG content of 15.91%, 12.20% higher than photoautotrophically grown cultures. Glycerol also improved the quality of the lipids produced, as 34.94% of the TAGs were saturated fatty acids, as compared to just

16.91% in the photoautotrophic cultures.[117] However, when used as a sole carbon source, glycerol had a pronounced lag phase before entering exponential phase, likely due to the lack of cellular machinery to properly metabolize it. Additionally, glycerol inhibits the pentose phosphate pathway, leading to a decrease in nucleotide production needed for cell division.[118] By using a 2-step batch culture in which cells were initially provided 10 g/L glucose before being dosed with an additional 10 g/L glycerol in stationary phase, cells experienced a 1.4-fold increase in growth and a 13.85% increase in lipid content compared to batch fed, with an overall lipid content of 36.39% and productivity of 729.67 mg $\cdot$ L^{-1} $\cdot$ d^{-1}. Lipid yield was best when using crude glycerol rather than analytical grade glycerol, which is promising for biodiesel production as the energy investment is lower than if needing processed glycerol.[119]

In addition to providing substrates for metabolism, exogenous carbon sources can also be used strategically to inhibit pathways that pull energy away from lipid production. Xylose, for example, is a waste product of the pulp and paper industry and is a major component of hemicellulose, a less rigid structural polymer than cellulose but still abundant in nature.[120] However, xylose has been found to be toxic in many different algal and bacterial species due to its interference in metabolic pathways.[121] While *C. vulgaris* was capable of growing heterotrophically on xylose alone, cultures had a decreased performance compared to photoautotrophic cultures as the monosaccharide initiated a loss in chlorophyll content with a subsequent increase in lipid content, but after 24 h, also resulted in the shrinkage of cells. The bleaching effect caused by xylose is species specific, not due to acidification of the medium, and not due to photo-oxidative stress. Xylose caused a similar effect to nitrogen deprivation without the budget-limiting step of centrifugation. Using xylose as an alternative to nitrogen deprivation, wherein cultures are dosed approximately 24 h prior to harvest, is a method through which lipid

productivity could have a three times increase using a fraction of time and expense required with nitrogen deprivation. Additionally, most of the xylose is still present in the media following inhibition, allowing for recycling of the raw material.[122]

Nutritional Supplementation with Waste Water Sources

While mixotrophic growth clearly improves lipid and biomass productivity, the cost of exogenous carbon sources causes challenges when scaling up production. In order to thwart the added cost while providing the same benefit of mixotrophic growth, researchers and entrepreneurs have employed various waste effluents as sources for both exogenous carbon as well as inorganic minerals. This has been of particular advantage to industries that produce large amounts of unmarketable waste – such as dairy farms or piggeries – as they produce waste with high concentrations of nitrogen that directly benefit algal growth.

Piggery wastewater in particular is of serious environmental concern as over 11 million tons of piggery wastewater is generated in China alone on a yearly basis.[123] While its abundant concentrations of nitrogen, phosphorus, and essential minerals makes it an ideal feedstock for microalgae growth, it also contains high concentrations of ammonium, which is toxic to microalgae.[124] However, by diluting it with media or distilled water, this toxicity was mitigated, generating algae with 28% lipids per dry mass.[99] Ammonium toxicity can also be avoided in wastes with high organic carbon contents, such as sewage waste, as the benefit of assimilating the carbon source outweighs the inhibitor effect of high ammonium concentrations.[106] Sewage contains an abundance of volatile fatty acids, which can be directly incorporated into the cells, generating lipid contents around 20%.[82, 106]

Table 2. Summary of waste water sources used for *C. vulgaris* cultivation and their potential for biodiesel production.

Waste source	Lipid rate (g · L^{-1} ·d^{-1})	Lipid %	Biomass (g · L^{-1})	Source(s)
Artificial wastewater	0.044 – 0.147	20 – 42	0.28 – 0.89	[78]
Cheese whey	0.253	30	3.58	[79]
Cyperus esculentus	0.381	34.44	4.43	[80]
Dairy waste	0.044	14.38	0.25 – 1.87	[81-84]
Ethanol thin stillage	1.1	43	5.8 – 9.8	[85]
Food waste	0.064	8.58 - 31	0.37 – 3.8	[86-88]
Glycerol waste	0.163	39	2.92	[89]
MSG effluent	0.005 – 0.013	13.47 – 25.40	0.35 – 1.02	[90]
Municipal wastewater	0.021 – 0.575	8.73 – 33.49	0.12 – 2.0	[82, 91-96]
Orange peel extract	0.022	12.27	2.2	[97]
Organic fertilizer	0.001	18.1	—	[98]
Piggery waste	0.093 – 0.28	16.9 - 28	0.75 – 1.68	[99-101]
Pine wood	0.072 – 0.319	21 - 32	0.69 – 4.94	[102]
Saline effluent	0.020 – 0.054	12 - 41	0.059 – 1.13	[103-105]
Sewage sludge	0.066 – 0.20	20.01	0.5 – 4.23	[82, 106]
Soy whey	0.2	11	2.5 – 6.3	[85]

While manure and sewage-based waste waters are useful nutrient sources for microalgae, they also generate large concentrations of microbial contaminants, which can overtake the growth of *C. vulgaris* when presented without pretreatment.[93] This can be remedied through the use of treated municipal wastewater, which can be pre-treated through sterilization, ultrasonic

cavitation, or ultraviolet light before microalgae cultivation without large-scale modifications to existing wastewater treatment plants.[91] Municipal wastewater provides a wide range of lipid contents in *C. vulgaris*, dependent on the addition of exogenous carbon as well as the presence of a light source. While heterotrophic growth presents an economic advantage through the dismissal of artificial light requirements, it also requires heavy supplementation through acetate or glucose in order to reach its full potential, dramatically increasing the cost of the growth medium.[96] However, in mixotrophically grown cultures, the use of carbon supplementation can prevent the need for internal aeration normally used for aerobic digestion of municipal waste.[95] This, when combined with the fact that algae can be used for profit via value added products as well as with the quick digestion time (approximately 2 days) and the lack of temperature control, increases the profitability and feasibility of microalgal biofuel feedstocks. Furthermore, if a credit of $0.40 m^{-3} is considered for primary wastewater treatment by algae, then it would cost approximately $231.59 to produce 1 ton of algal biomass. Assuming an optimized lipid content of at least 42%, algal biofuels would now be competitive with petroleum up to $63.97 per barrel.[47, 78] As of March 27, 2019, petroleum was priced at $59.19.

To avoid the added costs of water treatment, several groups have successfully utilized high saline effluents for microalgal growth. High saline effluents, including those from real tidal saline waters, have too high of saline concentrations to sustain bacterial growth, reducing the potential of contamination considerably.[104] Since *C. vulgaris* is robust, it can easily survive in high saline water, maintaining an osmotic equilibrium with the surrounding media.[105] However, once the media is deplete of nitrogen, the excess salinity acted as an environmental stressor, inducing increases in lipid synthesis similar to that of induced nitrogen depletion.[103] This effect is also salt-specific: while KCl resulted in the aforementioned stressed state upon nitrogen

28

depletion, high sodium in the media induced a stressed state before nitrogen depletion, showing immediate increases in algal lipid generation upon exposure. Thus waste-processing centers could strategically utilize the concentrations of saline effluents to expose cultures to high sodium solutions directly before harvest, ensuring that the lipid content is as high as possible prior to processing for biofuel production.

Nutrient Deprivation for Enhanced Lipid Production

Nutrient deprivation is currently recognized as the most successful and widely used strategy for increasing lipid production in biofuel feedstocks.[125] Nitrogen deprivation is the most widespread, as the method is inexpensive, easy to manipulate and fine tune, and has a reliably significant impact on lipid content in most algal species. *C. vulgaris* is particularly susceptible to these effects; in a study with 10 other species of algae, *C. vulgaris* had both the highest overall growth rate as well as the largest increase in lipid content in response to nitrogen deprivation.[70]

A challenge of nitrogen deprivation, outside of issues with economic feasibility due to the need for large-scale centrifugation, is the overarching effects on cellular morphology. While an ideal microalgae would be able to rapidly accumulate lipids while continuing to grow in number, this is impossible under nitrogen deprivation as protein synthesis, a nitrogen-dependent process, is severely limited, leading to a stagnation in cellular division.[77, 126] Additionally, photosynthesis is highly impacted, with chlorosis occurring within 48 h of nitrogen depletion with a subsequent decrease in photochemical energy conversion accompanied by increases in non-photochemically active carotenoid pigments.[127-128] A decrease in photosynthetic activity results in decreasing of reducing equivalents needed for lipid synthesis, limiting the overall potential of lipid yield.[76] An interesting byproduct of nitrogen limitation is that of fast carbohydrate increase, with cells reaching nearly 50% carbohydrates per dry mass within the first 48 h of depletion.[126] Since the

29

primary storage component of microalgae under physiologically ideal conditions is starch, the increase in carbohydrates may be accounted for by a decrease in starch demand as the metabolic flux for other carbon-dependent pathways decreases, increasing the dissociation of individual monosaccharides from starch macromolecules. While this process increases the overall available energy content of the microalgae, it is not helpful for biofuel production as carbohydrates can only be used to generate ethanol, rather than the drop-in ready biodiesel produced from TAGs. TAG accumulation increased following monosaccharide release from starch, with increases beginning 48 h of nitrogen deprivation.[126]

Regiments of sulfur deprivation have also generated enhanced lipid production, with deprivation conditions resulting in 1.5 – 2.4 fold higher lipid contents.[129] As with nitrogen deprivation, the cells first increased their overall concentration of carbohydrates before increasing their TAG production. Additionally, there is evidence of decreased protein synthesis as cell numbers stagnated while cell dry mass continued to increase, though not as much as the cells in the replete conditions. Like nitrogen deprivation, the sulfur deprivation resulted in changes to the ultrastructure of the chloroplast, as decreases in the size of the chloroplast observed using transmission electron microscopy corresponded with increases in starch accumulation, before the appearance of larger lipid droplets occurred. Interestingly, glucose consumption continues after the onset of sulfur depletion. This indicates that, unlike with nitrogen depletion, carbon metabolism is still active within cells, rather than macromolecular bioconversion alone.[130]

While both nitrogen and sulfur deprivation result in increases in overall lipid content, this does not extend to all nutrients, showing how further pathway analysis is needed in order to determine the causes of increasing lipid flux. A notable mineral that is needed both for cell

division as well as lipid synthesis is phosphorus, without which the cells cannot thrive. Phosphorus deprivation alone does not enhance lipid productivity, but excess phosphorus in the absence of nitrogen availability increased overall lipid content, with an increase in TAGs needed for biofuel production, specifically.[131] In fact, in nitrogen-deprived conditions, cells that are exposed to excess phosphorus have increased overall rates of lipid production and uptake the phosphorus at a rate nearly four times higher than cells in nitrogen replete conditions.[132] This is likely due to the need for ATP generation; as the cells are unable to produce excess NADPH through the downregulation of the photosynthetic electron transport chain, the cells are more likely to rely on ATP synthesis from oxidative phosphorylation in the mitochondria.

Further work for using *C. vulgaris* for biofuels

C. vulgaris encapsulates many of the qualities most desirable for algal biofuel feedstocks; it is stable and robust against pathogens and other contaminants, it can survive and thrive in waste waters, it requires little additional nutrients and can utilize a variety of exogenous carbon sources, and it can survive in a variety of light conditions, including both excessive light and heterotrophic growth.[57] However, despite over 20 years of biofuel-related research using *C. vulgaris* for biodiesel production, very little overall progress has been made.

Part of the problem in previous years has been the reliance on fragile model organisms, such as *Chlamydomonas reinhardtii*, that share many homologous proteins with *C. vulgaris* but are too genetically complex to model the pathways that need to be engineered in *Chlorella*. Now that *C. vulgaris* has been fully sequenced, there will be a decreased in reliance on other organisms and, with increased database annotations, the possibility of directly engineering enhanced lipid pathways through genetic transformations. While transfecting *C. vulgaris* has

31

been shown to be challenging, improvements in genetic technologies, such as CRISPR-Cas9 systems, increase the possibility of better engineering algal strains for biofuel production.[133]

However, while lack of genetic sequencing and manipulation has decreased the rate of continuing research, problems peppered throughout the decades of *C. vulgaris* research generate a highly problematic research library that is challenging to condense for the optimization of algal biofeedstocks. The first problem comes from differing strains: *C. vulgaris* is ubiquitously grown on nearly every continent leading to large strain varieties with differing phenotypes. While some researchers include the specific strain and location in their published work, many do not; additionally, many researchers use "mined" algal colonies from local waterways, which, without genetic or ribosomal confirmation, cannot be absolutely confirmed to be *C. vulgaris.* Furthermore, updates to species' classifications over the years have generated new species of *Chlorella* that were previously included under the *C. vulgaris* umbrella, such as *Chlorella protethecoides*, a *Chlorella* strain with an unusually high lipid content under normal conditions. Without more specific strain selection or reporting, it is difficult to determine which optimization methods found in the literature will be most effective for industrial purposes.

Additionally, the methods of data collection vary widely across the field of algal biofuels, with differences in both the analytical methodology as well as the notation used to describe production. While some researchers use 'specific growth,' a rate generated from the product of time and dry mass productivity, other publications refer only to the growth as a function of media volume, or else the mass of growth as a function of time alone. This continues for lipid analysis: many papers report the rate of production while others report content percent alone; some researchers report total lipids while others report neutral lipids and/or TAGs. These inconsistencies make it nearly impossible to make overarching conclusions as to the state of

optimization for *C. vulgaris* for use in biofuels and make it equally challenging to generate new experiments that either corroborate or expand on pre-existing datasets.

Conclusion

Algal biodiesel has the potential to make a meaningful impact on the overall use of fossil fuels by diversifying the energy sector with a renewable, carbon neutral fuel source that will not compete with other agricultural products. *C. vulgaris*, with its ability to survive in nutrient deficient conditions and without arable land, is a potential biofeedstock that must be further optimized before it is economically feasible for large-scale production. While over 20 years of research have provided a wealth of literature characterizing the effects of stressors and other growth conditions on the alga, standardization of analytical methods as well as the incorporation of direct genetic manipulations are needed to further explore the potential for *C. vulgaris* to be used on an industrial scale for the production of biodiesel.

CHAPTER 3

CHARACTERIZING THE EFFECT OF POAST ON *CHLORELLA VULGARIS*, A NON-TARGET ORGANISM

Amanda L. Smythers, Armin Garmany, Nicole L. Perry, Ethan L. Higginbotham, P. Ethan Adkins, Derrick R.J. Kolling*

Department of Chemistry, Marshall University, 1 John Marshall Drive, Huntington, WV, 25755, United States

*Corresponding author

Herbicides may cause unexpected damage to non-target organisms as it is challenging to predict undesirable biotic interactions. Poast is a widely used herbicide formulation that contains sethoxydim and targets the acetyl-CoA carboxylase of perennial grasses. In this study, *Chlorella vulgaris*, a unicellular green microalga, was exposed to a 0.08% working concentration of Poast

and the physiological and biochemical changes that took place were monitored using biochemical assays, fluorometry, oximetry, and immunoblotting. Within 15 min, severe photosynthetic damage was observed through a reduction in oxygen production and a reduced rate of electron transfer beyond photosystem II. In addition to direct damage to the photosynthetic machinery, it was shown that cells experienced membrane fragmentation. Within 30 minutes, over 90% of the exposed cells were nonviable. However, sethoxydim, the active ingredient, did not cause detrimental effects when applied along with mineral spirits. A synergistic or additive effect cannot be ruled out. This data suggests that Poast has the potential to cause severe harm to unicellular phototrophs in the case of herbicide over application or runoff.

Introduction

Herbicides are widely used in agriculture to promote the growth of target plants through the inhibition or by hindering competitors. These herbicides typically rely on compounds targeting specific proteins essential for plant survival, such as those needed for photosynthetic electron transfer or macromolecule synthesis. Herbicides affecting photosynthesis can be effectively monitored using the OJIP fluorescence transient, through which it is possible to infer changes in electron transfer throughout the entire electron transport chain. In fact, this is the most efficient system through which to monitor in vivo samples exposed to photosynthesis inhibiting herbicides, such as diuron, hexazinone, and atrazine.[134-136]

Herbicides are typically effective in small concentrations but are commonly mixed with carriers, wetting agents, or spreaders to make commercial formulations. These formulations are optimized to make handling easier, improve the performance of the active ingredient, and to minimize the adverse effects on non-target organisms.[137] However, the impact of the herbicide

formulation has the potential to be vastly different than that of the active ingredient without additives, causing unforeseen effects when introduced into the environment. These interactions can result in an increased toxicity as well as a decrease in species specificity that may be difficult to predict.[138] Therefore, to properly gauge the potential environmental effects of various agricultural run-offs, it is prudent to use commercial formulations to ensure the data will be more physiologically relevant.[139]

Sethoxydim is a member of the cyclohexanedione herbicide family used to inhibit plastid homomeric acetyl-CoA carboxylase (ACCase), the rate-limiting enzyme in lipid synthesis, in monocotyledonous and adventitious grass species. Specifically, it blocks the biotin-binding site, preventing the carboxyltransferase partial reaction from occurring.[140] This ACCase inhibitor is commonly used as post-emergence herbicide to protect broad-leaved crops such as cotton, soybean, sugar beet and tobacco against undesired annual grasses, wild oats, volunteer cereals and quackgrass. Sethoxydim is amphipathic and non-volatile, two desirable herbicide characteristics. Additionally, it has the advantage of being isomerically selective, easily degradable, and it can be used at dosages lower than 300 g ha^{-1} .[141] Sethoxydim is commercially available as Poast where it is concentrated at 13% (w/v), or 366 mM. Sevilla-Moran et. al (2017) used a Microtox toxicity test and found the Poast formulation caused increased toxicity to *Vibrio fischeri*, a bioluminescent bacteria, when compared to the sethoxydim alone.[138] However, there are no known studies on the effect of this formulation on unicellular phototrophic organisms.

Poast is used in large agricultural settings and has the potential to run off into streams and other natural waters where it could disturb the biotic environment. To determine the potential detriment of this disturbance, *Chlorella vulgaris*, a unicellular freshwater microalga, was exposed to a 0.08% (v/v) concentration of Poast (approximately 20x less than the manufacturer's

36

recommended concentration of 1.5%), after which the cultures were assayed for cell viability and their biochemical components were monitored at 12-h increments. While the formulation would be diluted with time and additional water volume, fields (due to pooling), shallow streams, and small ponds could potentially experience a direct effect following run off or drifting. 0.08% was chosen as it was the lowest concentration that results in complete culture death during one growth cycle. Even at this seemingly low concentration (relative to the working concentration), catastrophic effects were documented in *C. vulgaris*. One may expect to see this concentration in transient pools that appear in crop fields and surrounding areas. Organisms found in nearby shallow ponds and streams could be strongly affected. In addition, the amphipathic or nonpolar nature of some of the herbicide formulation components could result in aggregation and higher local concentrations (even in larger bodies of water) due to their low miscibility. There are many studies in the literature that concern the effects of herbicides, herbicide run-off dynamics, and herbicide formulations as they concern run-off and negative effects on non-target species.[142-145] To further characterize the effects of the herbicide formulation on *C. vulgaris*, oximetry and the chlorophyll *a* (Chl *a*) OJIP fluorescence transient were utilized to assay for changes in photosynthetic activity.

Materials and Methods

   Reagents

   D-Glucose, erythrosine, and the Folin-Ciocalteu reagent were acquired from Sigma-Aldrich Inc. (Dermstadt, DE). NaOH, sucrose, and MES monohydrate were purchased from Columbus Chemical Industries (Columbus, WI), EMD Millipore (Billerica, MA), and Alfa Aesar (Haverhill, MA), respectively. The remaining reagents, unless otherwise specified, were obtained through Fisher Scientific (Hampton, NH).

Strain and culture growth conditions

Batch cultures of *Chlorella vulgaris* were maintained on lysogeny broth agar plates and inoculated into 25 mL of modified Chlorella medium supplemented with 20 g/L of dextrose into 50-mL sterile Erlenmeyer flasks top capped with aluminum foil.[76] Cultures were grown in triplicate, using a 1-mL inoculum from a stationary phase culture and kept under constant white light conditions of 30 μmol photons · m-2 · s-1 at 25 °C at an orbital rotational speed of 100 rpm.

For sethoxydim-formulation-treatment experiments, cells were dosed with Bonide Grass Beater with Poast Plus (Bonide Products, Inc., Oriskany, NY) at 36 h to establish a working concentration of 0.08% (v/v) within cultures. Control cultures were dosed with an equal volume of Jasco mineral spirits (W.M. Barr, Memphis, TN), the solvent used in suspending the formulation.[146]

Spectroscopic cell density

Cell density (turbidity) was obtained using a Shimadzu UV-1800 spectrophotometer (Shimadzu Corp., Kyoto, JP) at 750 nm as previously described.[76]

Pigment extraction

Pigments were extracted as previously described and measured from 470 to 700 nm. Chlorophyll *a,* Chlorophyll *b* (Chl *b),* and total carotenoids were calculated using the following equations:[76, 147]

$[\text{Chl } a] = (12.47 \times \text{Abs}_{665.1}) - (3.62 \times \text{Abs}_{649.1})$

$[\text{Chl } b] = (25.06 \times \text{Abs}_{649.1}) - (6.5 \times \text{Abs}_{665.1})$

$[\text{Carotenoids}] = [\ (1000 \times \text{Abs}_{480}) - (1.29 \times [\text{Chl } a]) - (53.78 \times [\text{Chl } b])\ ] / 220$

Cell viability

Cells were combined at a 1:1 ratio with 2.5% (w/v) erythrosine and counted using a Neubauer improved disposable hemocytometer (Electron Microscopy Sciences, Hatfield, PA) with a VWR VistaVision light microscope at 1000x magnification. Non-viable cells were stained pink while viable cells remained the characteristic *Chlorella sp.* green.[148] Cell counts used the average of four 2.5×10^{-7} mL squares, adjusted for dilution. Measurement was conducted in triplicate for all cultures.

Cell dry weight measurement

Dry mass was measured using 1 mL of cells per filter rather than 0.5 mL as previously reported.[76]

Lipid extraction and lipid dry weight analysis

Lipid extractions were performed using a modified methyl *tert*-butyl ether extraction similar to the method published by Matyash et al. (2008).[149] Two 1-mL samples were pelleted and the supernate discarded. Cell pellets were lysed with 1 mL of methanol and incubated in a 9-mL tube with 6 mL of methyl *tert*-butyl ether for 1 h before adding 1.5 mL of ultrapure H_2O and incubating for another 15 min. Suspensions were centrifuged for 15 min at 10,000 x*g* and the organic layer was removed by a Pasteur pipette into a pre-weighed 4-cm tube and dried under constant airflow. The extraction was done twice to ensure close to complete recovery of lipid mass. Tubes were weighed on a Secura 125-1S analytical balance (Sartorius, Göttingen, DE).

Carbohydrate quantification

Carbohydrates were quantified using the acid-phenol test.[150] In brief, 100 µL of sample was collected in triplicate from each culture and pelleted, discarding the supernate. The pellet was resuspended with 100 µL of ultrapure H_2O before adding 500 µL concentrated H_2SO_4 and

vortexing. After a 15-min incubation at room temperature, 100 μL of 5% (w/v) phenol in ultrapure H_2O was added and vortexed. After 15 min, 600 μL of ultrapure H_2O was added and thoroughly vortexed before finding the absorbance of each sample at 490 nm using a Shimadzu UV-1800 spectrophotometer. Calibration curves were prepared daily using a freshly prepared 0.05 mg/mL D-glucose stock solution.

Protein extraction and quantification

Protein quantification followed the method of Lowry et al. (1951) as modified by Price (1965).[151-152] A stock of Lowry Reagent D was prepared daily in a 48:1:1 ratio of Lowry Reagents A (2% w/v Na_2CO_3 in 0.1N NaOH), B (1% w/v NaK Tartrate), and C (0.5% w/v $CuSO_4 \cdot 5H_2O$). The Folin-Ciocalteu reagent was prepared daily with a 1:1 ratio of ultrapure H_2O. To quantify the protein in the cell medium, 50 μL of culture medium was added to individual microcentrifuge tubes in triplicate followed by 950 μL Lowry Reagent D and immediate vortexing. Samples were then incubated for 10 min at room temperature before adding 0.1 mL of diluted Folin-Ciocalteu reagent and vortexing again. The samples were incubated 30 min at room temperature and the absorbance of each sample was measured at 600 nm using a Shimadzu UV-1800 spectrophotometer. Calibration curves were prepared daily using a 2-mg/mL bovine serum albumin stock solution.

For intracellular protein quantification, proteins were extracted from cells following the method of Slocombe *et al.* (2013).[153]

Oxygen evolution *in vivo*

Photosynthetic oxygen production was measured using a Clark-type electrode (Hansatech, UK) at 18 °C. Oxygen measurements were conducted by exposing 200 μL of cell suspension to a 1700-μmol photons $\cdot$ m^{-2} $\cdot$ s^{-1} white light after a 5-min dark adaptation phase.

High light intensity was chosen in order to ensure light saturation of photosystem II—the initial rate of oxygen production was measured, normalized to Chl *a* and used for comparison.

Chlorophyll fluorescence induction *in vivo*

Photosynthetic electron transfer was inferred from Chl *a* fluorescence using a Photon Systems Instruments FL 3500 fluorometer. Cuvettes were loaded with 3 mL of clean (non-herbicide exposed) modified Chlorella cell medium before adding 60 μL of algal cell suspension and dark-adapting it for 5 min. Measurements were conducted at room temperature. Fluorescence data was collected using FluorWin connected to the Photon Systems Instrument. The OJIP protocol included a 1-s actinic illumination using 630-nm light at an intensity of 2,400 μmol photons m^{-2} s^{-1}. Fluorometry parameters were calculated as outlined by Stirbet et al. (2018) and Chen and Cheng (2009).[154-155] For a comprehensive review, including mathematical derivations and conflicting interpretations, see Strasser et al. (2004), Stirbet and Govindjee (2011), Kalaji et al. (2014), and Kalaji et al. (2017).[156-159]

Photosystem II-enriched membrane preparation

Photosystem II-enriched membranes from *Spinacia oleracea* were prepared as described previously.[160-161]

SDS-PAGE electrophoresis and immunoblotting

The effect of Poast on PsbO, the largest extrinsic protein of PSII, was observed by exposing PSII-enriched membranes of *S. oleracea* to it or to mineral spirits (for controls) for 5 min. PSII-enriched membranes have been widely used as a model system to test the effects of various inhibitors and other compounds that directly or indirectly target the many components of PSII. Following this treatment, PSII-enriched membranes were centrifuged at 3,000 x*g* for 5 min and resuspended in K3 buffer (50 mM MES, 35 mM NaCl, 0.3 M sucrose). For electrophoresis,

0.60 µg of protein was added to each lane of a 12% SDS-acrylamide gel and run for 1.5 h at 15

mA using a Biorad mini-PROTEAN Tetra cell chamber. Following electrophoresis, the gel was

transferred using wet-transfer onto nitrocellulose at a constant voltage of 100 V for 1 h, followed

by three 5-min washes with 5% nonfat milk buffer.[162] The membrane was incubated overnight at

4 °C with a 1:5,000 dilution of polyclonal PsbO antibody (Agrisera, Vännäs, SE) in blocking

buffer. Following incubation, the membrane had three 5-min washes with tris-buffered saline

with Tween (TBS-T) before incubating for 1 h with a 1:2,500 dilution of donkey anti-rabbit

secondary antibody (SouthernBiotech, Birmingham, AL). After three 5-min washes with TBS-T,

the membrane was exposed to enhanced chemiluminescent developer (Fisher Scientific) for 10

min before imaging using a FluorChemE (Cell Biosciences, Heidelberg, Vic., AU). FIJI software

was used for blot image analysis.[163]

Statistical analysis

Fluorometry data was analyzed through one-way repeated measures analysis of variance

(ANOVA) conducted with SPSS. To correct for possible violations of sphericity the

Greenhouse-Geisser correction was used. When $p \leq 0.05$, paired t-tests between the control and

the treated time points were conducted. The Holm-Bonferroni method was used to maintain the

family-wise error rate below 0.05 for each fluorometry parameter.

The remaining data was analyzed through multiple comparisons of means conducted

using Welch's t-tests. The family-wise error rate for each figure was maintained at 0.05 through

the use of the Holm-Bonferroni method, unless stated otherwise. Due to the conservative nature

of the Holm-Bonferroni method, p values ≤ 0.05 were reported to allow for open interpretation.

Results

Cultivation of *Chlorella vulgaris* under herbicide exposure

Comparison of cell growth with and without the addition of the herbicide was carried out

in 50-mL Erlenmeyer flasks. Up until 36 h, the control and herbicide-treated cultures showed

nearly identical growth with no statistical differences, as was expected (Figure 8). This growth
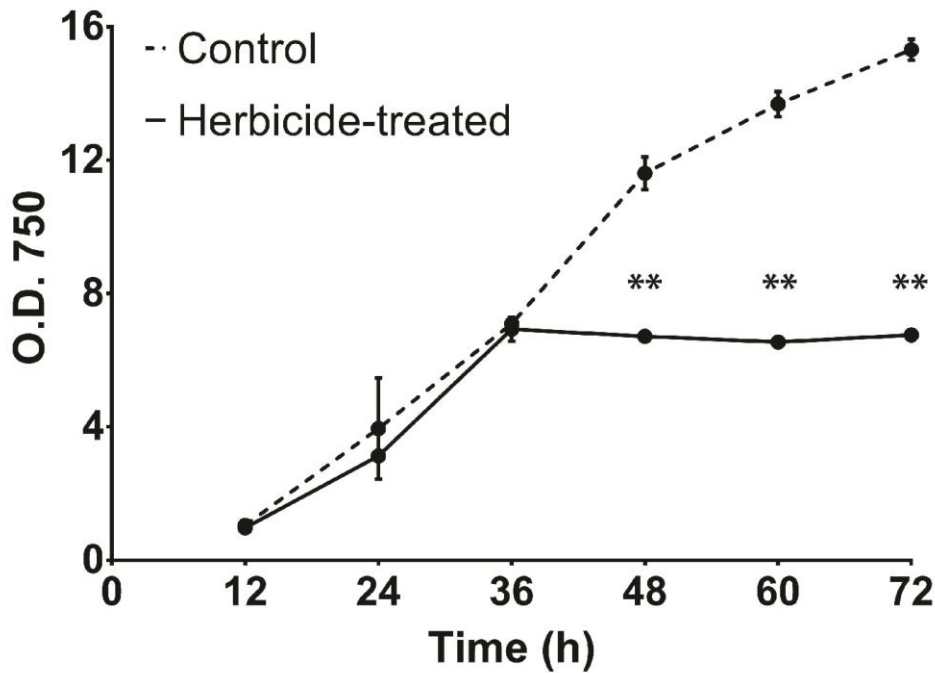
Figure 8. The optical density of algal cultures was measured every 12 h at 750 nm. **
indicates a statistically significant difference between control and herbicide-treated group
means at that specific time point, determined via the Holm-Bonferroni method. * indicates p≤
0.05 between control and herbicide-treated group means at that specific time point but no
statistical significance using the Holm-Bonferroni method. Error bars indicate standard
deviation of the measurement.

pattern matches our previously published results of heteromixotrophic cultures.[76] After being

treated at 36 h by mineral spirits (control) and herbicide, the growth curves no longer match. The
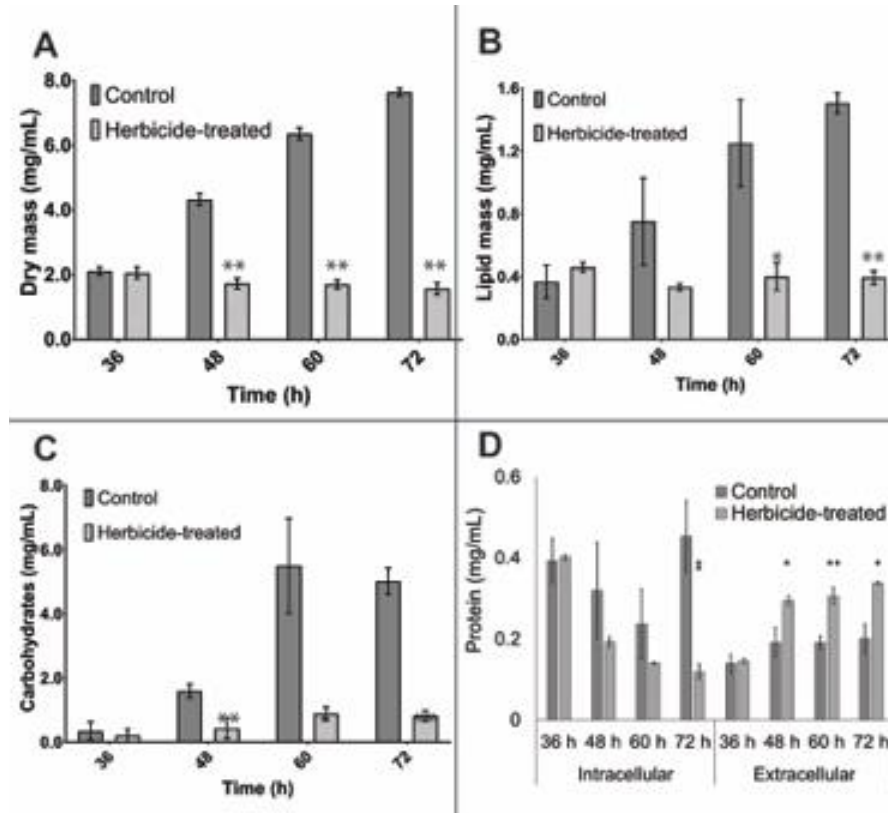
Figure 9. The composition of sethoxydim exposed and control cultures. (**A**) The algal dry mass was measured every 12 h beginning at 36 h, with the first measurement taking place prior to mineral spirits (control) and herbicide-treated dosage. (**B**) The lipid mass of algal cultures was measured gravimetrically every 12 h beginning at 36 h, with the first measurement taking place prior to mineral spirits (control) and herbicide dosage. The algae was exposed to mineral spirits and herbicide following the 36 h measurement. (**C**) The intracellular accumulation of carbohydrates was measured every 12 h beginning at 36 h using the acid-phenol method. The algae was exposed to mineral spirits (control) and herbicide following the 36 h measurement. (**D**) Intracellular and extracellular protein were measured every 12 h beginning at 36 h using the Lowry assay. For A – C, ** indicates a statistically significant difference between the control and herbicide-treated group means at that specific time point, determined via the Holm-Bonferroni method. * indicates $p \leq 0.05$ between control and herbicide-treated means at that specific time point but no statistical significance using the Holm-Bonferroni method. For D, * are used to designate statistical significance for the extracellular fraction while ‡ are used to designate statistical significance for the intracellular fraction. **/‡‡ indicates a statistically significant difference between control and herbicide-treated group means of the designated fraction at that specific time point, determined via the Holm-Bonferroni method. */‡ indicates $p \leq 0.05$ between control and herbicide-treated group means of the designated fraction at that specific time point but no statistical significance using the Holm-Bonferroni method. Error bars in all panels indicate standard deviation of the measurement.

control culture continues its exponential growth, slowing down as it approaches stationary phase

44

at 72 h. The herbicide-treated culture, however, appears to immediately enter stationary phase from exponential phase, or some form of stasis, with a 3% drop in optical cell density in the first 12 h of inhibition that remains steady throughout the experiment up to 72 h (36 h post-inhibition).

While the changes in optical density and dry mass appear to be the same, detailed inspection of the herbicide-treated cells reveals that the dry mass decrease is larger in magnitude than the decrease in optical density (Figure 9 (A)). At 36 h, there is no statistical difference between the control and the herbicide-treated cultures when measuring dry mass or turbidity. Continuing to 48 h, the control dry mass increases by 52%, while the herbicide-treated culture drops by 15%. At 72 h, the control group reaches its maximum mass of 7.64 mg $\cdot$ mL^{-1}, while the herbicide-treated group ends at 1.58 mg $\cdot$ mL^{-1}, a 23% decrease from the pre-inhibition point. Therefore, while the control group has a Pearson coefficient denoting linear correlation between O.D.$_{750}$ and dry mass as previously reported (R = 0.98467), this correlation is absent in the herbicide-treated group post-dosage (R = 0.65863), indicating that while cellular content has decreased, overall cell number has likely remained steady.[76] This was confirmed via cell counting, where herbicide-treated cell numbers stayed constant within error after dosing.

Pigment accumulation and chlorosis

Pigments were extracted and recorded every 12 h. The accumulation of Chl *a* is of particular interest as it loosely correlates with photosynthetic activity. Up until 36 h, the control and herbicide-treated cultures exhibit nearly identical concentration of Chl *a* (~30 µg $\cdot$ mL^{-1}) with no statistically significant difference, as expected from the turbidity results (Figure 10). Following dosage at 36 h, the control group reaches a plateau within 12 h, matching previously published results that show chlorophyll slowing in accumulation before turbidity enters the final

45
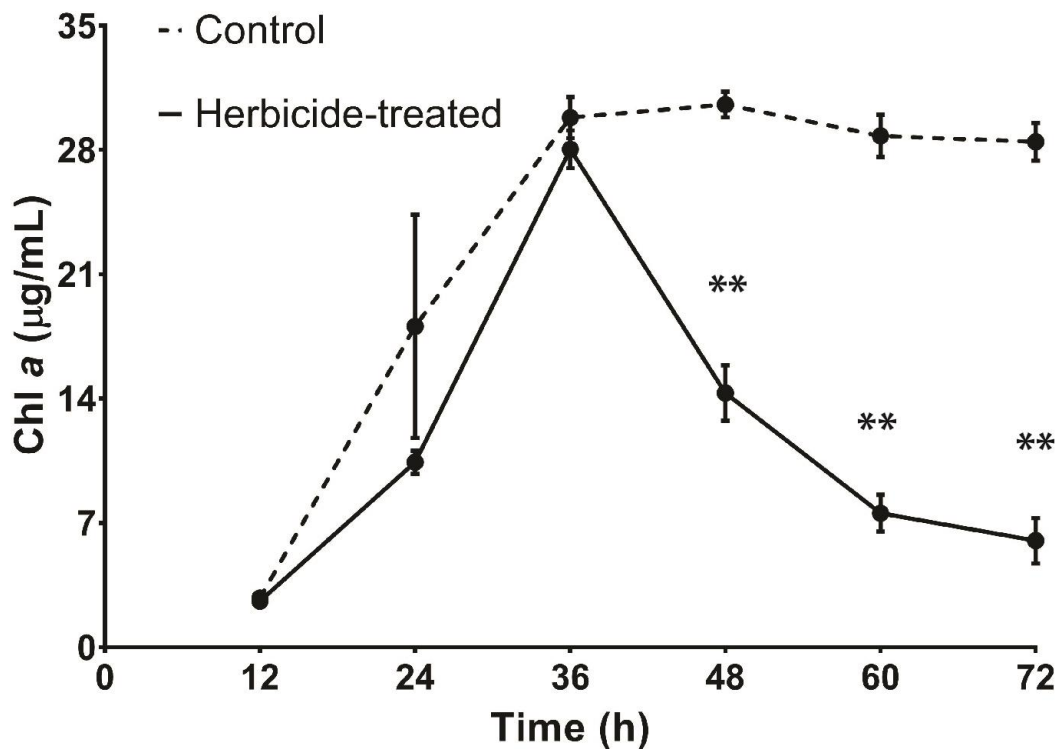
Figure 10. Chl a was extracted and measured at 649.1 nm and 665.1 nm every 12 h. ** indicates a statistically significant difference between control and herbicide-treated group means at that specific time point, determined via the Holm-Bonferroni method. * indicates $p \leq 0.05$ between control and herbicide-treated group means at that specific time point but no statistical significance using the Holm-Bonferroni method. Error bars indicate standard deviation of the measurement.

stationary phase.[76] The herbicide-treated group, however, experiences dramatic chlorosis in the first 12 h of inhibition, equating to a 49% drop in Chl *a* by 48 h. This chlorosis continues until it reaches 6.0 µg · mL^{-1}, a 79% decrease post-inhibition. Carotenoids and Chl *b* follow the same trend, experiencing chlorosis immediately after dosing and remaining near 1 and 2 µg · mL^{-1} at 72 h, respectively (data not shown).

Cell viability

Cell viability was initially assessed at 12 h post inhibition, at which point all cells were non-viable (data not shown). To better understand the rate of cell death, cell viability was assessed 15 min before inhibition, immediately after adding the herbicide formulation, 15 min

46

after inhibition, and 30 min after inhibition. The 15 min pre-inhibition and immediately after

adding the herbicide appear to be consistent and have values within error, with 2.38 x 10^8 and

2.17 x 10^8 cells, respectively. These time points showed 100% viability of cells, with no pink

cells detected under 1000x magnification. 15 min later, however, the cells were only 45% viable,

followed by 12% at 30 min post-inhibition. By 1 h post-inhibition, there were no visible viable

cells. In addition, exposing *C. vulgaris* to 0.08% sethoxydim in mineral spirits alone showed no

effect as determined by a cell viability assay 30-min post-exposure (data not shown).

Lipid, protein, and carbohydrate analysis of cells exposed to herbicide

To assess the intracellular metabolic changes occurring within the cells after herbicide

exposure, lipid, carbohydrate, and protein accumulations were assessed at 36, 48, and 72 h. The

lipid mass, assessed gravimetrically using the method of Matyash et al. (2008), mirrors the dry

mass and optical density (Figure 9(B)).[149] At 36 h, the control and herbicide-treated groups had a

lipid mass of 0.37 and 0.46 mg · mL^{-1}, respectively, equating to approximately 17% of their

cultures' total mass. As expected, the control cultures continue to accumulate lipids, ending at

1.51 mg/mL, accounting for about 25% of the culture's total mass. This data fits with previous

study's early-stationary phase lipid data. The herbicide-treated cultures' lipid accumulation

follows the trend shown by optical density, in which it decreases by 28% over the first 12 h post-

dosage and then remains constant until ending with 0.39 mg · mL^{-1} at 72 h.

The intracellular carbohydrates of the herbicide-treated group show a significant

difference from the control at 48 h and 72 h (Figure 9(C)). At 60 h, the Holm-Bonferroni

analysis shows a lack of statistical significance, although Welch's t-test produces a p-value of

0.025, indicating significance before the more conservative Holm-Bonferroni correction.

However, unlike the dry mass and O.D.$_{750}$ data, the intracellular carbohydrates appear to increase

in concentration until 60 h, after which it remains constant. While it is possible the cells are metabolizing other biochemical components to form carbohydrates, this seems unlikely. It is more likely the intracellular carbohydrates are an artifact of a permeable cellular wall and membrane, as assessed through the cell viability assay.

As the needs of cells change, the expression of their proteome changes as well. This is experimentally indicated through the changing protein concentration of the control cultures, which decreases from 36 to 60 h before undergoing a sharp increase at 72 h (Figure 9 (D)). The herbicide-treated samples follow a similar pattern as the control with an initial 51% drop 12 h post-inhibition. Simultaneously, the herbicide-treated cultures have an increase in extracellular protein statistically different from the control, a statistical difference present throughout the remaining growth cycle. Ultimately, the herbicide-treated cultures end with 0.34 mg of protein · mL^{-1} of culture located extracellularly (Figure 9(D)). When paired with the loss of intracellular protein, this indicates that 68% of the intracellular protein lost from the herbicide-treated cultures between 36 and 72 h can be accounted for extracellularly. When normalized to cytosolic concentration (using cell counts and an average cellular diameter of 5 µm), the intracellular protein in the herbicide-treated cultures decreases from 73.7 mg/mL intracellular protein to 35.4 mg/mL intracellular protein. During this time, the extracellular protein has an increase of 27.3 mg/mL, showing that 71% of the intracellular protein loss can be accounted for extracellularly after 12 h of herbicide exposure. At the terminal time point, the intracellular protein decreases to 21.8 mg/mL, while the extracellular increases to 35.2 mg/mL, showing that 68% of the total protein loss ultimately ends up in the extracellular medium.

From 36 to 72 h, the herbicide-treated cultures decrease in dry mass by 23% (Figure

9(A)). Using the difference in biochemical components from 36 to 72 h, the largest component

comes from protein loss, making up 59% of the lost dry mass; following protein comes lipids

with 15% and pigments with 6% (Figure 11). This leaves 20% of the dry mass loss unaccounted

for. It would be beneficial for future experiments to use liquid chromatography mass
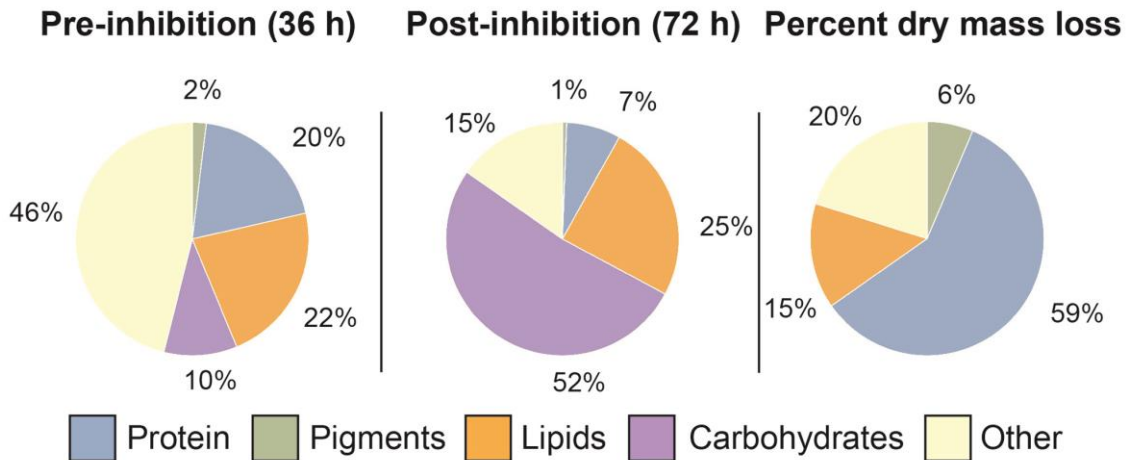
Figure 11. The compositions of pre and post inhibition cultures. (From left) The pre-exposure cellular composition, the post-exposure cellular composition, and the percent of dry mass lost through loss of macromolecules.

spectrometry to determine the change in intracellular metabolites before and after herbicide

exposure.

Photosynthetic capacity measured using *in vivo* oxygen evolution and chlorophyll fluorescence induction

In order to establish the photosynthetic changes accompanying herbicide exposure,

oxygen evolution was measured using a Clark-type electrode. Prior to adding the Poast, the algae

produced 241 μmol $O_2 \cdot$ (mg Chl *a*)$^{-1} \cdot$ h^{-1} (Figure 12(A)). After adding the Poast, however, this

decreased to 67.8 μmol at the first time point following exposure (5 min and 15 s after exposure,

the quickest time point available due to the necessity of transfer to the chamber and the 5 min
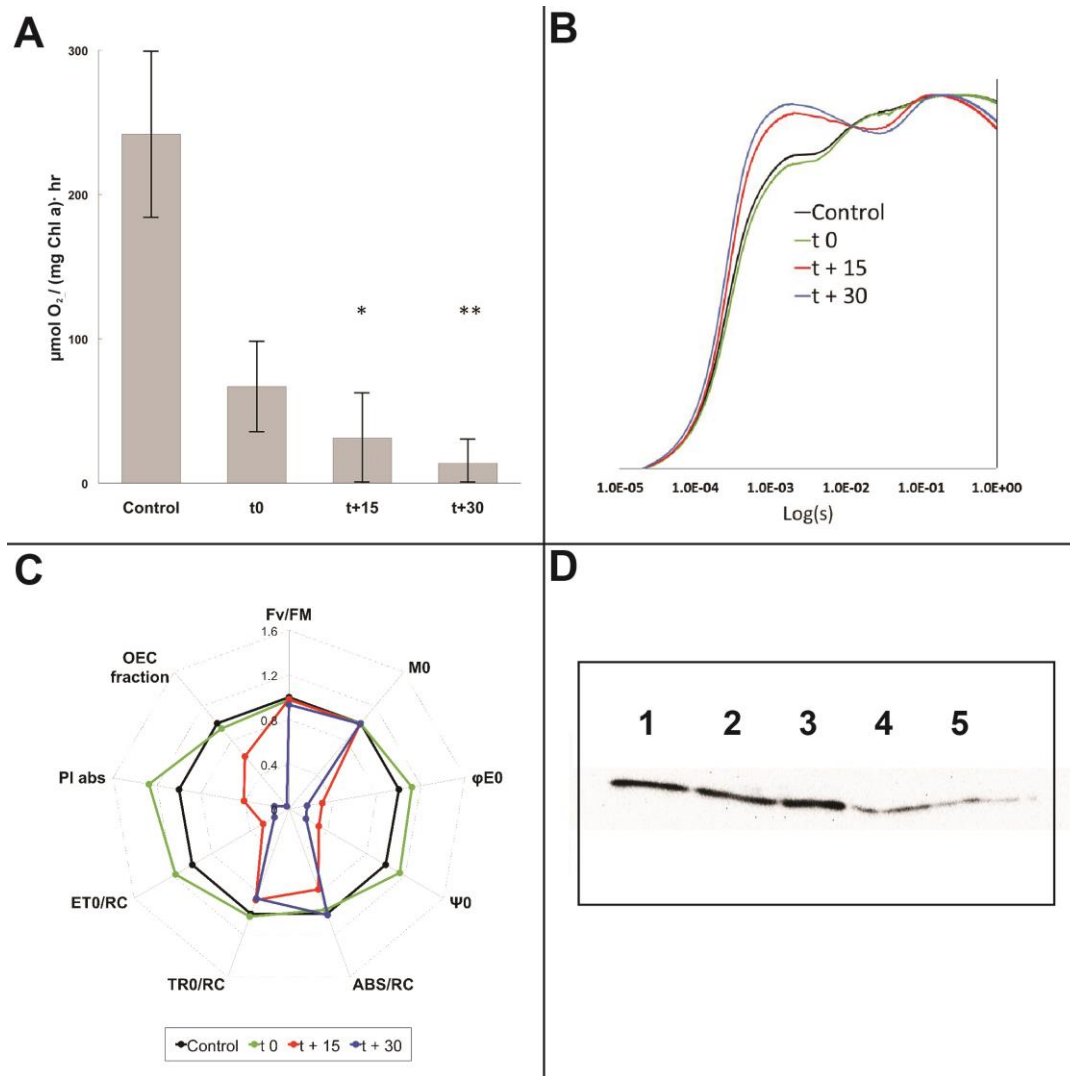
Figure 12. Photosynthetic measurements of sethoxydim exposed cells. (**A**) The oxygen production of algal cultures exposed to herbicide was measured following a 5-min dark adaptation in μmol O_2 / (mg Chl *a*)· hr. The control was measured 15 min prior to herbicide dosing and the following measurements were taken immediately after dosage and dark adaptation (t 0), 15 min post-dosage and dark adaptation (t + 15), and 30 min post-dosage and dark adaptation (t + 30). Error bars indicate standard deviation of the measurement. (**B**) The chlorophyll *a* transient (OJIP curves) of algae exposed to herbicide, beginning at t 0. The control was measured 15 min prior to herbicide dosing and the following measurements were taken immediately after dosage and dark adaptation (t 0), 15 min post-dosage and dark adaptation (t + 15), and 30 min post-dosage and dark adaptation (t + 30). Transients are double normalized where $F_t = [F_t-F_0]/F_v$. (**C**) Parameters derived from fluorescence transients, normalized where control = 1. (**D**) Immunoblot of enriched PSII particles exposed to mineral spirits (control) and herbicide for 5 min. Signal shows PsbO, a protective extrinsic protein in the thylakoid lumen. Lane 1: No treatment, Lane 2-3: Mineral spirit treatment, Lanes 4-5: Poast treatment.

dark adaptation), which lowered again to 31.5 and 13.8 μmol O_2 · (mg Chl *a*)$^{-1}$ · h^{-1} at 15 min and

30 min following exposure, respectively. This indicates that oxygen production decreases by

50

94.3% in the first 30 min of exposure, demonstrating major damage to the photosynthetic apparatus. This was also confirmed using PSII-enriched membranes from *S. oleracea*, although these stopped all oxygen production at the first time point following exposure, likely because of the easier accessibility to the disrupted thylakoid membranes. PSII-enriched membranes also experienced no change in oxygen production when exposed to mineral spirits, analytical grade sethoxydim suspended in mineral spirits, naphthalene, or 20% (v/v) triton-X, all components believed to be in the Poast herbicide formulation (data not shown).[146]

The OJIP fluorescent transient was used to assay the integrity of PSII in vivo. Using this method, the kinetics of PSII are inferred, specifically the reduction of Q_A and Q_B, thus showing the availability of reaction centers to utilize photons for photochemical processes rather than thermochemical processes or fluorescence. Using the log-based plot, it is possible to view the OJIP curve, also known as a Kautsky induction, where the O-step represents F_0, or minimal fluorescence and the point at which all reaction centers are open, and the P-step represents F_M, or maximal fluorescence and the point at which all reaction centers are closed.[157] This OJIP curve in the first time point of the herbicide-treated cultures appears to have a heightened J-step (while this step is usually 60% of total fluorescence intensity, the curve generated has about 80% fluorescence intensity at the J-step), which instead likely stems from using an asynchronous culture grown in constant light (Figure 12(B)). However, since the cells were grown in identical conditions, the OJIP curve could be used effectively to compare the changes in photosynthetic activity caused by Poast exposure. Immediately after herbicide exposure (taken at 5.25 min post-exposure due to the necessity of transfer and dark adaptation), there is a slight decrease in intensity of the O-J and J-I phases, indicating a decrease in the maximum photosynthetic quantum yield. While this intensity increases after 15 min, the curve also breaks from the OJIP

51

pattern, with a prominent change near the J-step making it impossible to differentiate the J-I phase from the transient.

While the relative intensities of the OJIP curves allow visual comparisons of electron flux over time, Strasser's JIP test, using the raw data rather than the normalized curves, allows a better idea of electron flux of the steps in electron transport beginning in PSII and ending in PSI (Figure 12(C)).[164] F_v/F_M is the most frequently used parameter and represents the maximum quantum yield of PSII photochemistry for a dark-adapted state. After herbicide exposure, it showed a 7% decrease in overall quantum yield, which, although small, was shown to be statistically significant ($F(1.578, 3.516) = 84.15$, $p = 0.002$). Additionally, the Abs/RC, the absorption flux per reaction center, remains similarly unchanged, but with no statistically significant difference at any time point. Meanwhile, several parameters show a significant difference after herbicide exposure, including ET_0/RC- showing the electron transport flux leading to a reduction of electron carriers beyond Q_A, Ψ_0 – indicating the probability that a trapped exciton is used for electron transport beyond Q_A, φ_{E0} – revealing the quantum yield of the electron transport beyond Q_A, and PI_{abs} –the performance index on an absorption basis, all of which decreased by over 80% following 30 min of herbicide exposure.

Immunoblot of PsbO following herbicide exposure

The change in the pattern of the OJIP curve could indicate damage to PSII. To gauge the potential damage occurring at the site of the oxygen evolution complex (OEC), PSII-enriched membranes of *S. oleracea* were exposed to the herbicide formulation before probing for the 33 kDa extrinsic protein, PsbO, which functions as a protective barrier around the OEC and is used as an indicator as to whether or not OEC-depleted PSII has been created (Figure 12(D)).[165] After

5 min of Poast exposure, analysis showed a decrease of 64% of PsbO when compared to the control.

Discussion

Herbicide exposure compromises the cell wall and membrane

Biochemical changes to *C. vulgaris* were monitored following the addition of Poast, a sethoxydim-containing herbicide, to a working concentration of 0.08% (v/v). After 15 min of exposure, 55% of cells were non-viable, as shown through an erythrosine dye test. This increases to 88% 30 min after exposure and is accompanied by complete stasis in cell growth monitored via O.D.$_{750}$ (Figure 8). Although breaks in the cell wall and membrane are observed after 15 min (indicated through the pink coloration of the erythrosine cell viability assay), the distinguishable breakdown of macromolecules takes considerably longer. As a supplemental experiment, the rate of Chl *a* chlorosis was monitored following herbicide exposure for 12 h. While the Chl *a* of these cultures decreased approximately 43% by the 12 h point, it took 4 h before there was a distinguishable difference between the control and herbicide-treated samples. Therefore, while the herbicide was toxic enough to disrupt the cell wall and membrane, it was not able to fully induce degradation of the light harvesting antennas of PS I and II for several hours. This is likely occurring via the uncoupling of LHCs from PSI and PSII, but will require measurements from a 77 K fluorometer to confirm.[166]

The above conclusion is supported by the protein data, which demonstrates that while there is a decrease in intracellular protein after 12 h, much of this decrease can be accounted for by the increase in protein found in the extracellular medium, contributing evidence that the cells are extruding or leaking their contents as a result of cell wall damage rather than completely degrading their macromolecules (Figure 9(D)). However, the decrease in intracellular protein is

not accounted for by extracellular proteins; however, when considered in the context of chlorosis, it suggests intracellular enzymatic degradation may be occurring simultaneously. These data, in addition to the separation between membrane and cell wall seen via light microscope, support the existence of programmed cell death occurring, as characterized with *Chlorella saccharophila* under heat stress.[167] Therefore, while the herbicide treatment causes cell wall and membrane degradation within 15 min, it is possible that the treatment also initiates programmed cell death. Further experiments are needed to study the expression of caspase-3 and confirm the activity of the apoptotic pathway.

Herbicide exposure causes irreparable damage to photosynthetic machinery

Photosynthetic activity was monitored via oxygen evolution and the OJIP Chl *a* fluorescence. While it took hours to observe a decrease in pigment accumulation, the change in photosynthetic activity—like the change in cell viability—was more immediate. While the cell viability test did not show changes until 15 min after dosing, the oxygen production decreased by 72% immediately after exposure (Figure 12(A)). Although the immediate post-exposure point in oxygen evolution represents 5.25 min post exposure (due to the need for transfer and dark adaptation), it still shows how quickly damage begins to accumulate in the cell.

Using the Chl *a* fluorescence transient, we were able to gather information as to the location of damage within PSII. Since the ABS/RC remains unchanged, meaning the effective antenna size of the reaction centers are unchanged, it is unlikely that the architecture of the light harvesting antennas have changed (a smaller antenna would have a smaller absorption capacity per reaction center, thus causing ABS/RC to decrease).[168] While F_v/F_M is used to indicate photosynthetic efficiency, it is more accurately a quantitative assessment of the overall availability of open reaction centers, as it indicates the yield of the reduction of plastoquinone at

Q_A. When combined with information on changes in rates of oxygen evolution, it appears that the damage to the photosynthetic apparatus is only at the site of the OEC. Additionally, parameters (ET_0/RC, Ψ_0, φ_{E0}, and PI_{abs}) showing the sharpest decrease are all related to the transfer of electrons beyond PSII, all of which show a statistically significant difference beginning at 15 min post-dosage (Figure 12(C)). These decreases, combined with the decrease in oxygen evolution, suggest that the damage to PSII is at the OEC. This is further supported by the changing shape of the OJIP transient curve upon exposure to Poast: the near maximum fluorescence occurring near 1.45 ms, just before where the J-step should be (2 ms), is indicative of the a delayed J-step. The delayed J-step indicates damage to the OEC as modeled by Lazár et al (1997).[135] Just after the J-step, there is a characteristic dip in fluorescence indicating the oxidation of the quinone pool on the acceptor side, further indicating damage to the OEC (Figure 12(B)).[155, 158, 164, 169] Additionally, there were significant differences in the calculated active OEC fraction, indicating that the percent active OECs (as compared to the before herbicide dosage measurement) dramatically decrease by 30 min of herbicide exposure.

The loss of PsbO confirmed via immunoblotting of PSII-enriched membranes following 5 min of herbicide exposure, in addition to the fluorescence data indicating a loss in OEC function, suggests a component of the herbicide is interfering with the interactions between the extrinsic and integral protein system. Since PSII is located within the grana stacks of the thylakoid membranes in the chloroplast, the near immediate decrease in oxygen evolution suggests the damaging component(s) of the Poast formulation is capable of permeating through membranes rapidly, making it a potentially catastrophic environmental toxin. However, it does not appear to be the active ingredient alone doing the damage: when PSII-enriched membranes of *S. oleracea* were exposed to sethoxydim suspended in mineral spirits, there was not a

significant change in oxygen production (control: 79.53 µmol O_2 mg chl a^{-1} hr^{-1} ± 5.43;

sethoxydim exposed: 69.63 µmol O_2 mg chl a^{-1} hr^{-1} ± 8.50). In addition, exposure of *C. vulgaris*

cultures to a 293-µM working concentration sethoxydim (in mineral spirits) resulted in no

change in cell viability at 30 min post-exposure. The same result was observed when the PSII-

enriched membranes were exposed to naphthalene (122.34 µmol O_2 mg chl a^{-1} hr^{-1} ± 23.70) ,

another component in the herbicide indicated on the Poast MSDS (Bonide Products 2011), as

well as a solution of 20% (v/v) Tween 20 (Fisher Scientific; 77.87 µmol O_2 mg chl a^{-1} hr^{-1} ±

6.09), a polyethylene glycol similar to those used in industrial herbicides.[170] Therefore, it appears

as though one of two scenarios is occurring: either there is a combinatory effect between the

chemicals within the herbicide formulation causing it to be more toxic than intended, or one of

the proprietary ingredients within the formulation is the cause of the damage. Without the full list

of chemicals within the formulation, we are unable to identify the damaging agent(s).

The rapid permeability through membranes, combined with the near instant damage to

the photosynthetic apparatus, makes high concentrations of Poast particularly harmful to

unicellular (and possibly multicellular) phototrophs, a non-target organism for this herbicide.

Therefore, if Poast was subjected to runoff or spilled into a waterway, it may cause a great deal

of damage to the phototrophic community, including the ability to prevent the oxygenation of the

waterway, an event that would negatively affect higher-order organisms that rely on phototrophs

for aquatic oxygen.

CHAPTER 4

CHLORELLA VULGARIS BIOACCUMULATES EXCESS MANGANESE UP TO 55X UNDER PHOTOMIXOTROPHIC CONDITIONS

Department of Chemistry, Marshall University, 1 John Marshall Drive, Huntington, WV, 25755, United States

*Corresponding author

Manganese is a transition metal that can accumulate in waterways in concentrations above natural abundance due to the mining, metallurgy, and agricultural industries. While manganese is an essential mineral for plants and all other life, excess exposure causes a variety of health issues for vertebrates and invertebrates—in humans, this includes impotence, decreased cardiac function, and manganism, a neuropathological condition similar to Parkinson's disease. While chemical technologies for manganese removal are abundantly available, the high solubility of manganese in aqueous solutions causes steep decreases in removal efficiency and generates hazard waste that can be problematic to store. *Chlorella vulgaris*, a robust, unicellular green alga, offers an environmentally friendly alternative to chemical methods with the added

economic potential of generating value-added products. In this study, *C. vulgaris* was exposed to increasing concentrations of manganese and monitored for bioaccumulation and adsorption. Additionally, cells were monitored for biochemical changes by assaying for terminal biochemical composition and determining photosynthetic activity throughout the life cycle of the culture. Evidence suggests that *C. vulgaris* can bioaccumulate manganese to an intracellular concentration of 733.3 mM and remove up to 56.74 % of the manganese from highly concentrated media through both intracellular bioaccumulation and membrane-bound adsorption. Interestingly, the cultures exposed to high concentrations were able to accumulate manganese up to 55x the external concentration without experiencing inhibitory effects resulting from metal toxicity. Furthermore, cultures exposed to increased manganese displayed higher amounts of protein biosynthesis and an increase in photosynthetic capacities, potentially related to structural changes in the light harvesting antenna complexes of photosystem II.

Introduction

Manganese is a naturally abundant transition metal with two oxidation states that are soluble in water, Mn(II) and Mn(VII).[171] While not common in its elemental form, it is a component of over 100 minerals, most notably MnO_2, $MnCO_3$, and $MnSiO_3$, and is most commonly found in its divalent state.[172] Manganese accumulates in waterways, ground water, and surface water in concentrations above natural abundance due to industrial steel production and manufacturing,[173] mining and smelting,[174] and agricultural processes, specifically the use of pesticides.[175] While manganese is an essential micronutrient for humans for its role in bone mineralization, cellular protection, enzymatic processes, and metabolic regulation, excessive exposure causes manganism, a neuropathological condition similar to Parkinson's disease.[176]

Furthermore, manganese overexposure has been shown to cause impotence,[177] changes in cardiac function,[178-179] infant mortality,[180-181] and other life threatening diseases.[182]

There are a variety of chemical methods through which to remove manganese from aqueous solutions including chemical precipitation,[183-189] flotation, [190-192] ion exchange, [184, 193-194] oxidation, [188, 195-196] filtration,[184, 195, 197-198] and adsorption,[199-202] among others. [171] However, even the most economic methods are hindered by the high stability of manganese in solution, requiring large investments to effectively remove, resulting in excessive volumes of hazardous waste that are difficult and environmentally problematic to store.[203] Phytoremediation offers an alternative solution that is cost-effective, environmentally friendly, solar-driven and, through the generation of value-added products, economically fortuitous.[204-208]

Chlorella vulgaris is a unicellular green alga with a rapid growth rate and natural resistance to harsh conditions including nutrient limitation, excessive or deficient light availability, and fluctuating temperatures.[75, 131, 209-211] Additionally, *C. vulgaris* has been shown to accumulate or adsorb a variety of bio-available environmental contaminants, such as magnesium,[212] lead,[213] antimony, [214] cadmium,[215] uranium,[216] and hexachlorobenzene, [217] among others. However, overexposure to many contaminants, specifically transition and heavy metals, often led to cell toxicity, inhibiting the potential of long-term phytoremediation efforts. [218]

While manganese is toxic in high concentrations to vertebrates, it is a key component of photosynthesis, as the oxygen-evolving complex of photosystem II (PSII) requires four manganese ions for catalytic activity.[59] In order for efficient photoassembly, the process through which free inorganic cofactors combine into the semi-cubane structure known as the oxygen evolution complex, it is necessary to have excess manganese, as spontaneous disassembly and reassembly occur as a protective mechanism against photoinhibition.[219] Therefore, it is likely that

C. vulgaris¸ whose chloroplast makes up approximately 80% of its internal volume, actively transports manganese when available to serve as excess stores for its photosynthetic machinery.[75, 220] To determine the ability of *C. vulgaris* to bioaccumulate manganese and to ascertain its potential for phytoremediation efforts, batch cultures were exposed to increasing concentrations of $MnCl_2$ and monitored via inductively-coupled plasma optical emission spectroscopy (ICP-OES) for both internal and membrane-bound manganese concentrations. To measure toxicity potential, physiological characterization of growth rate, pigment accumulation, and terminal biochemical composition were monitored. Additionally, chlorophyll *a* fluorescence (OJIP) and oximetry were used to monitor photosynthetic capacity throughout manganese exposure.

Materials and Methods

Reagents

D-Glucose, erythrosine, the Folin-Ciocalteu reagent, ICP-grade Mn^{2+}, and 70% analytical grade nitric acid were acquired from Sigma-Aldrich Inc (Dermstadt, DE) and NaOH was purchased from Columbus Chemical Industries (Columbus, WI). The remaining reagents, unless otherwise specified, were obtained through Fisher Scientific (Hampton, NH).

Strain and culture growth conditions

Cultures of *C. vulgaris* (Carolina Biological Supply) were maintained on lysogeny broth agar plates and for batch cultures, inoculated into 25 mL of modified *Chlorella* medium supplemented with 20 g/L dextrose into 50-mL sterile Erlenmeyer flasks capped with aluminum foil.[76] Cultures were grown in quadruplicate, using a 1-mL inoculum from stationary phase culture and kept under constant white light at 30 µmol photons $\cdot$ m^{-2} $\cdot$ s^{-1} at 25 °C at an orbital rotational speed of 100 rpm.

Experimental design

Prior to culture inoculation, manganese-deprived modified *Chlorella* medium was dosed with an autoclaved stock of $MnCl_2$ and ultrapure water, ensuring that all cultures had equal concentrations of all other medium components. The control cultures' media was dosed to generate a working concentration of 0.07 mM manganese, the standard concentration for modified *Chlorella* medium. Experimental cultures' media were raised to 17.5 mM and 35 mM manganese, 250 and 500x the control, respectively. Cultures were maintained until 84 h, at which point they were in stationary phase.

Spectroscopic cell density

Cell density (turbidity) was obtained using a Shimadzu UV-1800 spectrophotometer (Shimadzu Corp., Kyoto, JP) at 750 nm as previously described.[76]

Pigment extraction

Pigments were extracted as previously described and measured from 470 to 700 nm.[76] Chlorophyll *a* (Chl *a*), Chlorophyll *b* (Chl *b*), and total carotenoids were calculated using the following equations:[147]

[Chl *a*] = (12.47 x $Abs_{665.1}$) – (3.62 x $Abs_{649.1}$)

[Chl *b*] = (25.06 x $Abs_{649.1}$) – (6.5 x $Abs_{665.1}$)

[Carotenoids] = **[** (1000 x Abs_{480}) – (1.29 x [Chl *a*]) – (53.78 x [Chl *b*]) **]** / 220

Inductively coupled plasma optical emission spectroscopy

The intracellular and membrane-bound manganese were determined every 24 h using an Agilent Technologies 5110 ICP-OES (Santa Clara, CA). To separate the fractions, 250 µL of cells were pelleted by centrifuging at 13,400 x g for 5 min and removing the supernate. The cells were washed three times with manganese-deprived modified *Chlorella* medium, centrifuging

between each wash. Prior control tests indicated that three washes ensured that all non-bound manganese was removed before analysis. Following the washes, the cell pellet was resuspended in a pH 7 phosphate buffer containing 1 mM EDTA and 10 mM NaCl. After thoroughly vortexing for approximately 30 s, the cells were centrifuged again and the supernate, containing the membrane-bound manganese, was removed and saved for later analysis.[221] The cell pellet, containing the intracellular manganese fraction, was resuspended in 200 µL of ultrapure H_2O before transferring to 6 mL borosilicate tubes containing 2.86 mL of 70% analytical grade HNO_3. Samples were diluted to 100 mL using an acid-washed volumetric flask and syringe filtered into sterile 15-mL conical tubes. The supernate was prepared the same as the intracellular pellet, with the exclusion of adding H_2O and without syringe filtering.

Samples were analyzed at a wavelength of 257.61 nm and viewed under radial mode. The samples had a read time of 10 s. The ICP was set to a nebulizer flow of $0.70 \text{ L} \cdot \text{min}^{-1}$, a plasma flow of $13.0 \text{ L} \cdot \text{min}^{-1}$, and an auxiliary flow of $1.00 \text{ L} \cdot \text{min}^{-1}$. Each measurement was taken three times and blanks were measured after every 4 samples. A 9-point standard curve was prepared daily via serial dilution using ICP-grade manganese standard.

Cell dry weight measurement

Dry mass was measured using 1 mL of cells per filter rather than 0.5 mL as previously reported.[76]

Biochemical composition

Terminal lipid, carbohydrate, and protein concentration were assayed as previously described.[27]

Oxygen evolution *in vivo*

Photosynthetic oxygen production was measured using a Clark-type oxygen electrode (Hansatech) at 25 °C as previously described.[27] Oxygen measurements were conducted by exposing 1:1 diluted cell suspension in modified *Chlorella* media to a 1700-μmol photons$\cdot$ m^{-2} $\cdot$ s^{-1} white light after a 5-min dark adaptation phase. High light intensity was chosen in order to ensure light saturation of PSII —the initial rate of oxygen production was measured, normalized to Chl *a*, and used for comparison across manganese concentrations.

Chlorophyll fluorescence induction *in vivo*

Photosynthetic electron transfer fluxes were inferred from Chl *a* fluorescence using a Photon Systems Instruments FL 3500 fluorometer as previously described.[27] The OJIP protocol included a 1-s actinic illumination using a 630-nm light at an intensity of 2,400 μmole photons m^{-2} $\cdot$ s^{-1}. Fluorometry parameters (JIP test) were calculated as outlined by Stirbet, et al. [222]

Statistical analysis

Statistical analyses were performed with GraphPad Prism 7.01 (GraphPad Software, Inc.). Optical density, pigment, and fluorometry data were analyzed through two-way repeated measures analysis of variance (ANOVA) using a Bonferroni correction to maintain a family-wise error rate below 0.05. The remaining data were analyzed through multiple comparisons of means conducted using Welch's t-tests. The family-wise error rate for each figure was maintained at 0.05 through the use of the Holm-Bonferroni method. Statistical significance is indicated numerically through increasing asterisks, where * indicates $p \leq 0.05$, ** indicates $p \leq 0.01$, *** indicates $p \leq 0.005$, and **** indicates $p \leq 0.001$. Figures show the means of quadruplicate data and the error bars denote the standard error of the measurement.

Results

Cultivation of *C. vulgaris* in the presence of increased manganese

Cells were inoculated into 50-mL Erlenmeyer flasks containing manganese

concentrations of 0.07 mM (control), 17.5 mM, and 35 mM and optical density and pigment

concentration was monitored every 12 h throughout the growth cycle (Figure 13). While subtle,
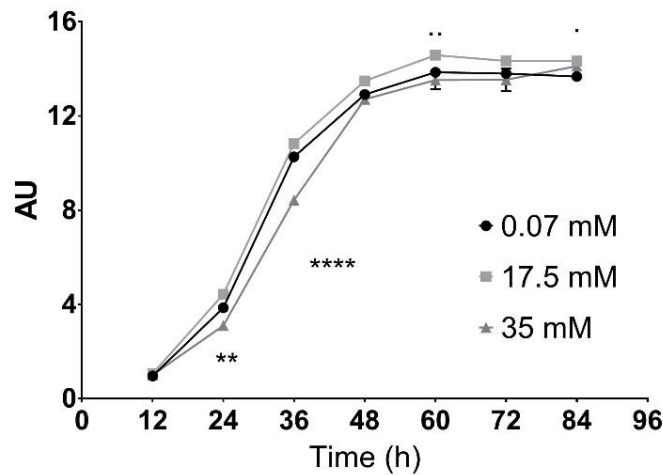
Figure 13. The optical density measured at 750 nm of manganese-exposed cultures taken over time. Error bars represent standard error of the measurement. Asterisks (*) are used to indicate statistically significant differences between the 35 mM cultures and the control while the middle dots (·) are used to indicate statistically significant differences between the 17.5 mM cultures and the control. Further information on statistical analysis can be found in the materials and methods section.

the 35 mM cultures experience a slightly elongated lag phase, with statistically significant

decreases in optical density compared to the control at 24 and 36 h. However, following the 36 h

measurement, the 35 mM cultures have a higher rate of cell division than the control (measured

through the slope of the line between the 36 and 48 h time points), resulting in a near identical

optical density beginning at 48 h and continuing through stationary phase, with no significant

differences when compared to the control. This extended lag phase was more pronounced with

higher concentrations of manganese, although the terminal optical density still reached that of the

control cultures (data not shown). The cultures grown in 17.5 mM manganese, (containing 250x the manganese than that of the control) only had a statistically significant difference in optical density when compared to the control at hours 60 and 84, showing that the cultures have superseded the growth of the control cultures once in stationary phase. However, the maximum difference between the culture sets is only 0.727 AU (at 60 h), representing a mere 5% increase compared to the control, thus showing that the difference between the two culture sets is practically negligible. The difference between the 17.5 mM and the 35 mM cultures, however, are statistically significant at all points except the first and last time point, with a difference of up to 27% at 36 h. Therefore, while increasing manganese concentration does not appear to have a toxic effect on the overall growth of the cells, it is important to note that it has a statistically significant inhibitory effect on growth rate in highly excessive concentrations.

In addition to monitoring the optical density every 12 h, cultures were also assayed for total pigment concentration as an indicator of metabolic health. While increased manganese availability did not generate long-term growth inhibition when compared to the control, it significantly decreased pigment accumulation at every time point beginning at 36 h, with the exception of the 17.5 mM manganese culture (Figure 14a). However, beginning at 48 h, the 17.5 mM manganese culture also had a significantly decreased pigment accumulation compared to the control that was maintained throughout the remaining growth cycle. While excess manganese inhibited accumulation of all pigments, it had a heightened effect on Chl *a*, resulting in the increased manganese cultures having a Chl *a* deficit at all time points (Figure 14b). Unlike the optical density which showed an increased lag phase but similarity in terminal density, the peak Chl *a* concentrations in the 17.5 and 35 mM manganese cultures were 24.8 and 22.9 $\mu g \cdot mL^{-1}$,
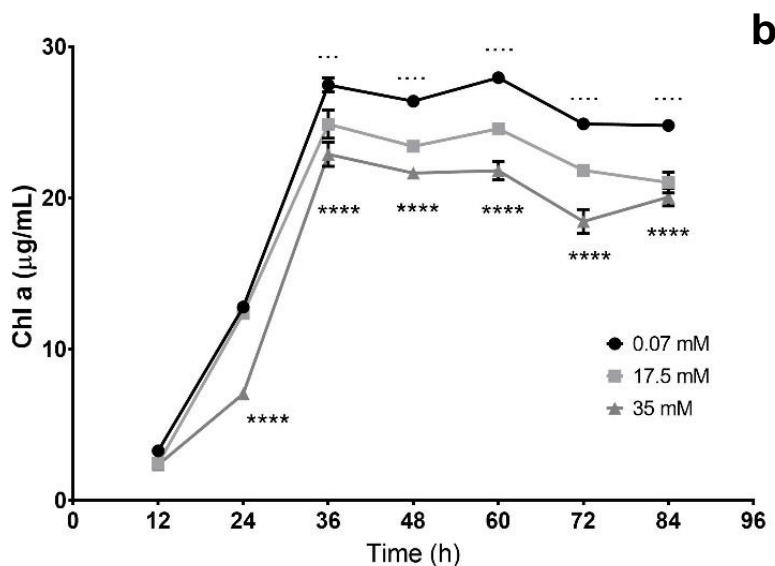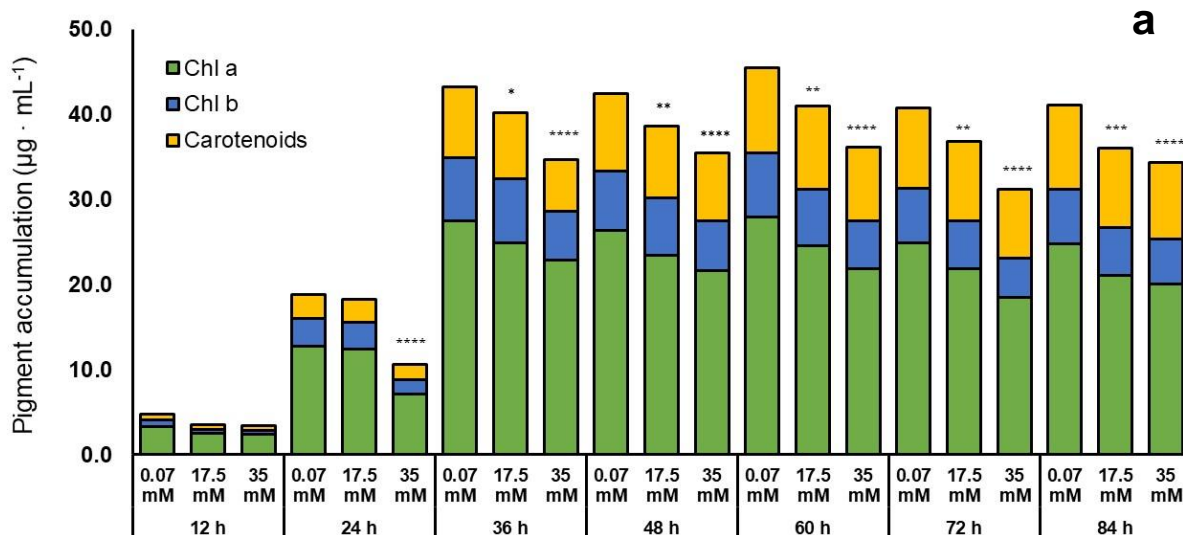
Figure 14. Pigment accumulation in manganese exposed cultures. (a) The pigment accumulation of manganese cultures taken over time. Asterisks (*) indicate statistical significance with the control, where * indicates $p \leq 0.05$, ** indicates $p \leq 0.01$, *** indicates $p \leq 0.001$, and **** indicates $p \leq 0.0001$. **(b)** The chl *a* concentration of manganese-exposed cultures taken over time. Error bars represent standard error of the measurement. Asterisks (*) are used to indicate statistically significant differences between the 35 mM cultures and the control while the middle dots (·) are used to indicate statistically significant differences between the 17.5 mM cultures and the control. Further information on statistical analysis can be found in the materials and methods section.

respectively, an 11 and 18% decrease when compared to the 0.07-mM-manganese culture peak

Chl *a* of 28.09 µg·mL^{-1}.

Intracellular and membrane-bound manganese accumulation

To determine the capacity of *C. vulgaris* to bioaccumulate manganese, the intracellular

and membrane-bound manganese concentration was assayed using ICP-OES every 24 h

beginning 12 h after inoculation (Figure 15). The intracellular concentration was then converted
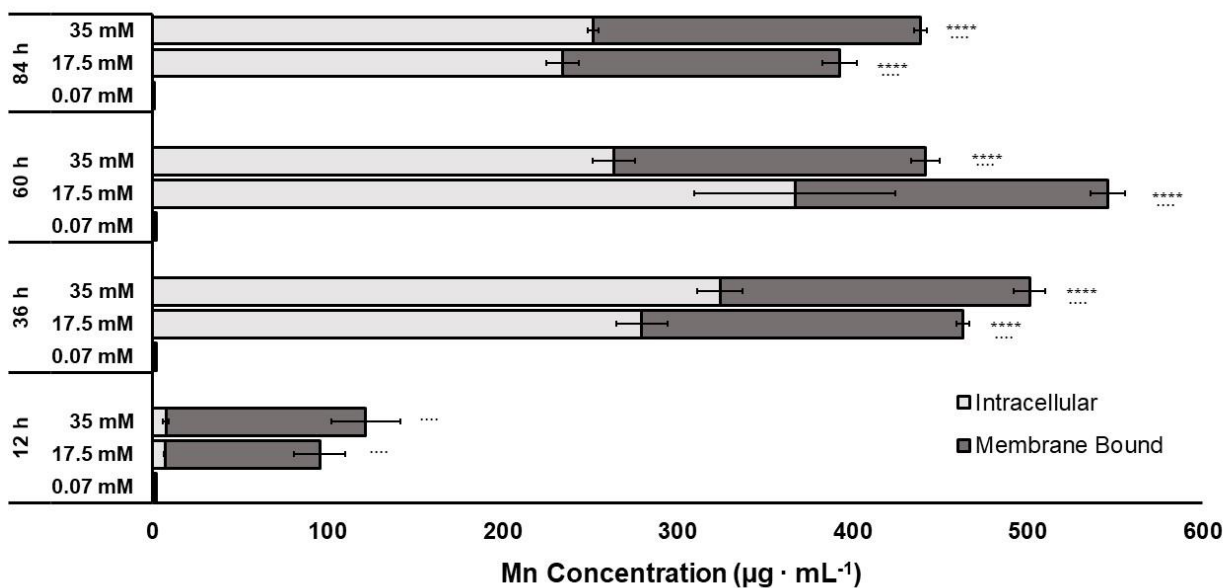
Figure 15. The concentration of intracellular and membrane bound manganese assayed via ICP-OES over time. Error bars represent the standard error of the measurement. Asterisks (*) indicate statistically significant differences of the intracellular manganese with that of the control, while the middle dots (·) are used to indicate statistically significant differences of the membrane-bound manganese with that of the control.

to molarity using a previously determined average cell diameter of 5 µm (the average found

using confocal microscopy) and a correlation curve between optical density and cell number

(Table 3). At 12 h, the control cultures had an intracellular manganese concentration of 1.425 ±

0.1739 µg · mL^{-1} , or 24.57 mM, while the 17.5 mM cultures had accumulated 6.931 ± 2.680 µg

· mL^{-1} and the 35 mM cultures had accumulated 5.800 ± 4.413 µg · mL^{-1}, a molarity of 106.4 and

95.04 mM, respectively. All cultures reached their maximum intracellular concentrations 24 h

Time post-inoculation	Initial concentration (mM)	Cell number (cells · mL^{-1})	Intracellular Mn (mM)	Adsorbed Mn (pg · cell^{-1})	Percent Mn removed
12 h	0.0700	1.615×10^7	24.57	2.516×10^{-2}	47.54
	17.50	1.761×10^7	106.4	4.956	9.935
	35.00	1.685×10^7	95.04	7.006	6.476
36 h	0.0700	1.491×10^8	2.646	2.022×10^{-3}	44.66
	17.50	1.570×10^8	495.0	1.167	48.13
	35.00	1.228×10^8	733.3	1.439	26.05
60 h	0.0700	2.004×10^8	1.981	7.818×10^{-4}	41.17
	17.50	2.111×10^8	483.9	8.460×10^{-1}	56.74
	35.00	1.956×10^8	373.9	9.098×10^{-1}	22.96
84 h	0.0700	1.978×10^8	0.2374	6.199×10^{-2}	7.579
	17.50	2.072×10^8	314.4	7.622×10^{-1}	40.81
	35.00	2.041×10^8	342.4	9.146×10^{-1}	22.80

Table 3. The intracellular and adsorbed manganese per cell in molarity and pg/cell. The cell number was determined using a correlation curve between cell number and turbidity while the molarity was determined using a previously determined average cell diameter of 5 µm. All numbers represent the mean of four replicates.

later, when the control culture had an internal manganese concentration of 2.646 mM and the 17.5 and 35 mM cultures had internal concentrations of 495.0 and 733.3 mM, respectively. The membrane-bound manganese follows a similar trend, with the 0.07 mM and 17.5 mM cultures staying within error of the membrane-bound accumulation at 36 h. Following 36 h, the cells increase in number while the total biomass associated accumulation stays within error of the peak mean, resulting in an overall drop in intracellular molarity. However, for all cultures (including the control), the internal molarity greatly exceeds that of the surrounding media, demonstrating a natural bioaccumulation of manganese in excess of equilibrium.

Terminal biochemical composition of manganese-exposed cell cultures

Macromolecule composition sheds light on overarching metabolic changes. For this reason, dry mass, proteins, lipids, and carbohydrates were all quantified at 84 h, the terminal
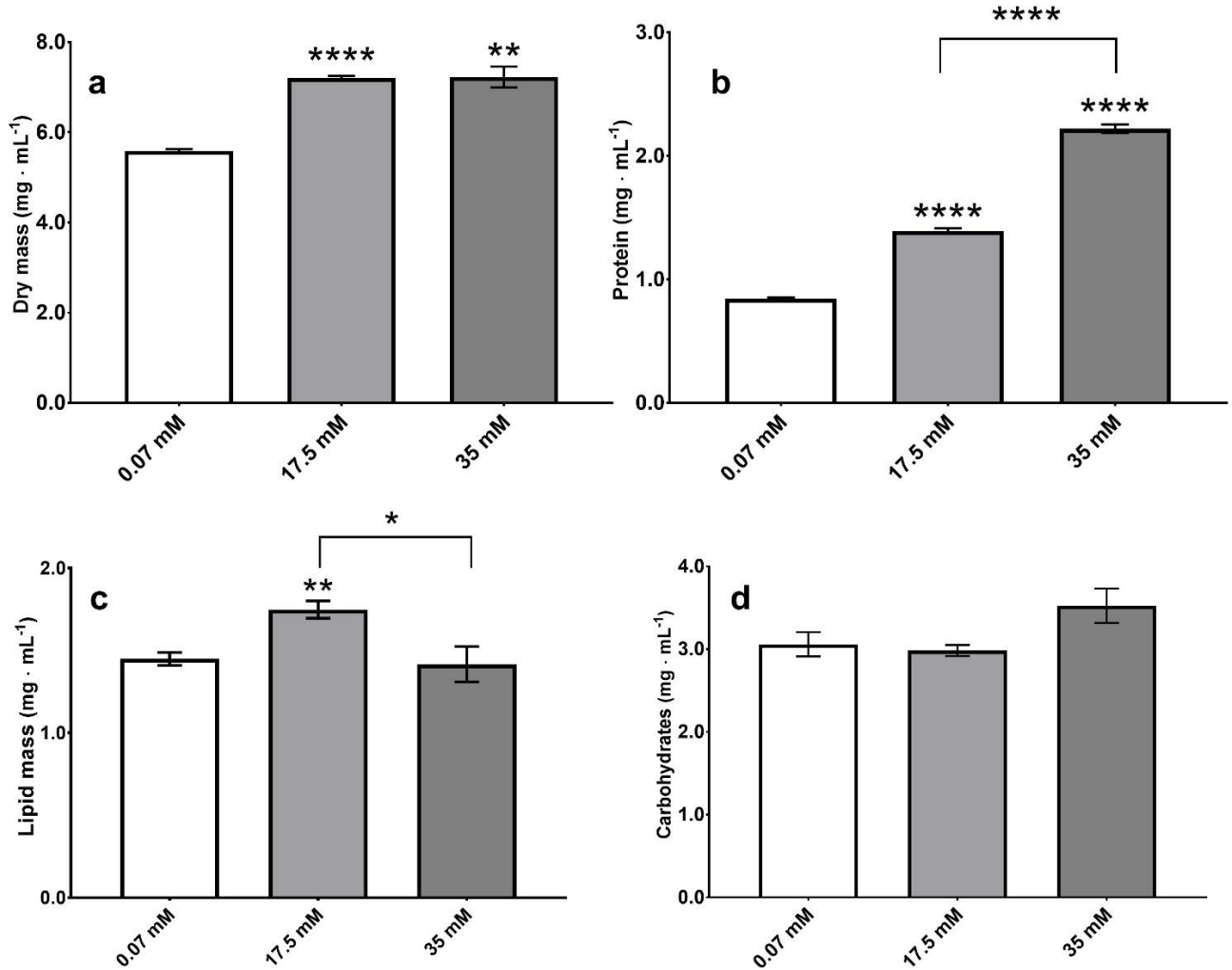
Figure 16. The terminal dry mass (a), protein content (b), lipid mass (c), and carbohydrate content (d) of manganese exposed cells. Error bars represent the standard error of the measurement. Unless indicated, asterisks (*) indicate statistical significance from the control cultures. Further information on statistical analysis can be found in the materials and methods section.

point, in order to gauge the metabolic health of the cultures following manganese exposure. The difference in overall dry mass between the control and experimental cultures was significant for

both manganese concentrations, with terminal dry mass concentrations of 5.59, 7.21, and 7.23

mg · mL^{-1} for the 0.07, 17.5, and 35 mM cultures, respectively (Figure 16a). However, only the

terminal protein concentration showed a statistically significant difference in both cultures when

compared to the control, with p ≤ 0.001 when comparing both the 17.5 mM and 35 mM

manganese cultures (Figure 16b). The 17.5 mM and 35 mM culture had 1.39 and 2.22 mg · mL^{-1}

protein at the terminal point, respectively, showing a 39 and 62% increase over the 0.84 mg ·

mL^{-1} measured from the control culture.

The 0.07, 17.5, and 35 mM cultures accumulated lipids with terminal concentrations of

1.45, 1.75, and 1.42 mg · mL^{-1}, respectively, consisting of 25.9, 24.3, and 19.6% of their total

dry mass (Figure 17). While the lipid concentration was statistically significant when comparing
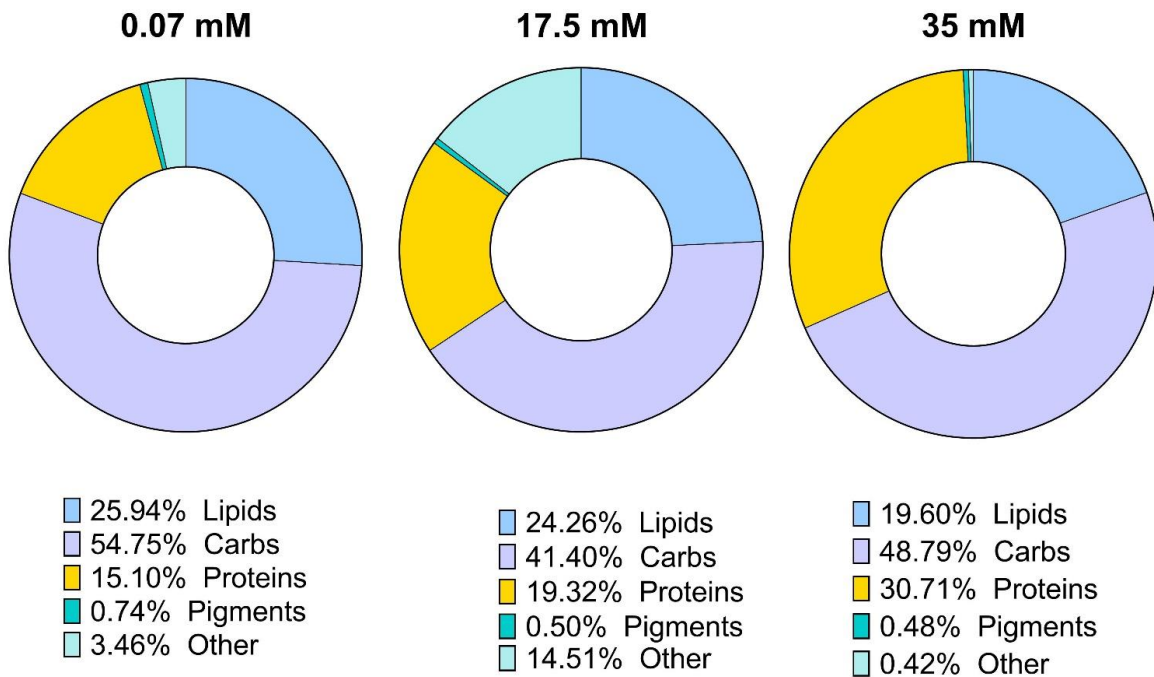
Figure 17. The macromolecule concentrations normalized to dry mass for the manganese-exposed cultures assayed at 84 h, the terminal point of growth.

the 17.5 mM manganese culture to the control ($p \leq 0.01$) and the 17.5 mM manganese culture to

the 35 mM manganese culture ($p \leq 0.05$), there was not a significant difference between the

highest manganese exposure and the control (Figure 16c). Additionally, the carbohydrate

concentration did not show a significant difference when comparing the high manganese cultures

with the control or the high manganese cultures to each other (Figure 16d).

Photosynthetic efficiency of manganese exposed cultures

Cells were monitored every 12 h beginning at 24 h post-inoculation for photosynthetic

efficiency using oximetry and the Chl *a* polyphasic fluorescent transient. The higher manganese
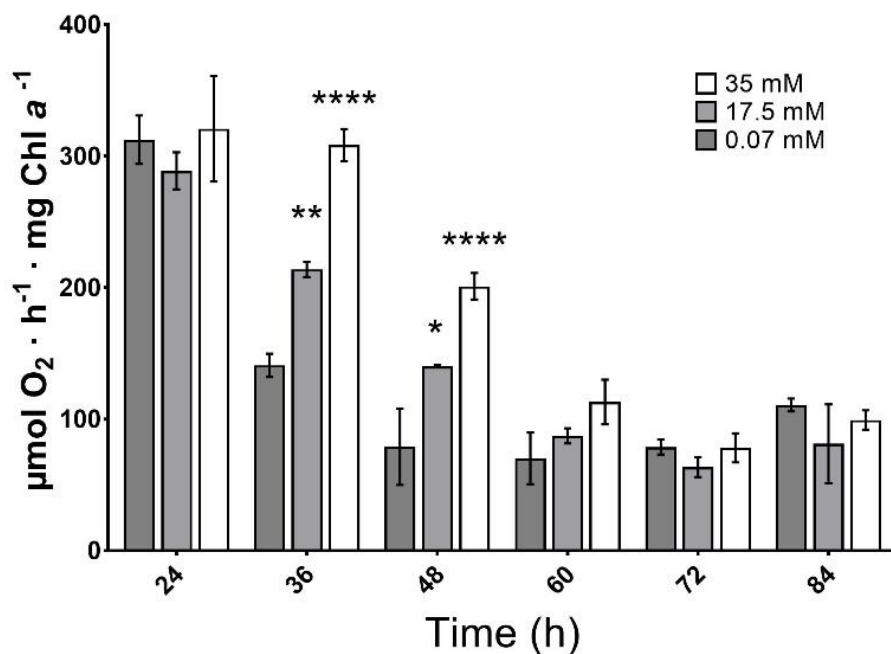
Figure 18. The oxygen production of manganese-exposed cultures taken over time.
Error bars represent the standard error of the measurement. Asterisks (*) indicate the
statistical significance as compared to the control group. Further information on statistical
analysis can be found in the materials and methods section.

cultures experienced a higher rate of oxygen production from 36 through 60 h post-inoculation,

with a statistically significant difference found at both 36 and 48 h, during which the cultures

were in exponential phase (Figure 18). The most significant difference is observed at 36 h,

71

during which time the cells are in mid-exponential growth phase and the 17.5 mM and 35 mM

manganese cultures produce 34 and 54% more oxygen, respectively. As the oxygen production is

normalized to the concentration of Chl *a* and both the 17.5 mM and 35 mM cultures have

significantly less chlorophyll than the control, it is possible that the active reaction centers are

using photons more efficiently in cells exposed to high levels of manganese.

In order to gather more evidence as to the efficiency of photosynthesis, the Chl *a*

polyphasic fluorescent transient was collected and analyzed every 12 h beginning at 24 h post-

inoculation. Once normalized to the control = 1, it is possible to visualize the difference in
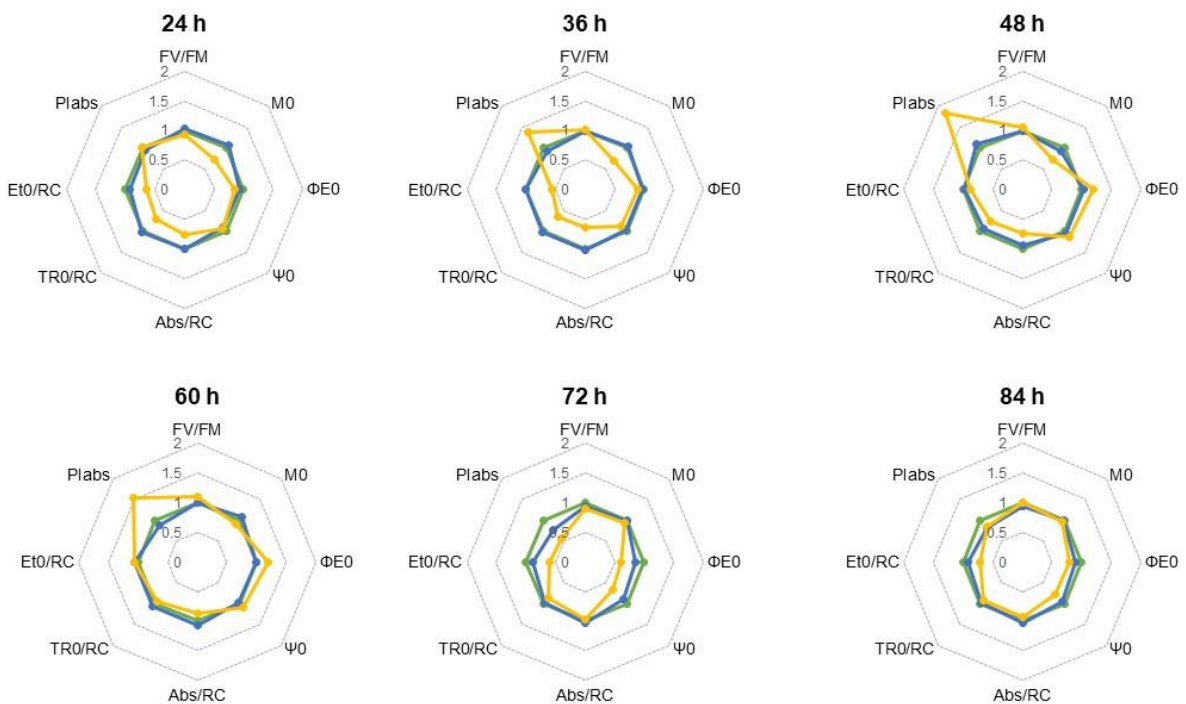
Figure 19. Spiderweb plots of JIP test parameters derived over time using the Chl a fluorescent transient, normalized where the 0.07 mM culture = 1. Green lines represent the 0.07 mM manganese cultures, blue lines represent the 17.5 mM manganese cultures, and yellow lines represent the 35 mM manganese cultures.

	24 h			36 h			48 h			60 h			72 h			84 h		
	0.07 mM	17.5 mM	35 mM	0.07 mM	17.5 mM	35 mM	0.07 mM	17.5 mM	35 mM	0.07 mM	17.5 mM	35 mM	0.07 mM	17.5 mM	35 mM	0.07 mM	17.5 mM	35 mM
F_V/F_M	0.529	0.544	0.488	0.590	0.583	0.601	0.550	0.543	0.578	0.488	0.487	0.535	0.475	0.448	0.427	0.447	0.422	0.444
M0	1.434	1.517	1.019	2.165	2.229	1.467	2.012	1.844	1.474	2.023	2.159	1.855	2.345	2.344	2.217	2.427	2.378	2.327
Φ_{E0}	0.134	0.125	0.115	0.160	0.153	0.142	0.139	0.144	0.167	0.105	0.103	0.126	0.099	0.085	0.061	0.080	0.072	0.063
Ψ_0	0.254	0.230	0.235	0.270	0.263	0.236	0.254	0.265	0.288	0.215	0.212	0.236	0.209	0.189	0.136	0.179	0.171	0.140
Abs/RC	3.624	3.622	2.729	5.027	5.176	3.196	4.901	4.618	3.583	5.219	5.612	4.533	6.243	6.455	6.045	6.624	6.789	6.111
TR_0/RC	1.921	1.971	1.332	2.966	3.025	1.921	2.695	2.509	2.071	2.568	2.738	2.429	2.964	2.889	2.585	2.957	2.867	2.709
Et_0/RC	0.488	0.454	0.313	0.801	0.796	0.453	0.683	0.666	0.597	0.545	0.579	0.574	0.618	0.545	0.368	0.530	0.489	0.382
PI_{abs}	0.106	0.099	0.107	0.107	0.097	0.146	0.085	0.093	0.155	0.052	0.046	0.079	0.039	0.029	0.022	0.027	0.022	0.023

Table 4. The JIP test parameters calculated using the polyphasic Chl a fluorescent transient. Grey fill indicates a statistically significant difference from the control cultures.

derived parameters using spiderweb plots (Figure 19). While the normalized values between 0.07 mM manganese and 17.5 mM manganese show few differences, the 35 mM cultures have substantial changes throughout the growth cycle. Most noteworthy is the increase in the performance index per reaction center (PI_{abs}), which is significantly higher at hours 36 – 60, and significantly lower at hour 72 (Table 4). This is paired with an overall decrease in absorption per reaction center (Abs/RC), indicating that it is likely the effective antenna size of the reaction centers have decreased in higher manganese cultures as smaller antennas result in a smaller absorption capacity per reaction center.[168] Although the PIabs and Abs/RC of the 35 mM culture is significantly larger during exponential phase, an increase in Fv/Fm, a measure of photosynthetic efficiency through a quantitative assessment of the overall availability of open reaction centers, occurs in early stationary phase, indicating that *C. vulgaris* experiences a lengthened peak photosynthetic capacity under increased manganese. This was shown to a larger extent when the alga was exposed to manganese concentrations beyond 35 mM (data not shown). Additionally, M0 (rate of primary photochemistry at Q_A) and TR_0/RC (trapped energy flux per

reaction centers at t = 0) show significant increases in exponential phase, further demonstrating an overall increased photosynthetic capacity.

Discussion

C. vulgaris **actively accumulates manganese in excess of equilibrium**

Large concentrations of manganese adsorbed to the surface of *C. vulgaris* cells in high-manganese cultures beginning 12 h after inoculation. Soon after, the cells began intracellularly accumulating manganese, and by 36 h post-inoculation, cells reached their peak, containing 495.0 and 733.3 mM manganese for the 17.5 and 35 mM cultures, respectively. These intracellular concentrations of manganese are significantly higher than the manganese concentrations found in the surrounding media, suggesting that either manganese is actively transported across the cell wall and membrane or that manganese is stored in cellular compartments, decreasing the effective intracellular concentration and allowing for passive transport. The intracellular accumulation also greatly exceeds that of the membrane bound manganese for all time points except for 12 h post-inoculation. This is likely due to a phenomena in which there are two distinct stages in algal metal uptake: a quick initial adsorption followed by intracellular accumulation over time.[212] While the mass of biomass-associated manganese remains virtually unchanged after the first 36 h of the growth cycle (Figure 15), the intracellular molarity of the cells begins to decrease, demonstrating that the cells do not continue to actively accumulate manganese while they finish their exponential rate of cell division (Table 3).

From these observations, it can be inferred that the cells actively regulate the uptake and storage of manganese. The data show that cells in lag and early exponential phase adsorb the manganese and actively increase the intracellular concentration beyond equilibrium while those in late exponential and stationary phase no longer continue increasing their overall manganese

74

accumulation. Based on previous work, it is possible that this is linked to nutrient availability: as the cells deplete their dextrose stores in late exponential phase, they have less excess energy stores to use for active transport across the membrane.[76] Additionally, when nutrients are in short supply, the cells are more likely to switch from protein biosynthesis pathways, many of which require metal cofactors, to lipid biosynthesis pathways, meaning the excess metals would no longer serve an immediate biochemical purpose. Another potential reason for the decrease in manganese bioaccumulation is due to the decrease in photosynthetic activity (Figure 18). Photosynthesis, which requires manganese for the water oxidation complex, reaches peak productivity in early exponential phase before decreasing steadily over the remaining life cycle as shown through both the oxygen production as well as the Chl *a* fluorescent transient (Table 4). When paired with the manganese accumulation data, it is possible that the rate of photosynthesis mediates the uptake of metals and metal storage. Further experiments should expose heterotrophic cell cultures to increased manganese to determine the extent photosynthesis has on mediating metal uptake.

Phytoremediation efforts require that the algae are capable of accumulating intracellular concentrations of contaminants in excess of equilibrium, which all cultures, including the control, achieve successfully. The 17.5 mM cultures were able to remove the maximum percent of manganese from the surrounding cultures, removing 56.74 % at 60 h post-inoculation. Even the control cultures were able to remove up to 47.54 % of the manganese in the surrounding media, showing how *C. vulgaris* can be used to remove manganese at both high and low concentrations. However, like all systems, *C. vulgaris* is limited: in experiments with manganese increased beyond 35 mM, the cells did not accumulate any excess above that of the 35 mM cultures. That being said, the quick rate of accumulation would allow for a fast harvesting time

of manganese-accumulated cultures, increasing the feasibility of using *C. vulgaris* for the remediation of manganese-contaminated waterways.

Excess manganese does not significantly inhibit metabolic pathways

Other studies have established inhibitory effects on *C. vulgaris* caused by metal toxicity for a variety of metals, including cadmium, lead, copper, zinc, and chromium.[218, 223] The inhibitory effects included decreased growth, decreased pigment accumulation, decreased protein content, and decreased photosynthetic efficiency – all at concentrations in the micromolar range. However, while high manganese concentrations did lead to significant decreases in overall pigment accumulation, it had a limited effect on cell growth and biochemical composition, with high manganese cultures increasing their protein content beyond that of the control (Figure 16b). Similarly, high manganese cultures had an increased photosynthetic capacity, producing more oxygen when normalized to Chl *a* and showing increases in several derived parameters from chlorophyll fluorescence (Figures 18 & 19). While manganese exposure did somewhat increase the lag phase in the 35 mM cultures, this was not enough to significantly inhibit cell growth; in fact, statistical analysis using a linear regression model could detect no differences in rate between the three growth curves (p = 0.982) (Figure 13). These physiological characterizations, paired with erythrosine cell viability tests that indicated no decreases in cell viability caused by high manganese (data not shown), confirm increased manganese exposure does not have a significant inhibitory effect on *C. vulgaris*.

Most interesting was the increase in photosynthetic capacity, which was linearly increased at manganese concentrations beyond 35 mM (data not shown). While the increased oxygen production suggests an upregulation in linear electron transfer (Figure 18), the derived fluorescence parameters suggest that the phenomenon may be more complex (Figure 19). If the

increased oxygen production was related to an upregulation in PSII activity and linear electron transport, it would be expected that both Chl a and F_v/F_m, the quantum efficiency parameter most specifically linked to PSII function, would increase. However, high manganese cultures accumulated significantly less Chl a (Figure 14b) and the 35 mM cultures only have statistically higher F_v/F_m values at 24 and 60 h post-inoculation. While the 17.5 mM manganese cultures have significantly higher rates of oxygen production at 36 and 48 h, the derived electron flux parameters are not significant at any time point when assayed through the JIP test (Table 4). The largest changes are seen in specific fluxes, including both Abs/RC and TR_0/RC, the absorption per reaction center and trapped energy flux per reaction center at t = 0, respectively, both of which are significantly decreased in 35 mM manganese cultures. Simultaneously, the 35 mM cultures experience an increase in PI_{abs}, the performance index of photosynthetic electron transfer on an absorbed photon basis, demonstrating an increased efficiency of photon use. This suggests that there are structural changes taking place, wherein the light harvesting antenna complexes are absorbing fewer photons, potentially leading to increasing photosynthetic efficiency due to a decrease in nonphotochemical quenching pathways. As excess manganese is also required for photoassembly following the turnover of PSII D1 dimers due to photoinhibition, it is possible that increased concentrations of the ion enable a faster rate of photorepair, increasing the relative amount of active (reducing) reaction centers in high manganese cultures.[219, 224] Thus increased photosynthetic production under elevated manganese may potentially be both an artifact of changing PSII heterogeneity by structural differences in light harvesting antenna complexes (such as differences in the ratios of PSIIα to PSIIβ), as well as changes in the relative amounts of available reducing reaction centers. This is further suggested by the statistically significant decreases in M0 (the rate of primary photochemistry at

77

Q_A) at 24, 36, and 48 h, as smaller values would occur if more reaction centers were capable of reduction, as an increase in active Q_A sites would decrease the rate in which they are filled with plastoquinone, thus decreasing the rate at which the polyphasic fluorescent transient reaches the J step (Table 4). Further studies on PSII heterogeneity in high manganese exposed cultures are ongoing.

Conclusions

Manganese is a bioavailable water contaminant resulting from industrial processes including mining, metallurgy, and agricultural industries. Due to its high solubility in water, chemical methods of remediation are limited, with even the most efficient methods requiring an influx of materials and generating large amounts of environmentally problematic waste. *C. vulgaris*, a robust green alga, offers an environmentally friendly alternative to traditional chemical remediation strategies, as it is able to bioaccumulate manganese in intracellular concentrations in excess of equilibrium without metal toxicity or inhibitory effects. In fact, excess manganese improved the biochemical productivity of the alga, with increased protein production and an enhanced photosynthetic capacity over the cell's life cycle. Additionally, manganese was accumulated to a maximum concentration at only 36 h post-inoculation, making *C. vulgaris* a quick and efficient alternative to other remediation technologies. While more studies are required to determine the dependence of bioaccumulation on light availability and through it, photosynthetic function, the data suggests that *C. vulgaris* can be effectively used for phytoremediation of waterways up to 35 mM manganese.

CHAPTER 5

GLYCEROL METABOLISM IN BATCH-FED MIXOTROPHIC *CHLORELLA VULGARIS*

Introduction

The time has never been more appropriate, or more urgent, to invest in carbon neutral renewable energy sources. Of the 28% of total U.S. energy used for the transportation industry, 92% is petroleum based, making the transportation industry an easy target for biofuel replacements that can lead to rapid decreases in overall fossil fuel use.[225] Specifically, this replacement can be achieved using microalgae, aquatic microbial oxygenic photoautotrophs with the ability to grow in adverse environments using a variety of water sources, making them a promising source of energy that will not compete with agricultural resources.[69]

Based on current theoretical yields, it is estimated that microalgae can be up to 20x more productive per unit area than the most productive agricultural crops.[70] In order to realistically produce fuel on an industrial scale, microalgal lipid production must be increased. If this is accomplished, microalgae with 70% oil by biomass could satisfy 50% of the United States' transport fuel needs while using less than 2% of the existing cropping area used for fuel production.[47]

Chlorella vulgaris is a unicellular green alga with a high division rate, multiplying via autosporulation fourfold per day in optimal conditions.[75] This growth rate paired with an average 42% dry weight lipid content under nitrogen deprivation makes *C. vulgaris* a promising biofeedstock for large-scale biofuel production.[70] While *C. vulgaris* grows photoautotrophically, mixotrophically, and heterotrophically, research has linked the growth and lipid production rate of *C. vulgaris* with the availability of an exogenous carbon source and a light source, showing

79

how photosynthetic light reactions, while not explicitly linked to lipid metabolism, are an integral biochemical process for increased lipid productivity.[76] However, nitrogen deprivation, the most promising and well-researched method of increasing algal lipid production, has the potential to inhibit this activity, as it has been shown in *Chlamydomonas reinhardtii*, another chlorophyte, to decrease electron flux through the electron transport chain.[226] Therefore, to realistically increase algal biofuel feasibility, an approach needs to be found that increases lipid production without drastic decreases in photosynthetic capacity.

Attempts have been made to increase lipid production of *C. vulgaris* using a variety of carbon sources, including glucose[102, 115], xylose[122], sucrose[110], acetate[109, 113-114], sodium bicarbonate[109, 227-229], and glycerol[117-118], among others. The highest rate of lipid productivity has occurred using mixotrophic cultures supplemented with glucose, as previously reported.[76] However, the increase in lipid productivity does not necessarily correlate with an increase in triacylglycerols (TAGs), the most energy dense and therefore most desired lipid for biofuel production.[230]

To generate biodiesel, TAGs are transesterified to generate fatty acid methyl esters (FAMEs) and a glycerol byproduct.[231] It is estimated that biodiesel production will generate about 10% (w/w) glycerol, meaning that every gallon of biodiesel produces approximately 1.05 pounds (about 476 g) of crude glycerol.[232] If glycerol could be reused to generate more efficient algal feedstocks, the process would be less wasteful and more economically efficient. In fact, research has shown that adding glycerol in stationary phase after initially supplementing with glucose yields higher lipid production than either glucose or glycerol alone.[119] However, this study was completed using heterotrophic cultures, thus decreasing the overall potential for algal lipid production.

In this study, a two-stage batch fed system of glucose and glycerol was combined with the presence of constant light in order to generate a more productive biofuel feedstock. Glycerol uptake and lipid yield was monitored over time to find optimal harvesting time and glycerol dosage. Additionally, isotopically labeled glycerol was used to confirm that exogenously applied glycerol was incorporated directly into the TAG backbone. Results indicate that a two-stage mixotrophic carbon-supplemented culture has the potential to generate a more efficient algal culture for use in biofuels.

Materials and Methods

Reagents

D-Glucose was acquired from Sigma-Aldrich Inc. (Dermstadt, DE). The remaining reagents, unless otherwise specified, were obtained through Fisher Scientific (Hampton, NH).

Strain and Culture Growth Conditions

Batch cultures of *Chlorella vulgaris* were maintained on lysogeny broth agar plates and inoculated into 25 mL of modified Chlorella medium supplemented with 20 g/L of dextrose into 50-mL sterile Erlenmeyer flasks top capped with aluminum foil.[76,27] Cultures were grown in quadruplicate, using a 1-mL inoculum from a stationary phase culture and kept under constant white light conditions of 30 μmol photons $\cdot$ m^{-2} $\cdot$ s^{-1} at 25 °C at an orbital rotational speed of 100 rpm. For glycerol acclimation experiments, the glycerol addition was divided equally between three doses, given at 24, 48, and 72 h of growth. For the remaining glycerol experiments, glycerol-dosed cultures were dosed at 72 h of growth. All cells were grown to 144 h before harvesting for lipid analysis.

For 2-^{13}C glycerol experiments, cells were inoculated into 12 mL of modified Chlorella medium into 25 mL sterile Erlenmeyer flasks top capped with aluminum foil. Cells were dosed

81

with 20 g · L^{-1} 2-^{13}C glycerol (Omicron Biochemicals, Inc., South Bend, IN) at 72 h and harvested at 144 h.

Spectroscopic Cell Density

Cell density (turbidity) was obtained using a Shimadzu UV-1800 spectrophotometer (Shimadzu Corp., Kyoto, JP) at 750 nm as previously described.[76,27]

Cell Dry Weight Measurement

Dry mass was measured as previously reported by Smythers et al. (2019).[27]

Lipid Extraction and Lipid Dry Weight Analysis

Lipid extractions were performed as previously described using a modified methyl tert-butyl ether (MTBE) extraction similar to the method published by Matyash et al. (2008).[149] Two 1-mL samples were pelleted and the supernate discarded. Cell pellets were lysed with 1 mL of methanol and incubated in a 9-mL tube with 6 mL of methyl tert-butyl ether for 1 h before adding 1.5 mL of ultrapure H_2O and incubating for another 15 min. Suspensions were centrifuged for 15 min at 10,000 xg and the organic layer was removed by a Pasteur pipette into a pre-weighed 4-cm tube and dried under constant airflow. The extraction was done twice to ensure complete recovery of lipid mass. Tubes were weighed on a Secura 125-1S analytical balance (Sartorius, Göttingen, DE).

Biochemical *composition*

Terminal carbohydrate and protein concentration were assayed as previously described [27].

Oxygen evolution *in vivo*

Photosynthetic oxygen production was measured using a Clark-type oxygen electrode (Hansatech) at 25 °C as previously described [27]. Oxygen measurements were conducted by exposing 1:1 diluted cell suspension in modified *Chlorella* media to a 1700-µmol photons· m^{-2} ·

s^{-1} white light after a 5-min dark adaptation phase. High light intensity was chosen in order to ensure light saturation of PSII —the initial rate of oxygen production was measured, normalized to Chl *a*, and used for comparison across culture conditions.

Chlorophyll fluorescence induction *in vivo*

Photosynthetic electron transfer fluxes were inferred from Chl *a* fluorescence using a Photon Systems Instruments FL 3500 fluorometer as previously described [27]. The OJIP protocol included a 1-s actinic illumination using a 630-nm light at an intensity of 2,400 μmole photons $m^{-2} \cdot s^{-1}$. Fluorometry parameters (JIP test) were calculated as outlined by Stirbet, et al. [222].

Solid phase extraction

Solid phase extraction (SPE) was conducted using amino-propyl columns conditioned with 600 μL 7:1 acetone:H_2O and 2 mL hexane. Dried lipid extractions were suspended in 200 μL 100:3:0.3 hexane:MTBE:acetic acid and allowed to gravimetrically penetrate the column before being washed with 3 mL 100:3:0.3 hexane:MTBE:acetic acid. Sterols were eluted using 5 mL hexane before eluting triacylglycerols using 6 mL of 100:5:5 hexane:chloroform:ethyl acetate. Mono- and di-acylglycerols were eluted using 5 mL of 2:1 chloroform:isopropanol and free fatty acids were eluted using 6 mL 100:2:2 chloroform:methanol:acetic acid. Charged lipids were eluted using 6 mL of 10:5:4 methanol:chloroform:H_2O, after which 1 mL of chloroform and 2 mL H_2O were added to the eluent and shaken before using a Pasteur pipette to remove the bottom layer for analysis. All eluents were dried completely under vacuum until GC-MS preparation for analysis.[233]

Transesterification and methylation

Dried SPE elutions were suspended in 500 μL anhydrous diethyl ether before adding 10 μL methyl acetate and vortexing for 10 s. Following vortexing, 0.5 M anhydrous sodium

methoxide was added and the reaction was vortexed for another 10 s before incubating at RT for 5 min. After incubation, 15 µL of saturated oxalic acid in anhydrous diethyl ether was added and briefly vortexed before centrifuging at 1,500 xg for 2 min and drying under N_2.[234]

Gas-chromotography mass spectrometry

For SPE elutions, dried eluents were resuspended in 100 µL of 2:1 acetic anhydride: pyridine reagent and incubated at RT for 15 min. The samples were then dried under nitrogen and resuspended in ethyl acetate for GC-MS analysis. The suspended sample was transferred to a GC sample vial and injected onto a 5% diphenyl column with a diameter of 0.25 µm and length of 15 m (Restek; State College, PA). The GC was carried out at constant, splitless flow of helium at 2.0 mL per min. The inlet was set at 75 °C and the MS was set at 220 °C. The oven began at 75 °C and was ramped at 45 °C · min^{-1} until 160 °C, where it was held for 1 min. The oven was then ramped at 4 °C · min^{-1} until it reached 171 °C, after which it was ramped again at 45 °C · min^{-1} until it reached the terminal temperature of 220 °C. The MS began scanning at 1.5 min with a dwell time of 0.5 s for ions between 20 – 100 amu.[235]

For monitoring of exogenous glycerol uptake, 1 mL of culture was centrifuged at 13,000 xg for 5 min and 10 µL of the resulting supernatant was combined with 130 µL of BSTFA: pyridine reagent and heated at 90 °C for 15 min. The samples were then transferred to a GC sample vial and injected onto a 5% diphenyl column GC column. Helium flow was maintained at 1 mL · min^{-1} with a split ratio of 50:1. The inlet and MS were both set at 260 °C. The oven began at 100 °C and held for 1 min before ramping at 4 °C min^{-1} to 240 °C and holding for 15 min.[236] Samples were quantified using a 5-point standard curve.

Statistical analysis

The remaining data was analyzed through multiple comparisons of means conducted using Welch's t-tests. The family-wise error rate for each figure was maintained at 0.05 through the use of the Holm-Bonferroni method, unless stated otherwise. Statistical significance is indicated numerically through increasing asterisks, where * indicates $p \leq 0.05$, ** indicates $p \leq 0.01$, *** indicates $p \leq 0.005$, and **** indicates $p \leq 0.001$. Figures show the means of quadruplicate data and the error bars denote the standard error of the measurement.

Results

Cell growth for glycerol acclimation protocol

Previous publications have shown increases in TAG production in *C. vulgaris* through the application of exogenous glycerol up to 10 g · L^{-1}.[89, 117, 119, 237] However, these approaches applied the glycerol in a single dose, either upon inoculation or in stationary phase, subjecting the cells to large amounts of osmotic pressure. Since *Chlamydomonas reinhardtii,* a genetically more complex green algae with many homologous proteins to *C. vulgaris*, uses the glycerol transporter MIP1 to transport glycerol across the cell membrane, it was hypothesized that *C. vulgaris* could use exogenous glycerol more effectively if these transport proteins were upregulated, as it would relieve some of the osmotic pressure.[238] In order to achieve cost-effective upregulation, the cells were grown mixotrophically with 20 g · L^{-1} dextrose and the glycerol dose was divided into three equal increments applied at 24, 48, and 72 h post-inoculation. However, this caused a significant decrease in cell density paired with a significant decrease in overall lipid yield (Figure 20 (a)). Following the genomic sequencing of *C. vulgaris* in 2018, it was concluded that *C. vulgaris* does not possess the glycerol transporters found in *C.*

reinhardtii, thus requiring another approach for increasing lipid accumulation through glycerol supplementation.[56]
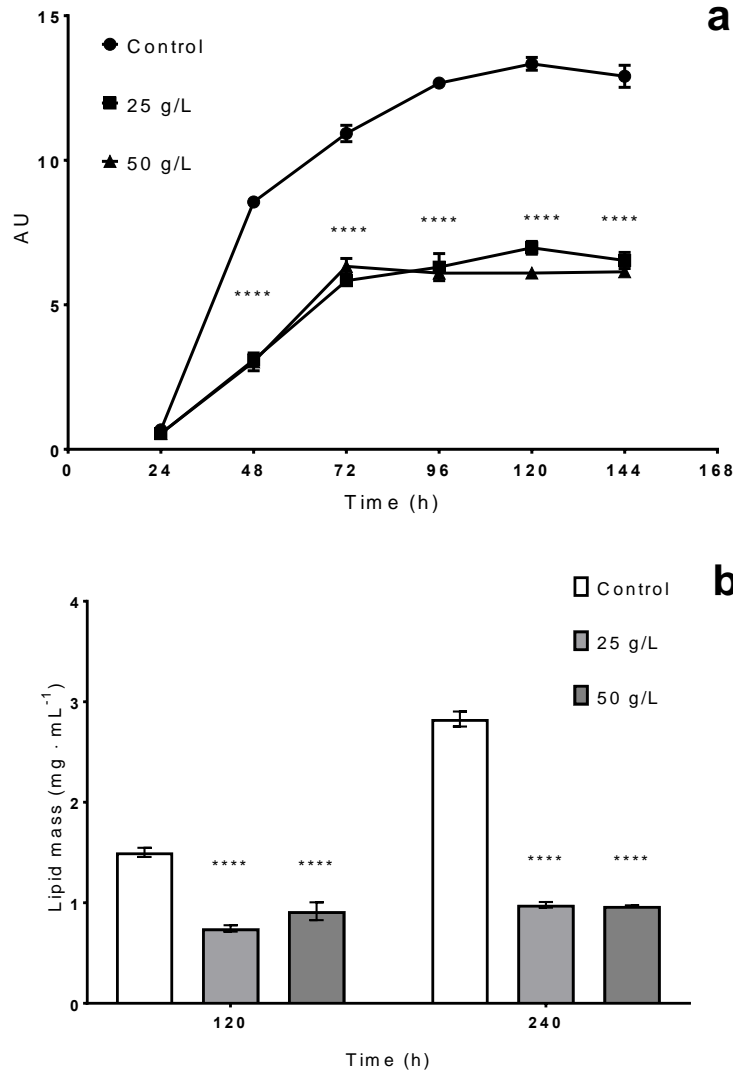
Figure 20. Cell growth under glycerol dosing. (a) The optical density of cells dosed with glycerol at 24, 48, and 72 h, to a total concentration of 0, 25, and 50 g/L glycerol. **** indicates p ≤ 0.001 for both 25 g/L and 50 g/L glycerol when compared to the control. **(b)** The lipid mass of cultures undergoing the glycerol acclimation protocol taken at 120 and 240 h. **** indicates p ≤ 0.001 when compared to the control.

Cell growth and lipid production following glycerol addition in stationary phase

To maintain cell density while subsequently increasing lipid yield and TAG accumulation, the cultures were dosed in stationary phase after being grown mixotrophically for

72 h. This two-stage fed batch system is similar to studies in the literature, with the added caveat of being conducted in constant light conditions, thus allowing the photosynthetic light reactions that previous research has linked to increases in lipid production to run continuously.[76, 119] After applying the glycerol, the cultures experienced a stagnation in cell density proportional to the concentration of added glycerol, with the control cultures continuing to experience a low rate of turbidity increase and the cultures with the highest concentration of glycerol experiencing no growth through the terminal point (Figure 21). This was reflected in the dry mass data as well, with the 10, 20, and 40 g · L^{-1} cultures increasing from 72 to 168 h by 23, 14, and 8%, respectively, while the control culture's dry mass increased by 26% in the same time frame (Figure 22). At the terminal point, this was reflected in significant differences between the control and glycerol-dosed cultures, with the 10, 20, and 40 g · L^{-1} cultures having a dry mass of 7, 22, and 26% less than that of the control, respectively.

Unlike the lipid results seen after the acclimation glycerol protocol, all cultures increased in lipid concentration over time (Figure 23). However, while the control cultures increased the
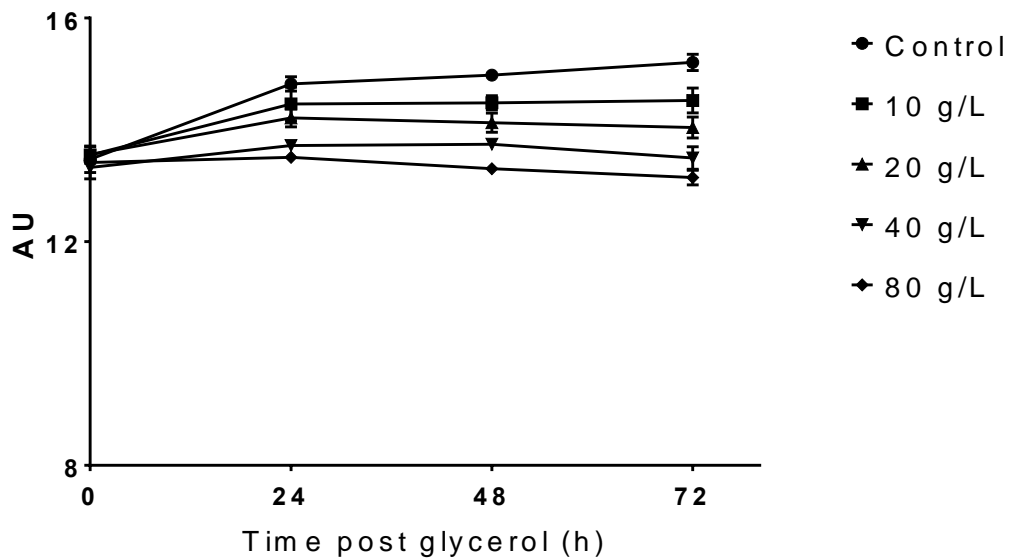
Figure 21. The optical density of cells dosed with glycerol at stationary phase.

87
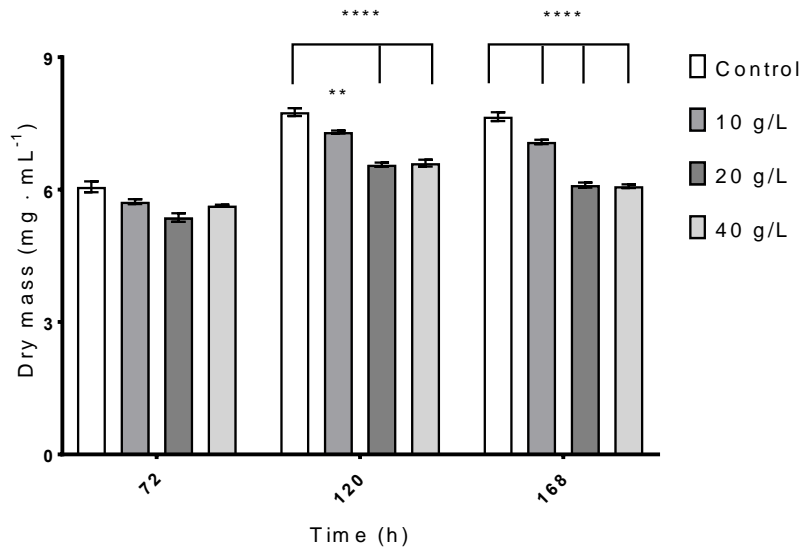
Figure 22. The dry mass of cells dosed with glycerol in stationary phase. * indicates $p \leq$ 0.05, ** indicates $p \leq 0.01$, *** indicates $p \leq 0.005$, and **** indicates $p \leq 0.001$.
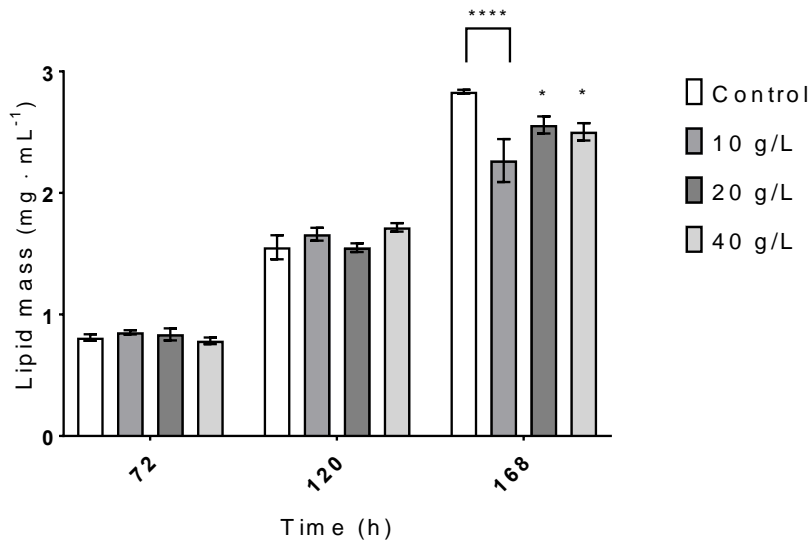
Figure 23. The lipid mass of cells dosed with glycerol in stationary phase. * indicates $p \leq 0.05$, ** indicates $p \leq 0.01$, *** indicates $p \leq 0.005$, and **** indicates $p \leq 0.001$.

rate of lipid production as time increased, finishing the growth curve with a rate of 0.640 mg · d⁻

¹, the glycerol-exposed cultures reached their highest rate of production after 120 h, with 0.403,

0.357, and 0.467 mg · d⁻¹ for 10, 20, and 40 g · L⁻¹ cultures, respectively. This correlates to

increases of 95, 85, and 119% of their lipid accumulation at 72 h of growth, with the control

increasing by 91% of their initial lipid accumulation, and small increases in lipids of the 10 and

40 g · L^{-1} cultures when compared to the control. At 168 h, however, the glycerol-dosed cultures
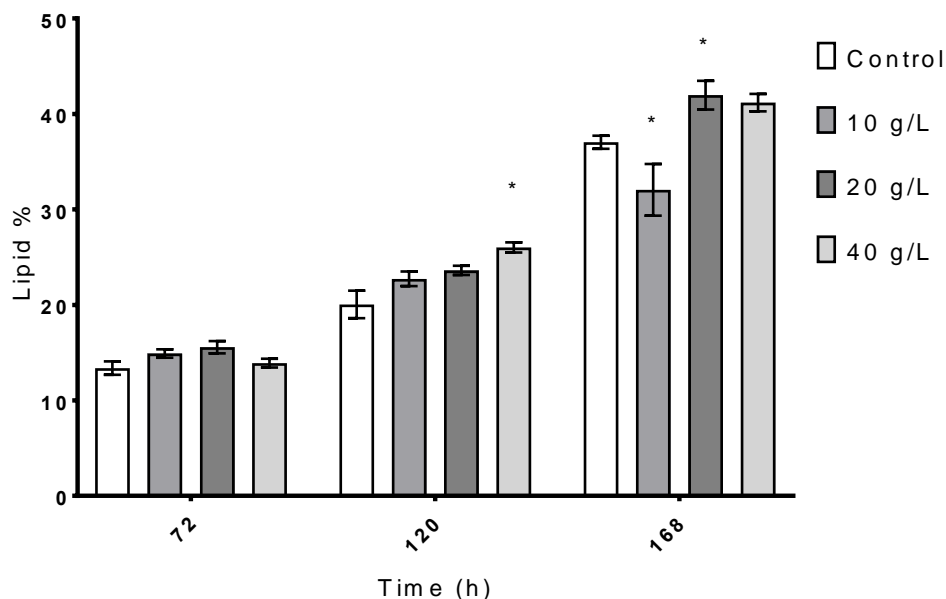
Figure 24. The lipid percent (m/m) of glycerol-dosed cultures taken over time. *
indicates p ≤ 0.05, ** indicates p ≤ 0.01, *** indicates p ≤ 0.005, and **** indicates p ≤
0.001.

had a significantly less terminal lipid yield than the control cultures, indicating that the cells

could not sustain the initial increase in lipid production long-term. When correlated with the dry

mass, glycerol-dosed cultures did have a larger lipid percent than the control beginning at 120 h,

with increases of 3, 4, and 6% for the 10, 20, and 40 g · L^{-1} cultures, respectively (Figure 24).

This trend continued at the 16 h time point for the 20 and 40 g · L^{-1} cultures, each having a lipid

percent of about 42%, 5% higher than that of the control cultures.

Glycerol consumption by *C. vulgaris* in stationary phase

In order to assess the glycerol consumption of *C. vulgaris* following dosing in stationary phase, cells were pelleted and the resulting supernatant was collected and analyzed for glycerol content using GC-MS. While decreasing in overall percent of initial glycerol consumed, the overall amount of glycerol consumed increased with dosage concentration, with the highest dose tested (63 g · L^{-1}) resulting in a glycerol consumption of approximately 25 g · L^{-1} (Figure 25).
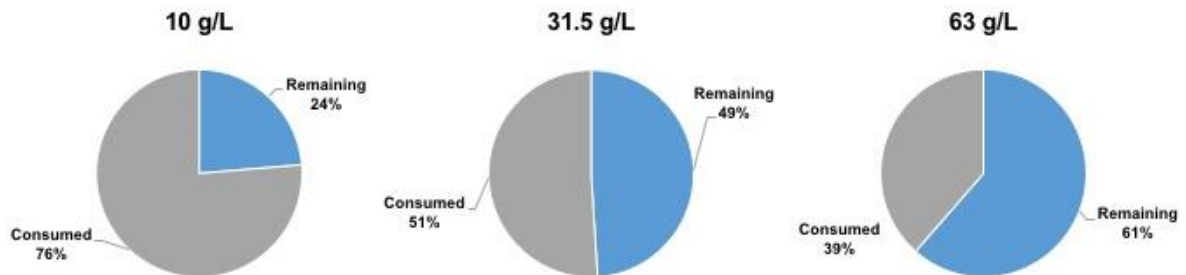
Figure 25. The glycerol consumed by dosed algae cells as quantified using GC-MS.

Lipid composition following glycerol dosage

To determine if the overall biochemical makeup of lipids had changed in the presence of glycerol, terminal lipids of 20 g · L^{-1} cultures and the control culture were fractionated using SPE and dried down for quantification (Figure 26). While the glycerol-exposed cultures had a 6% increase in free fatty acids when compared to the control, the TAG fraction only saw a 1.3% increase with a corresponding 5% decrease in the fraction containing monoacylglycerides (MAGs) and diacylglycerides (DAGs). The 20 g · L^{-1} cultures also had a minor decrease in phospholipids, with 16% of its lipids in the phospholipid fraction compared to 19% in the control.
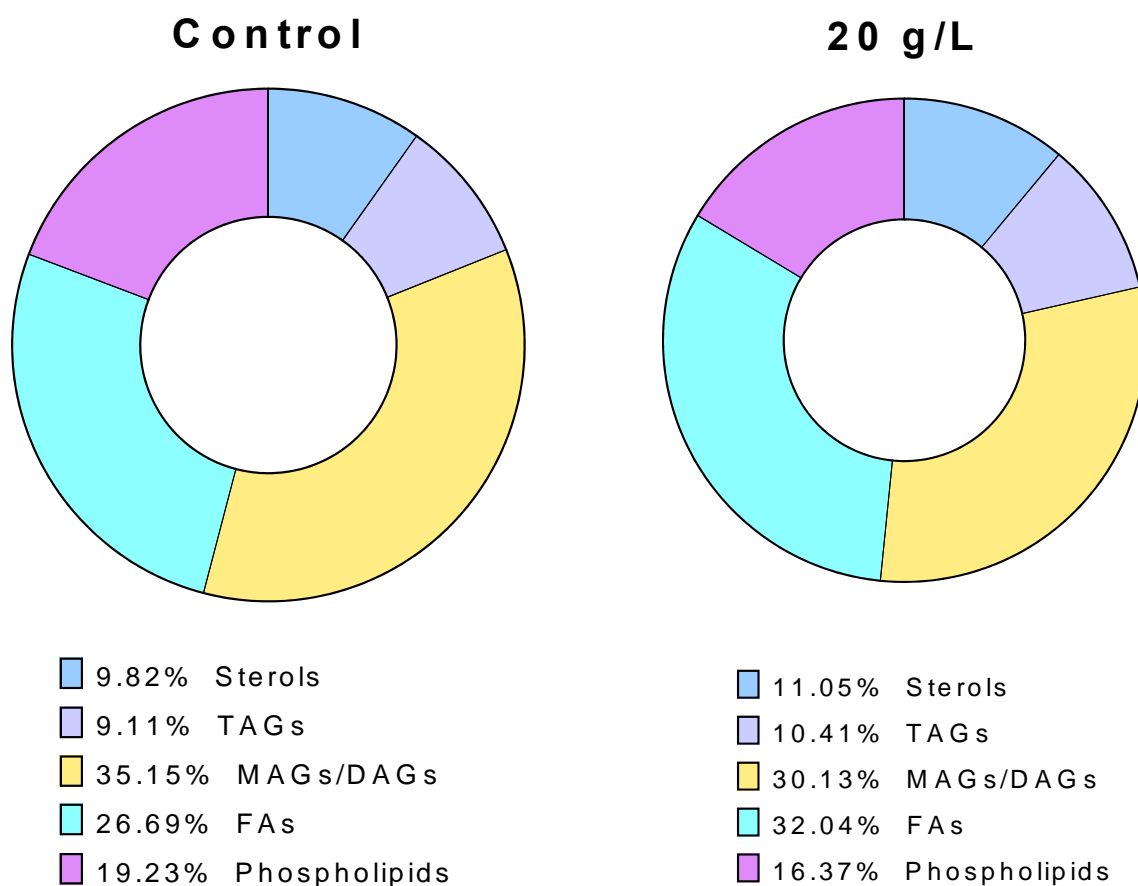
Figure 26. The composition of lipid samples fractionated through SPE.

Incorporation of isotopically labeled glycerol into the TAG backbone

Glycerol is synthesized in algae via an energy intensive pathway, through which glyceraldehyde-3-phosphate produced from glycolysis is enzymatically converted to glycerol phosphate, after which it is enzymatically acylated using glycerol 3-phosphate O-acyltransferase.[239] By adding glycerol exogenously, it was hypothesized that *C. vulgaris* would be able to skip the energy-intensive process of synthesizing glycerol *in vivo*, shifting the products of glycolysis toward energy storage via lipid synthesis pathways. The incorporation of glycerol into the TAG backbone was monitored through the use of isotopically labeled glycerol that was

applied to stationary cells at a concentration of 20 g · L⁻¹. Following 72 h of exposure, lipids

were extracted and fractionated via SPE and the TAG fraction was then transesterified,

acetylated, and analyzed using a GC-MS (Figure 27).[235] In the control sample, the backbone
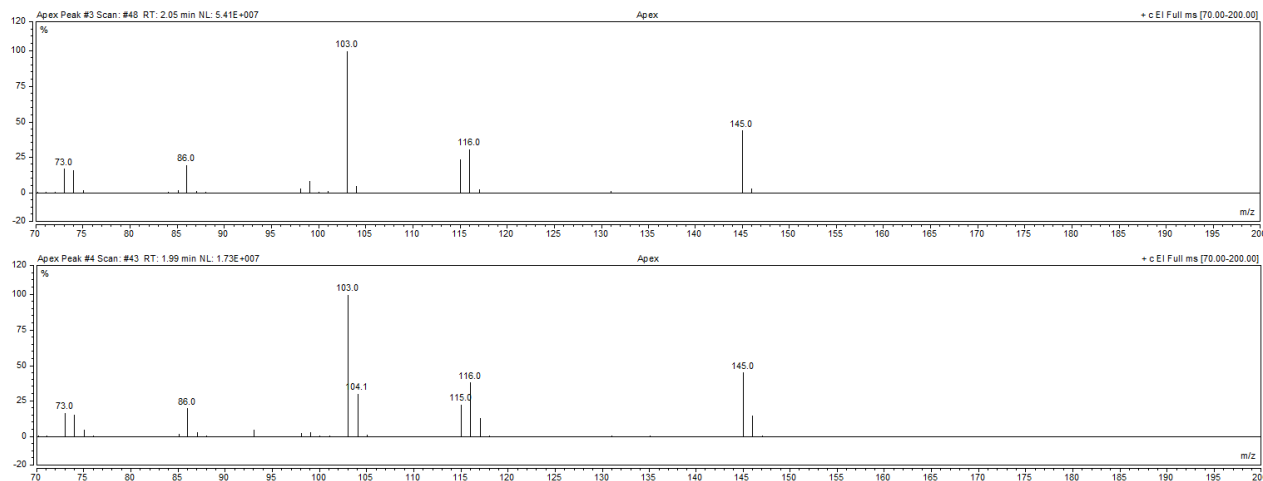
Figure 27. Mass spectra of glycerol dosed and non-dosed cultures. (Top) The mass spectrum
of the derivatized glycerol samples from the transesterified TAG fraction of the non-dosed algae
cultures. (Bottom) The mass spectrum of the derivatized glycerol samples from the transesterified
TAG fraction of the dosed algae cultures.

containing 103 amu peak has a +1 abundance of 5%, just above the theoretical abundance of 4%

expected in nature. On the 20 g · L⁻¹ glycerol sample, however, the 103 amu peak has a +1

abundance of 30%, 6x larger than that of the control, indicating the presence of more ¹³C than

that which is found under natural abundances. Since the glycerol was labeled on one carbon only

and glycerol is a 3-carbon molecule, an increased isotopic abundance to 30% could indicate that

a third of the glycerol used for TAG backbone generation was supplied exogenously rather than

being synthesized *in vivo*.

Photosynthetic capacity measured over time

In order to determine the changes to the photosynthetic apparatus following glycerol

introduction, both oxygen evolution and Chl *a* fluorescence were monitored every 12 h
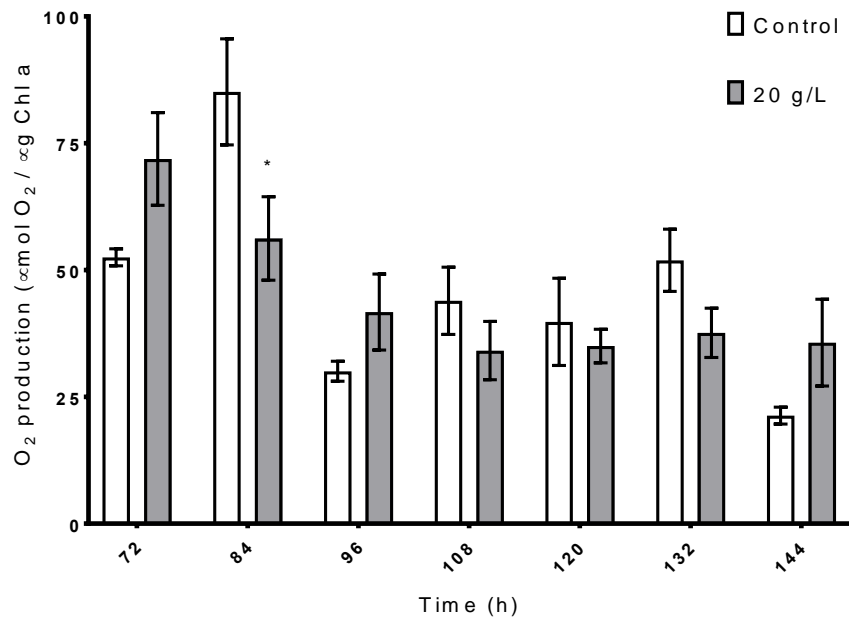
Figure 28. The oxygen production of cells with and without exogenous glycerol measured over time. * indicates p ≤ 0.05, ** indicates p ≤ 0.01, *** indicates p ≤ 0.005, and **** indicates p ≤ 0.001.

beginning at 72 h, the time at which cultures were dosed with glycerol. Oxygen production, an

indicator of both the health of PSII as well as the reliance on linear (rather than cyclic)

photosynthesis, had a statistically significant decrease at 84 h, 12 h after glycerol introduction, at

which point oxygen production was 34% less in the cultures exposed to glycerol when compared

to the control (Figure 28). For the rest of the growth curve, however, the oxygen evolution of the

glycerol-exposed and control cultures are within error of each other. Since photosystem II (PSII)

is known to degrade during stationary phase of cell cultures, it is likely that the glycerol sped up

this process initially, but not enough to outpace the natural degradation of the photosynthetic

apparatus *in vivo*.

The OJIP fluorescent transient was also used to assay the integrity of PSII *in vivo*. This

method allows for the inference of electron flux kinetics within PSII. Using this method, the

kinetics of PSII are inferred, specifically the reduction of Q_A and Q_B, thus showing the

availability of reaction centers to utilize photons for photochemical processes rather than thermochemical processes or fluorescence. Using the log-based plot, it is possible to view the OJIP curve, also known as a Kautsky induction, where the O-step represents F_0, or minimal fluorescence and the point at which all reaction centers are open, and the P-step represents F_M, or maximal fluorescence and the point at which all reaction centers are closed.[157] Plotting the OJIP curves of the 20 g · L^{-1} glycerol cultures over time allows further evidence of decreasing oxygen evolution: after the normal trace of the OJIP at 72 h, the remaining traces show an elevated OJ phase when compared to the IP phase, indicating damage to the oxygen evolution complex
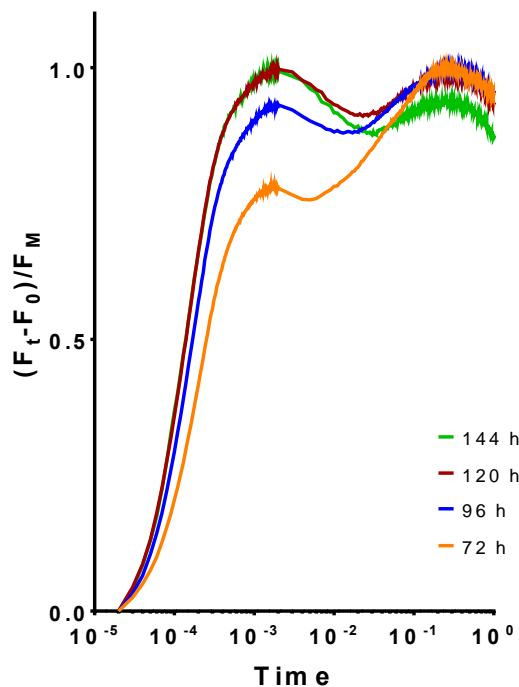
Figure 29. The normalized OJIP curves of glycerol-dosed curves taken over time.

(OEC) and substantiating the oxygen evolution findings (Figure 29).[27, 135] Just after the J-step, there is a characteristic dip in fluorescence indicating the oxidation of the quinone pool on the acceptor side, further indicating damage to the OEC.[155, 158, 164, 169]
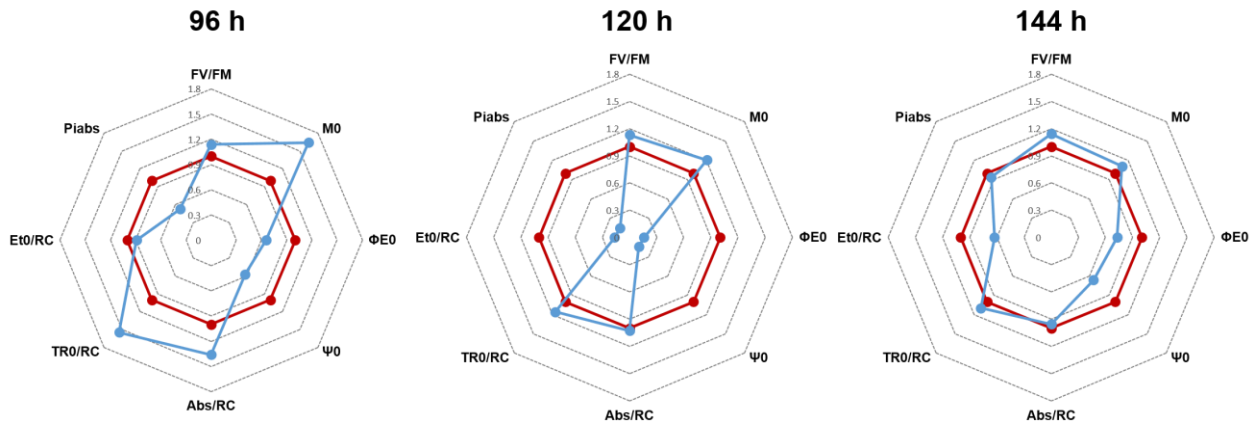
Figure 30. Spiderweb plots of JIP-test parameters derived from the Chl a fluorescent transient over time. Values are normalized to the control value at each time point in order to better visualize the difference between experimental groups.
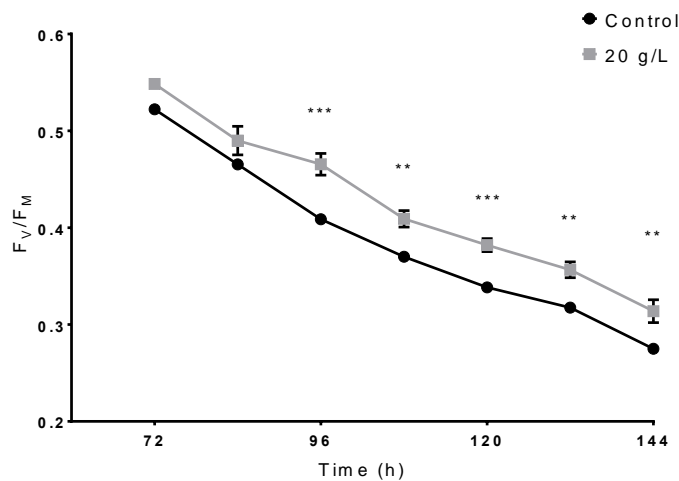
Figure 31. The FV/FM, or photosynthetic efficiency, of cell cultures taken over time. * indicates $p \leq 0.05$, ** indicates $p \leq 0.01$, *** indicates $p \leq 0.005$, and **** indicates $p \leq 0.001$.

While the relative intensities of the OJIP curves allow visual comparisons of electron flux over time, Strasser's JIP test, using the raw data rather than the normalized curves, allows a better idea of electron flux of the steps in electron transport beginning in PSII and ending in PSI (Figure 30)[164] F_v/F_M is the most frequently used parameter and represents the maximum quantum yield of PSII photochemistry for a dark-adapted state. Monitored over time, the F_v/F_M is significantly higher in the glycerol cultures when compared to the control beginning at 96 h, 24 h

after glycerol introduction (Figure 31). M0, the slope of the initial OJ phase, also increases

compared to the control, indicating an increase in the speed of the initial reduction of Q_A (Figure

31). This increase is accompanied by increases in the Abs/RC, or the absorption per reaction

center, an indicator of relative light harvesting antenna size, as well as TR0/RC, the trapped
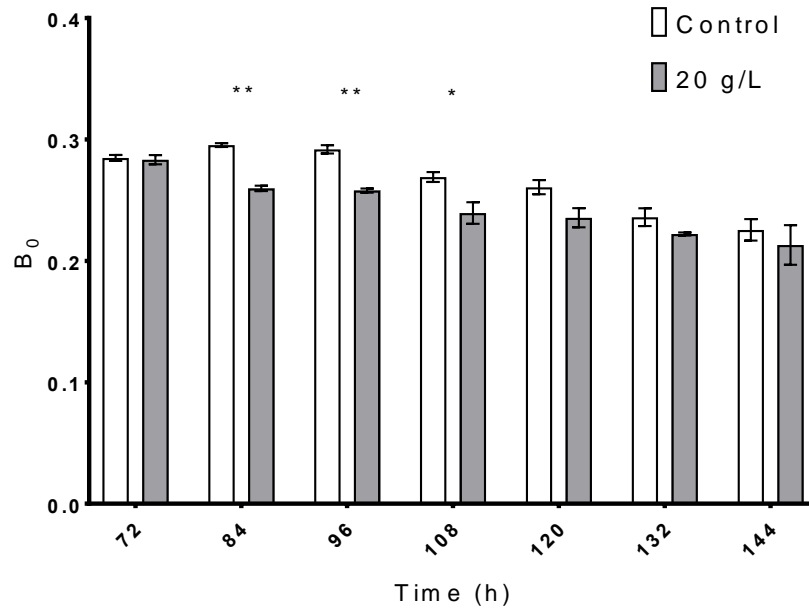
**Figure 32. The B0, or percent of non-reducing QB centers, taken over time in both
dosed and non-dosed cultures**. * indicates $p \leq 0.05$, ** indicates $p \leq 0.01$, *** indicates
$p \leq 0.005$, and **** indicates $p \leq 0.001$.

energy available per reaction center at the initial time point. However, several parameters

decreased in comparison to the control, including the PIabs, the performance index on a per

reaction center basis, as well as the $\phi E0$ and $\Psi 0$ parameters, the electron flux to PSI and the

probability that electrons reach PSI, respectively.

Using a double-hit method of collecting OJIP fluorescence, wherein the OJIP curve was

collected twice with a 1 s relaxation interval in between, it was possible to ascertain the

differences in percentage of Q_B non-reducing centers in the control compared to the glycerol-

exposed cultures. This is calculated through the equation:

$$B_0 = (F_V/F_M - F_V*/F_M*)/F_V/F_M$$

where F_V/F_M is derived from the first pulse and F_V*/F_M* is derived from the second pulse, before which the cultures were not dark adapted.[240] The glycerol cultures had a significantly higher percent of active Q_B reducing centers for the first 36 h after glycerol introduction, after which the control and glycerol-exposed cultures were within error of each other for the remainder of the curve (Figure 32).

Discussion

Correlation between glycerol incorporation and TAG production

Based on the lipid yield and dry mass data alone, it does not appear that exogenous glycerol plays a metabolic role in algal lipid biosynthesis. However, after quantifying the remaining extracellular glycerol using GC-MS, it was clear that the glycerol was being incorporated into the cell (Figure 27). Using the 2-^{13}C glycerol, it was determined that glycerol is, in fact, being directly incorporated into the backbone of TAGs, with a 26% increase in the abundance of [13]C. Interestingly, this did not correlate with a large increase in TAG percent; the glycerol-dosed samples had a 1% increase in TAGs compared to the control. However, this was accompanied by a 6% increase in free fatty acids and a 5 and 4% decrease in MAGs/DAGs and phospholipids, respectively. Previous research has shown that in the presence of environmental stressors, such as nitrogen deprivation, phospholipids are removed from the cell membrane and their fatty acids are removed and attached to glycerol for long-term storage as TAGs.[241] Every one mole of phosopholipids generates two moles of fatty acids; thus the 3% decrease in phospholipids paired with a 6% increase in fatty acids could indicate the removal of fatty acids from the phospholipid bilayer. Furthermore, while the control lipid composition includes more MAGs and DAGs than the glycerol dosed cultures, it is unclear if this is due to a flux toward

TAGs or toward phospholipids, as both lipid species share the acetylated glycerol precursors. Additionally, while the glycerol is consumed by the cells and is subsequently incorporated into the membrane, there is still much more free glycerol than there are TAGs (at the most, the cells produced 3 g · L^{-1} total lipids—all cultures consumed at least double the glycerol); for this reason it is possible that the stress from the osmotic pressure is contributing to the changing lipid metabolism and synthesis. This is also suggested by the decline in rate of lipid production. If the glycerol was being metabolized, but the lipid synthesis rates remained unchanged, this would imply that the glycerol synthesis steps of the pathway were not rate limiting; since the lipid rate decreases sharply despite the influx of additional carbon, it is likely the result of additional stress rather than the presence of glycerol, specifically. However, if the lipid synthesis pathways have, in fact, shifted toward TAG synthesis specifically are not decreasing in flux due to stress, it could be explained by the fact that TAG synthesis is a more energy intensive pathway that takes longer to complete.

Glycerol treatment has a negative effect on the plastoquinone pool

One of the benefits of using *C. vulgaris* as a biofuel feedstock is its ability to thrive both heterotrophically, photoautotrophically, and mixotrophically. However, mixotrophic growth has shown to result in the most production of lipids, as photoautotrophic cultures have decreased overall cell mass due to limits in carbon dioxide sequestration and heterotrophic cultures have limited available reducing equivalents due to the lack of the NADPH and ATP producing photosynthetic light reactions.[76] For this reason, it was hypothesized that glycerol supplementation in the presence of these light reactions would result in an overall greater flux toward TAG synthesis than if the glycerol was applied to a heterotrophic culture, as previously

published. Therefore, to monitor photosynthetic capacity, both the oxygen production and Chl *a* fluorescence were monitored over time.

The oxygen production showed a significant decrease after 12 h of glycerol exposure, after which it remained constantly within error of the control cultures. Since the photosynthetic electron transfer chain reaches its peak capacity in mid-exponential phase before being downregulated and degraded as the cells age, it would appear that while the glycerol caused an initial reduction in PSII activity, this was within the normal magnitude of age-dependent PSII downregulation, it was just expedited in the cultures by 12 h. This reduction in activity correlates with several reductions in Chl *a* fluorescence parameters, including the performance index, the electron flux out of PSII, and the probability that electrons reach PSI. However, it also correlates with increases in the rate of reduction of the Q_A site, FV/FM, and the percent of active Q_B reaction centers. These changes suggest that there may be an overall reduction in available plastoquinones as a reduction in plastoquinone availability would result in a faster rate of quinone reduction as well as a decreased rate of oxygen production, as PSII would be less active. Since the plastoquinone pool would be reduced quickly, it could appear as though PSII was more efficient, as measured through FV/FM, since an increase in flux of the initial QA reduction would result in a higher FV/FM value; the decreasing performance index, however, which offers a more holistic view of the activity of the photosynthetic electron transport chain, suggests that this is not the case.

Glycerol was used for external supplementation in order to directly impact the TAG synthesis pathway. Inadvertently, however, this could also affect other pathways that utilize glycerol or glycerol synthesis precursors and intermediates. This overlap could occur at two different points in metabolic pathways associated with plastoquinone synthesis.[242] If the

additional glycerol has increased the flux of metabolism toward lipid synthesis, this could be problematic for plastoquinone synthesis as acetyl-CoA, the primary building block of lipid synthesis, is also the primary building block needed for the synthesis of isopentenyl diphosphate isomerase, the substrate which is combined with dimethylallyl pyrophosphate to generate geranyl diphosphate via geranyl diphosphate synthase; this becomes farnesyl diphosphate before adding another isopentenyl diphosphate isomerase and dimethylallyl pyrophosphate to produce solanesyl diphosphate, which is used to generate methyl-solanesyl-benzoquinone, the direct precursor of plastiquinones. Redirecting acetyl-CoA to lipid production could stifle flux through this pathway, therefore decreasing overall plastoquinone production. Similarly, glyceraldehyde-3-phosphate, a precursor to *in vivo* glycerol synthesis, is combined with pyruvate to generate 1-deoxy-D-xylulose-5 phosphate, a precursor to the aforementioned dimethylallul pyrophosphate needed for plastoquinone synthesis.[243] If less glycerol is needed, this would contribute to a decreased availability of glyceraldehyde-3-phosphate, which could in turn decrease the flux toward plastoquinone synthesis. Further experiments should be undertaken to extract and quantify the plastoquinone pool to determine if the implied reduction in availability is real.

Conclusions

The use of exogenous glycerol is a promising method through which to recycle the primary byproduct of biodiesel production for direct incorporation into the TAG backbone. However, further optimization is needed to determine the conditions under which it can both contribute to increasing rates of TAG synthesis while simultaneously taking advantage of the energy producing light reactions of photosynthesis.

CHAPTER 6

THE PLASTICITY OF PHOTOSYSTEM II IN *CHLORELLA VULGARIS*

DEMONSTRATED BY INCREASING CONCENTRATIONS OF MANGANESE

Introduction

        Once responsible for the largest extinction event known on earth, oxygenic photosynthesis now sustains aerobic life through the generation of all atmospheric oxygen, making it easily the most important and fundamental biological mechanism on earth. For this reason it is of no surprise that this pathway has since evolved to be highly regulated and specific, enabling it to survive a variety of environmental stressors from the Archean era to the modern age.[244] Of the most dangerous environmental stressors are those that generate large amounts of reactive oxygen species (ROS), as the highly tuned electron transport mechanism relies on redox active metal cofactors to function effectively, including iron in cytochrome complexes b_{559} and b_6-f, iron-sulfur clusters in photosystem I (PSI) and ferredoxin, copper in plastocyanin, and manganese in the oxygen-evolving complex (OEC) of photosystem II (PSII).[59, 245] When tuned correctly, these metals generate on average a decreasing reduction potential throughout the photosynthetic electron chain, with electrons traveling "downhill" after being excited via photons at P680 in PSII. After transport to PSI, via plastocyanin, the electron is re-energized by another photon, allowing it to make the remaining reductions downhill again until it reduces ferredoxin reductase and is used to generate NADPH.

        Environmental stressors, however, can disrupt this pathway due to either photoinhibition, wherein PSII is damaged via a light-dependent disruption resulting in the release of manganese ions from the OEC, or by the inhibition of PSII damage repair.[246-247] These stressors often trigger the two modes of inhibition synergistically.[248-250] The overexposure of the photosynthetic

101

apparatus to metals, particularly redox-active transition metals, can result in an influx of damaging ROS, often caused by interactions with photosystems or their reaction intermediates. For example, excess Fe(III) can be reduced with $O_2^{-\bullet}$, which is generated along with H_2O_2 at the acceptor side of PSI following the transfer of electrons from reduced ferredoxin to O_2. After the reduction of Fe(III) to Fe(II), H_2O_2 and Fe(II) partake in the Fenton reaction, producing $HO^{\bullet}$ and $HO_2^{\bullet}$, arguably the most biologically damaging ROS.[251] Once these ROS accumulate, they can have a detrimental effect on the metabolism of the organism, as oxidative damage quickly spreads to lipids, proteins, and nucleic acids. In unicellular organisms, such as the unicellular green alga *Chlorella vulgaris*, this effect can be elevated by the lack of neighbor cells to help mitigate the oxidative burst as cells are limited by the redox-active enzymes that are present in that particular moment.[252] Heavy metals, including lead, cadmium, arsenic, and copper, among others, are known to inhibit photosynthesis and plant growth, decrease biosynthesis of pigment molecules, and decrease electron transport chain (ETC) phosphorylation, causing ETC dysregulation and dangerous ROS generation. However, ongoing research in the Kolling lab has shown that high concentrations of manganese enhances photosynthetic capacity rather than causing intracellular damage. This study seeks to determine the mechanism(s) through which this enhancement occurs.

Previous photosynthetic studies on manganese exposure (See Chapter 5) utilized oxygen evolution and chlorophyll *a* (Chl *a*) OJIP fluorescence to determine the photosynthetic efficiency of cells exposed to increasing concentrations of manganese. However, these methods are limited; although reaction centers are not homogenous and consist of various sub-populations, the parameters measured show the average of all reaction centers within the sample. While useful for determining the effect of abiotic stressors, this does not take into account the known

heterogeneity of both the antennas and reducing sites of PSII. The antennas of PSII are divided between PSIIα and PSIIβ reaction centers, where PSIIα refers to "super-complex" light harvesting antennas with large antenna sizes and high degrees of connectivity located into the thylakoid grana and PSIIβ refers to "core complex" light harvesting antennas with 2-3x smaller antennas and reduced connectivity located in the stroma-exposed region of the thylakoid.[253-254] Simultaneously, PSII reaction centers exist as either Q_B reducing or Q_B non-reducing, the latter of which is incapable of contributing to the reduction of the plastoquinone pool.[255] By using a variety of *in vivo* florescence measurements on *C. vulgaris* exposed to increasing concentrations of manganese, the mechanism of increased photosynthetic output could be better understood.

Materials and Methods

Strain and culture growth conditions

Cultures of *C. vulgaris* (Carolina Biological Supply) were maintained on lysogeny broth agar plates and for batch cultures, inoculated into 25 mL of modified *Chlorella* medium supplemented with 20 g/L dextrose. All cultures were grown in 50-mL sterile Erlenmeyer flasks capped with aluminum foil [76]. Cultures were grown in triplicate, using a 1-mL inoculum from a stationary phase culture and kept under constant white light at 30 µmol photons $\cdot$ m^{-2} $\cdot$ s^{-1} at 25 °C with an orbital rotational speed of 100 rpm (verified using a tachometer).

Experimental design

Prior to culture inoculation, manganese-deprived modified *Chlorella* medium was dosed with an autoclaved stock of $MnCl_2$ and ultrapure water, ensuring that all cultures had equal concentrations of all other medium components. The control cultures' media was dosed to generate a working concentration of 0.070 mM manganese, the standard concentration for modified *Chlorella* medium. Experimental cultures' media were raised from 50x (3.50 mM) to

1000x (70.0 mM) the control, each concentration produced in triplicate. Cultures were maintained under constant light and grown until they reached mid-stationary phase, shown through a spectroscopic cell density of between 8–10 AU.

Spectroscopic cell density

Cell density (turbidity) was obtained using a Shimadzu UV-1800 spectrophotometer (Shimadzu Corp., Kyoto, JP) at 750 nm as previously described.[76]

Pigment extraction

Pigments were extracted as previously described and measured from 470 to 700 nm. [76] Chl *a,* chlorophyll *b* (Chl *b),* and total carotenoids were calculated using the following equations:[147]

$[Chl\ a] = (12.47 \times Abs_{665.1}) - (3.62 \times Abs_{649.1})$

$[Chl\ b] = (25.06 \times Abs_{649.1}) - (6.5 \times Abs_{665.1})$

$[Carotenoids] = [\ (1000 \times Abs_{480}) - (1.29 \times [Chl\ a]) - (53.78 \times [Chl\ b])\ ] / 220$

Chlorophyll fluorescence induction *in vivo*

Photosynthetic electron transfer fluxes were inferred from Chl *a* fluorescence using a Photon Systems Instruments FL 3500 fluorometer as previously described (Chapter 3).[27] To ensure reproducibility between samples, algal cultures were diluted to 2 µg · mL^{-1} total pigments using medium of the same manganese concentration before dark adaptation and subsequent measurements. The OJIP protocol included a 1-s actinic illumination using a 630-nm light at an intensity of 2,400 µmol photons m^{-2} · s^{-1}. Fluorometry parameters (JIP test) were calculated as outlined by Stirbet, et al. [222]

To further increase understanding of the mechanisms at work and to estimate the relative amount of Q_B non-reducing centers, the double hit method was used, collecting Chl *a*

fluorescence data at two subsequent 1-s pulses. This method generates two OJIP transients that can be separated and normalized to t = 0.[240] While the first pulse was conducted following dark adaptation, meaning that all the reaction centers were open, the second pulse will only excite so-called "fast-opening" reaction centers, allowing for the calculation of non-reducing centers (centers which are unable to open in time for the second pulse) through the equation:

$$B_0 = (F_V/F_M - F_V*/F_M*)/F_V/F_M$$

where F_V/F_M is derived from the first pulse and F_V*/F_M* is derived from the second pulse. The relative amount of non-reducing Q_B reaction centers were also estimated by using the variable fluorescence of the OJ phase, calculated using the following equation:

$$V_J = (F_{2ms} - F_0)/F_V$$

generated using the OJIP produced by the first pulse. This is supported by the fact that high light intensities, such as the one used in this measurement, results in faster accumulation of Q_A^- and double-reduced Q_B centers, thus enabling estimation from the OJ phase rather than the terminal plateau.[256]

In addition to quantifying active Q_B centers, active Q_A reducing centers were quantified through the inhibition of PSII with 3-(3,4-dichlorophenyl)-1,1-dimethylurea (DCMU), a selective inhibitor that blocks the Q_B site.[257] When DCMU-inhibited cells are measured for Chl *a* fluorescence, the normal polyphasic transient is replaced by a single-phase plateau, indicating the reduction of Q_A to Q_A^-. By normalizing $F_0 = 0$ and integrating the resulting curve, the relative number of active Q_A centers can be determined.[258] Dark adapted samples were exposed to 50 mM DCMU for 10 min before measuring using the same protocol used for the JIP test. GraphPad Prism v.7.01 was used to perform the integrations following normalization.[240]

Q_A^- Reoxidation

Q_A^- reoxidation measurements were conducted using 20 data points per decade beginning at 50 µs and continuing for 120 s. The actinic flash had an intensity of 2,400 µmol photons m^{-2} · s^{-1} while the flash duration was for 50 µs. The measuring flash intensity was 24,000 µmol photons m^{-2} · s^{-1}. Cultures were diluted to 2 µg · mL^{-1} and dark adapted for 5 min prior to measurements.[240] The Q_A^- reoxidation decay was determined by fitting the data to a triexponential model:

$$F(t) = F' + A_1 e^{-K_1 t} + A_2 e^{-K_2 t} + A_3 e^{-K_3 t}$$

where F(t) is the fluorescence at time t, K_n is the rate constant, A_n is the amplitude of the fluorescence relaxation phase, and F' is the stable minimal fluorescence at the end of the decay.[259] The three phases are divided into fast, medium, and slow, wherein the fast phase is representative of the forward electron transfer from Q_A to Q_B centers containing a bound plastoquinone in the oxidized or semi-reduced form, the medium phase is representative of the Q_A centers that are waiting on plastoquinone to bind to the Q_B site in order to conduct forward electron transfer, and the slow phase is representative of the Q_A^- reoxidation that is dependent on the back reaction with the S-states of the OEC.[260] This slow phase recombination indicates that the PSII reaction centers are incapable of transferring an electron from Q_A^- to Q_B, therefore requiring the donor side of PSII. The percentage of this phase amplitude can be used to indicate the Q_B-nonreducing centers.[240] The curve fitting was performed in R.

S-states

The redox state of the OEC can be determined using short, actinic light flashes to sequentially advance from S0 to S4, where each S-state represents a different reduction state of the OEC.[261-262] The contribution of inactive PSII centers can be estimated by the difference

between the S4 $\to$ S0 fluorescence decay and the initial F_0, since the fluorescence decay following the fourth flash is primarily controlled by inactive centers.[263-264] S-states were measured through 4 saturating flashes at 80,000 µmol photons $m^{-2} \cdot s^{-1}$ voltage that were 100 µs in duration and 300 ms apart, each causing a single turnover of PSII.[240] Cells were dark adapted for 5 min prior to measurements.

Quenching analysis

When photons reach PSII reaction centers, they have one of three final destinations: they are used for photochemistry, they are emitted as fluorescence, or they are dissipated as non-photochemical quenching (NPQ), the latter of which releases the energy via heat. These three fates combine to be unity, indicating that a change in one abundance will result in proportional changes in the others. Thus by determining the amount of NPQ and photochemistry through fluorescence techniques, a total picture of photon fate can be generated.[265]

Quenching analysis was used on dark-adapted cells with an actinic intensity of 300 µmol photons $m^{-2} \cdot s^{-1}$, a saturating pulse intensity of 64,000 µmol photons $m^{-2} \cdot s^{-}$, and a measuring flash voltage of 80%. There was a dark relaxation duration of 20 s between pulses.[266] Photochemical coefficients were calculated as previously reported.[157]

Statistical analysis

Statistical analyses were performed with GraphPad Prism 7.01 (GraphPad Software, Inc.). Optical density, pigment, and fluorometry data were analyzed through two-way repeated measures analysis of variance (ANOVA) using a Bonferroni correction to maintain a family-wise error rate below 0.05. The remaining data were analyzed through multiple comparisons of means conducted using Welch's t-tests. The family-wise error rate for each figure was maintained at 0.05 through the use of the Holm-Bonferroni method. Statistical significance is indicated

numerically through increasing asterisks, where * indicates $p \leq 0.05$, ** indicates $p \leq 0.01$, ***

indicates $p \leq 0.005$, and **** indicates $p \leq 0.001$. Figures show the means of triplicate data and

the error bars denote the standard error of the measurement, unless otherwise specified.

Results

Photosynthesis performance

The most common parameter used for the measurement of total photosynthetic

performance is F_V/F_M, known as photosynthetic efficiency. This is measured through Chl *a* OJIP

fluorescence, through which dark adapted samples are exposed to a single saturating light pulse.
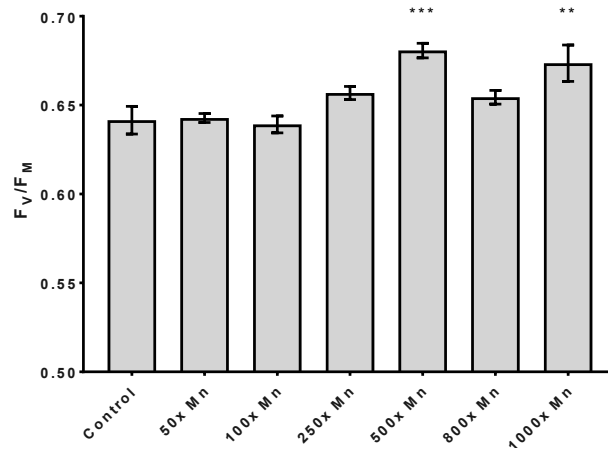
Figure 33. The FV/FM measured in exponential phase for cultures in increasing manganese concentrations. * indicates $p \leq 0.05$, ** indicates $p \leq 0.01$, *** indicates $p \leq$ 0.005, and **** indicates $p \leq 0.001$.

The *C. vulgaris* cultures were measured in mid-stationary phase, the phase in which previous

research has shown that they are in their highest photosynthetic efficiency. However, as the

concentration of manganese increased to over 100x the control concentration, the F_V/F_M

increased as well, with the 500 and 1000x concentrations exhibiting significantly higher F_V/F_M

than the control culture (Figure 33). This is of interest despite the seemingly insignificant

magnitude of increase as the maximum F_V/F_M value – that being the most efficient PSII is seen

in nature – occurs at an F_V/F_M value of 0.68, which the 500x manganese samples have reached

(0.68 ± 0.01). Therefore, it appears that manganese alone is able to increase photosynthetic

efficiency, as also shown in previous research in the Kolling lab (see Chapter 4). This increase
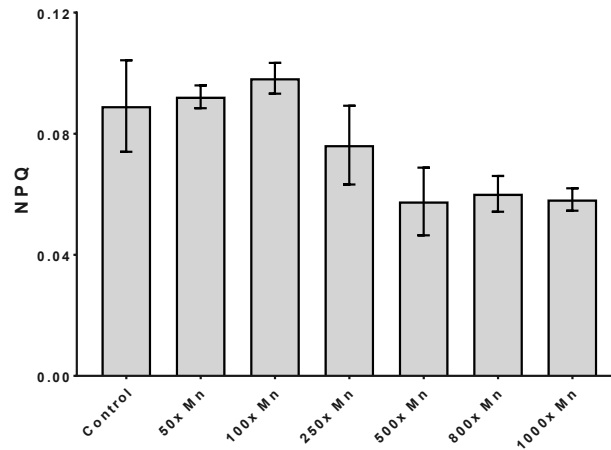
Figure 34. The non-photochemical quenching coefficient of cultures with increasing manganese concentrations. * indicates $p \leq 0.05$, ** indicates $p \leq 0.01$, *** indicates $p \leq 0.005$, and **** indicates $p \leq 0.001$.

could occur from either a decrease in NPQ or else an increased amount of reducing reaction

centers—or both. F_0, which is dependent on competition between fluorescence and other types of

exciton transfer (primarily photochemistry and NPQ), increased in the 500x manganese culture

and decreased in the 1000x manganese cultures. The F_M, a product of competition of internal

conversion alone, also increased in the 500x manganese and decreased in the 1000x manganese

cultures. The increases in F_M and F_0 for the 500x manganese cultures could both be due to an

increase in photosynthetic electron transfer, especially if corroborated through other fluorescence

measurements. Using a quenching analysis protocol in which the dark adapted cells were
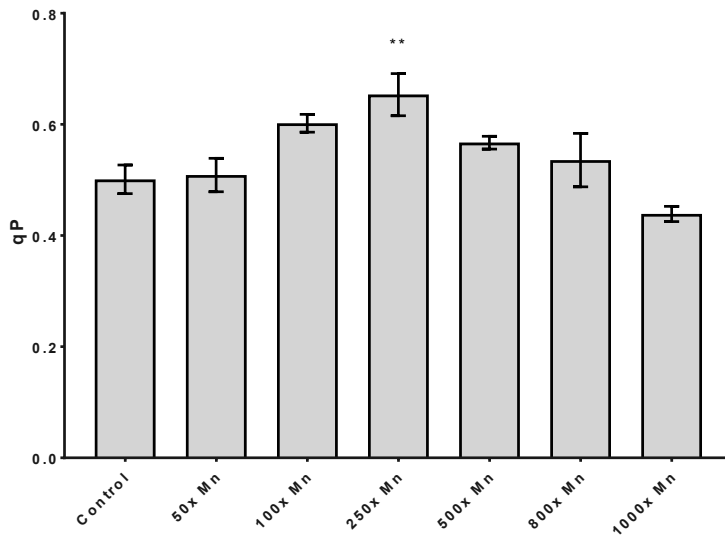
Figure 35. The photochemical coefficient of cultures exposed to increasing concentrations of manganese, measured through the quenching analysis protocol. * indicates $p \leq 0.05$, ** indicates $p \leq 0.01$, *** indicates $p \leq 0.005$, and **** indicates $p \leq 0.001$.

exposed to a saturating light pulse before adding actinic light and several subsequent saturating

pulses to the non-dark adapted samples, the elative amount of photons dissipated as NPQ was

determined. Both the 500x and 1000x manganese cultures dissipated fewer photons through

NPQ than the control cultures, demonstrating that although the 1000x manganese cultures had an

overall decreased photosynthetic capacity, the increased manganese did lead to an increase in

efficiency of photon usage, as more photons were used directly for photochemistry than

dissipative processes (Figure 34). While the 250x manganese culture resulted in a decreased

NPQ, it did not result in a significantly higher F_V/F_M; however, the mean was higher than that of

the control sample, showing that further experiments could establish a significant difference.

This is supported by qP, the photochemical coefficient for quenching analysis, which shows

increases in the 250 and 500x concentrations, though only the 250x manganese cultures

established a significant difference (Figure 35).

Another measurement of the capacity of photosynthesis is the rate at which the Q_A sites are reduced, which is addressed using the M0 parameter of the JIP test. This parameter is the equivalent of the slope of the OJ phase of the Chl a fluorescent transient, which begins when the plastoquinone pool is completely oxidized and ends at an undefined intermediary step in which the plastoquinone pool is only partly reduced. Outside of the 1000x concentration, there were not significant differences between the M0 values of the different concentrations of manganese, indicating that, until applied at excessive concentrations, manganese does not affect the kinetics of the Q_A site (Figure 36).
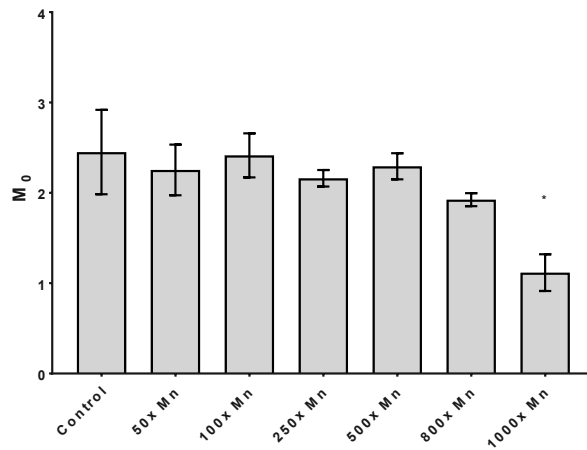
Figure 36. The slope of the OJ phase as derived from the Chl a transient, indicating the flux of the initial QA reduction. * indicates $p \leq 0.05$, ** indicates $p \leq 0.01$, *** indicates $p \leq 0.005$, and **** indicates $p \leq 0.001$.

The performance index per absorbed photon (PIabs), a parameter derived from the OJIP curve that considers the effect of photon absorption, transfer of excitons, and subsequent charge separation via electron transfer, was increased by 28, 26, and 125% when compared to the control in the 250, 500, and 1000x cultures, respectively, suggesting that manganese does not only impact the electron flow through PSII but that, when present in high concentrations, it affects the electron flow through the entire pathway. This is supported by an increase in the

probability of electrons that pass through PSI, as it is possible that either the intermediate

proteins or PSI is causing the increased performance index in high manganese cultures.

However, direct measurement of PSI is outside of the scope of this study as it requires a specific

fluorescence analysis (I820) and was unavailable.

Antenna complexes

Another parameter that is generated from the Chl *a* fluorescence induction curve is the

Abs/RC, or the average photons absorbed per reaction center. This parameter is used as an

estimation of the apparent antenna size as a larger antenna will result in increased absorption

capacity for photons, thus increasing Abs/RC. As the concentration of manganese was increased,

the Abs/RC increased with increases of 52, 65, 55, and 51% for the 50, 100, 250, and 500x

manganese concentrations, respectively (Figure 37). As seen with several other parameters, this
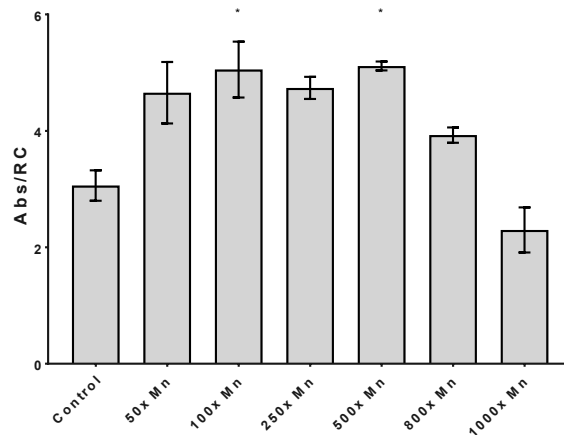
Figure 37. The Abs/RC of manganese-exposed cultures derived from the Chl a fluorescent transient. Abs/RC is indicative of the relative size of the light harvesting antenna complexes. * indicates $p \leq 0.05$, ** indicates $p \leq 0.01$, *** indicates $p \leq 0.005$, and **** indicates $p \leq 0.001$.

decreases at the 1000x manganese concentration, with the 1000x manganese culture having an

Abs/RC that is 75% of the control cultures. This suggests that manganese does lead to an overall

increase in antenna size for up to 500x manganese concentration, which also suggests an increase

112

in the ratio of PSIIα to PSIIβ reaction centers. As discussed previously, the light harvesting antennas can come in two sizes: the "super-complex" PSIIα centers and the "core complex" PSIIβ centers. Ongoing work is attempting to determine the ratio's dependence on manganese concentration by using the fast fluorescence induction, a method that uses a single-turnover saturating flash that generates a fluorescence induction rise. This rise is then mathematically fitted to a theoretical induction curve to determine the functional absorption cross section of the average antenna complex, the optical absorption cross section (absolute antenna size), the sigmoidicity, the PSIIα and PSIIβ stoichiometry, and the PSIIα and PSIIβ reaction center excitation rates. Additionally, the samples grown in increasing manganese concentrations will be analyzed using 77K fluorescence. This method freezes cells in liquid nitrogen and looks for fluorescence peaks at 685, 695, and 735 nm, in which the first two bands correspond to PSII and the last corresponds to fluorescence generated from PSI. By quantifying the ratios of the PSII-related fluorescence bands versus the PSI-related fluorescence bands, it is possible to determine the balance of the state transitions in the system. State transitions are a regulatory mechanism that balances the distribution of photons between PSI and PSII and decreases the likelihood of photoinhibition resulting from photoexcitation. If the system is weighted toward state 1, it indicates that the photons are being preferentially absorbed by PSI to excite P700; if the system is weighted toward state 2, it indicates that the photons are being preferentially absorbed by PSII to excite P680. Ongoing work is building a low-cost tabletop 77K fluorometer that will be used to generate this data.

Reducing centers

In addition to changing antenna structure, an increase in active reducing centers could result in an increased overall photosynthetic flux. In order to determine the relative amount of

113
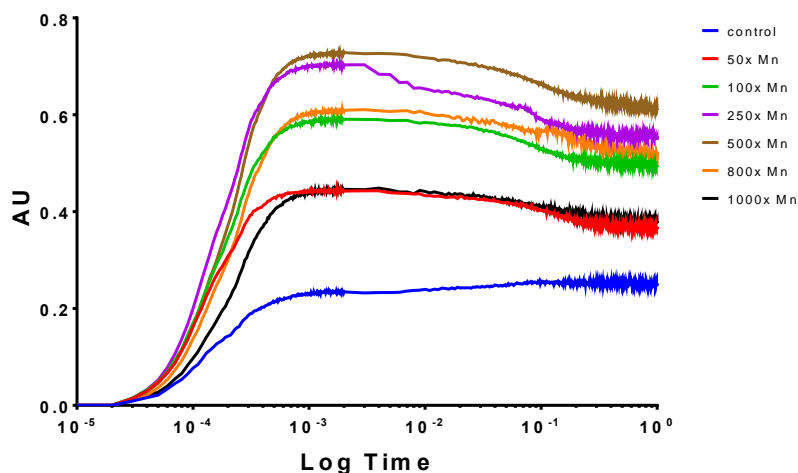
Figure 38. The Chl a fluorescent transient of manganese-exposed cultures dosed with DCMU before measurement. The curves are integrated in order to determine the relative quantity of active Q_A centers.
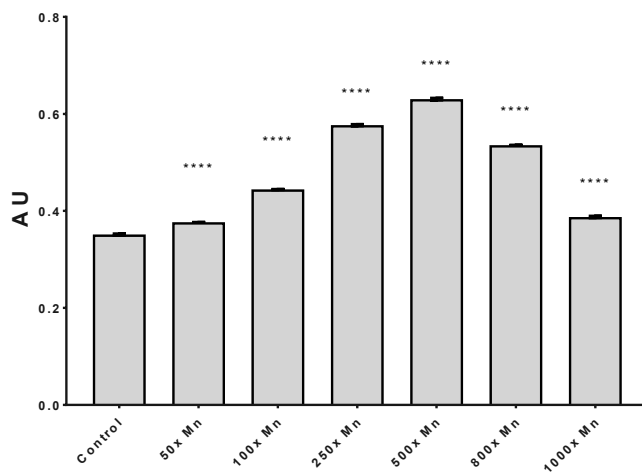
Figure 39. The quantification of QA centers derived from integrating the curves of figure 6. * indicates $p \leq 0.05$, ** indicates $p \leq 0.01$, *** indicates $p \leq 0.005$, and **** indicates $p \leq 0.001$.

active Q_A sites, the initial point of electron transport in PSII, the cells were exposed to DCMU, an herbicide that selectively binds to the Q_B site of PSII and inhibits electron transfer. The resulting fluorescent transient reaches its maximum output once all Q_A sites are reduced, generating a plot that can be integrated to determine the relative amount of active Q_A sites within

114
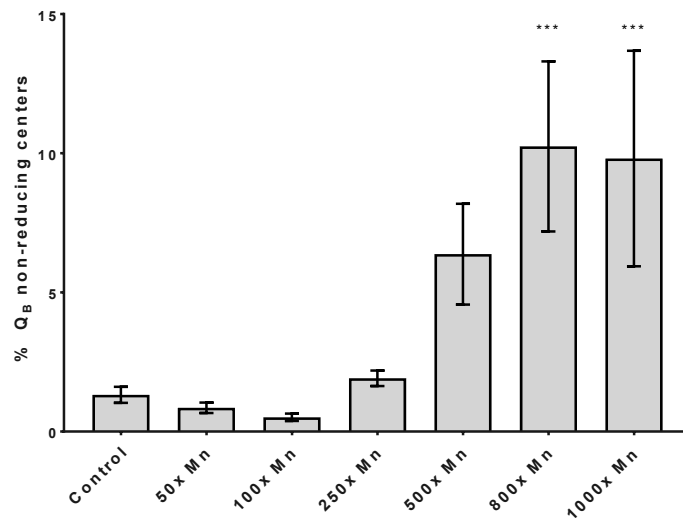
Figure 40. The percent of non-reducing QB centers as measured through the double hit method for OJIP fluorescence. * indicates $p \leq 0.05$, ** indicates $p \leq 0.01$, *** indicates $p \leq 0.005$, and **** indicates $p \leq 0.001$.
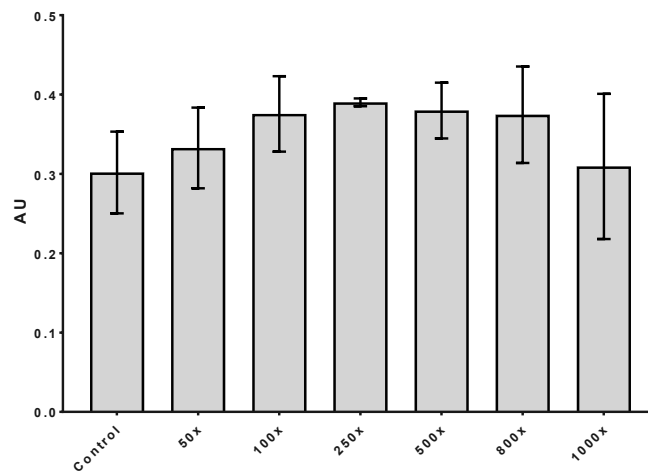
Figure 41. The relative quantity of non-reducing QB centers as measured through S-state fluorescence. * indicates $p \leq 0.05$, ** indicates $p \leq 0.01$, *** indicates $p \leq 0.005$, and **** indicates $p \leq 0.001$.

a sample (Figure 38). The resulting analysis suggests that manganese plays a positive role in increasing the activity of Q_A sites up to an extent, with the maximum number of active Q_A sites found at the 500x manganese concentration with a 76% increase over the control, after which the abundance decreased with increasing concentrations (Figure 39). Using the double hit method

115

for collecting the OJIP fluorescence transient, it was also possible to determine the relative amount of Q_B sites that were non-reducing. While it would be expected that Q_B site activity would increase with Q_A activity, this was not observed: instead, as the concentration of manganese increased, the relative amount of inactive Q_B centers increased as well (Figure 40). While this is problematic when put in the context of both the OJIP fluorescence and DCMU measurements, it is further corroborated by the analysis of the S-state fluorescence: the percent of non-reducing Q_B centers that contribute to fluorescence output increases with manganese concentration, although with the S-states fluorescence, it decreases again following the 500x manganese concentration (Figure 41). Likewise, the variable fluorescence at the J-phase of the OJIP curve decreases with manganese concentration, indicating a decreasing amount of Q_B reducing centers. Unlike the large differences seen with the double hit method, this analysis suggested that there was up to a 9% decrease in active reducing centers, with the 250x manganese concentration having the least amount of active centers. Given the conflicting data between these analyses, future work will seek out other ways to measure the activity of the Q_B centers in order to determine the most accurate way of generating the needed fluorescence data.

Conclusions

The results of this study suggest overall plasticity in the heterogeneity of PSII reaction centers in the presence of high levels of manganese, both in the terms of antenna size as well as reduction potential of the Q_A and Q_B sites. While preliminary analysis suggests an increased photochemical potential with 500x the control manganese concentration, much of the data is self-conflicting, indicating that further study is needed to sort out the inconsistencies in analysis. Further analytical techniques including 77K fluorescence and fast fluorescent induction should be used to gather further information about the efficiency of photon absorption and the

plastoquinone pool should be quantified using liquid chromatography in order to determine if there are any changes in plastoquinone availability that are affecting PSII functionality. Additionally, analysis of post-translational modifications of the photosynthesis-related proteins can give more evidence as to the regulatory mechanisms at play in the presence of high manganese concentrations.

CHAPTER 7

CONCLUSIONS AND FUTURE OUTLOOKS

C. vulgaris is a robust, single-celled green algae that contains a single chloroplast that can take up greater than 80% of its internal volume. This, when paired with its ability to survive harsh and nutrient-depleted conditions and also reproduce at an exponential rate, makes it an excellent model system for biological monitoring of contaminant effects, lipid metabolism, and fundamental photosynthesis research. However, this alga is used much less frequently than its long-time sequenced cousin, *Chlamydomonas reinhardtii*, despite the fact that *C. vulgaris*' adaptability and stability in adverse environments make it a better candidate for both phycoremediation efforts as well as optimization for use as a biofuel feedstock. These studies aimed to enhance the placement of *C. vulgaris* in this field of research through the optimization of physiological and photosynthetic characterization that can be applied to a wide range of studies.

Specific Aim 1 characterized the effect of Poast, an over-the-counter herbicide formulation used in the prevention of broad-leafed grasses, on *C. vulgaris*, a non-target organism. This study used concentrations more than 16x less than the manufacturers recommended usage concentration and found that despite the fact that *C. vulgaris* is not a target organism, it was severely inhibited after only 30 min of exposure, with less than 20% of the cells remaining viable. Furthermore, it was determined that one of the sites of action was at the OEC of PSII, despite the fact that sethoxydim, the labeled active ingredient, is supposed to be preferential to ACCase. *In vitro* studies tested sethoxydim, mineral spirits, naphthalene, and a polyethylene glycol, all substances known or inferred to be included in the herbicide formulation, but none of them recreated the inhibitory effect seen with the formulation.

Without further knowledge about components of the formulation, it is impossible to know whether one of the chemicals is specifically harmful to green algae or if multiple components are having a synergistic effect. While ^{1}H NMR was used to determine the identifiable components of the herbicide mixture, a more thorough analysis could be conducted through liquid chromatography fractionation followed by mass spectrometric analysis. However, even if specific chemical species could be successfully isolated, a methodological approach would have to be taken to determine the possibility of synergistic effects. However, since the formulation is proprietary, it is likely that further analysis would require permission from the manufacturer.

Specific Aim 2 sought to understand the capability of *C. vulgaris* to bioaccumulate manganese, as a possible route of phycoremediation for manganese contaminated waterways. While the literature has shown dramatic inhibitory effects for other metals including cobalt, iron, cadmium, copper, and others, excess manganese did not result in significant inhibitory effects, even at concentrations up to 500x that of the control. Additionally, the manganese was sequestered into the cells to concentrations greatly exceeding that of diffusion equilibrium, with a maximum of 55x the manganese content of the external media being held in the cells. While the manganese had a sharp increase in concentration throughout the first few points of the growth curve, it peaked in concentration around mid-exponential phase, despite the fact that cells continued to increase in number until the beginning of stationary phase. One potential reason for this phenomenon could be that the manganese sequestration is related to photosynthetic activity. Since both pigment content and photosynthetic activity peak near mid-exponential, this could potentially correlate with the intake of manganese, a mechanism that would allow cells to have excess manganese available in the case of PSII turnover due to photoinhibition or other

119

protective processes. Ongoing research is growing manganese-exposed cells in both mixotrophic and heterotrophic conditions to determine the light-dependency of manganese sequestration. A second potential contributor to the peak influx of manganese at mid-exponential phase is the availability of exogenous carbon sources. Previous work in the Kolling lab has shown that carbon availability becomes severely limited beginning in mid-exponential phase — which is also the reason why the cells stop dividing in the first place.[76] If the manganese is sequestered into the cells by active transport, this would further support the need for excess carbon availability in order to supply the energy investment for transportation.

While the expectation was for manganese to inhibit *C. vulgaris*, it instead increased photosynthetic flux, as seen through both the oxygen evolution probing as well as Chl *a* fluorescence. Since the light reactions of photosynthesis increase overall lipid production, it is possible that this effect could be utilized in order to improve the feasibility of *C. vulgaris* as a feedstock for biodiesel. However, data collected showed no increases in lipid production across manganese treatments, suggesting that additional environmental stressors would need to be applied in order to successfully utilize manganese for increased biodiesel feasibility. Ongoing research is seeking to combine manganese exposure with nitrogen deprivation, an established environmental stressor for increasing lipid yield, in order to see if the effect of having increased photosynthetic flux (and therefore increased production of reducing equivalents needed for lipid synthesis) results in further increases to lipid production under nitrogen deplete conditions.

Specific Aim 3 combined glycerol and constant light conditions in order to increase the lipid production in *C. vulgaris*. While lipid production itself was not increased significantly across glycerol-dosed cultures, the application of glycerol in early stationary phase did result in an increase in overall lipid percent for the 10 and 20 g · L^{-1}, as well as minor changes in the lipid

120

composition between treated and untreated cultures. Furthermore, it was found that the exogenously applied glycerol was directly incorporated into the TAG backbone. While the lack of increase in lipid production suggests that the production of glycerol is not rate-limiting within the cells, their ability to directly use glycerol is promising for the reduction of waste generated from biodiesel production, as 1 molar equivalent of glycerol will be produced for every 3 molar equivalents of fatty acids. If this can be reused for further lipid production, it could significantly reduce costs for biodiesel production.

This study does not support studies in the literature, which determined an increase in lipid flux following glycerol supplementation of heterotrophic cultures in stationary phase. This suggests that something along the photosynthetic pathway could be somehow inhibiting the flux toward TAG production, most likely through carbon fixation for carbohydrate production. Additionally, the glycerol-mediated degradation of the photosynthetic pathway suggests further convergences in pathways requiring further analysis. One possibility is that exogenous glycerol inhibits the plastoquinone synthesis pathway, decreasing the overall electron transfer capacity of the photosynthetic electron transport chain. This will be investigated through extraction and liquid chromatography based quantification of plastoquinones. Furthermore, additional photosynthetic studies will seek to understand the mechanism through which glycerol supplementation reduced the overall photosynthetic capacity of *C. vulgaris*.

Specific Aim 4 expanded on the previous manganese work by seeking to understand the mechanism through which manganese was increasing the overall photosynthetic flux of *C. vulgaris*. Using a variety of chlorophyll fluorometry techniques to test a wide range of manganese concentrations, it was concluded that while changes to photosynthetic heterogeneity do take place under increased manganese exposure, further analysis must be completed in order

to determine specifically how this is occurring. While the results thus far indicate an increase in the size of antenna complexes and an increase in active reducing sites, the use of 77K fluorometry as well as the fast fluorescent induction method will be better suited to provide more specific analyses. Additionally, combining these parameters with proteomic data could further increase the understanding of the effect of manganese on the photosynthetic electron transport chain.

REFERENCES

1.	Brasier, M. D.; Green, O. R.; Jephcoat, A. P.; Kleppe, A. K.; Van Kranendonk, M. J.; Lindsay, J. F.; Steele, A.; Grassineau, N. V., Questioning the evidence for Earth's oldest fossils. *Nature* **2002,** *416*, 76.

2.	Dalton, R., Squaring up over ancient life. *Nature* **2002,** *417*, 782.

3.	Khan, M. I.; Shin, J. H.; Kim, J. D., The promising future of microalgae: current status, challenges, and optimization of a sustainable and renewable industry for biofuels, feed, and other products. *Microbial cell factories* **2018,** *17* (1), 36-36.

4.	Hopkinson, B. M.; Dupont, C. L.; Allen, A. E.; Morel, F. M. M., Efficiency of the CO<sub>2</sub>-concentrating mechanism of diatoms. *Proceedings of the National Academy of Sciences* **2011,** *108* (10), 3830.

5.	Spolaore, P.; Joannis-Cassan, C.; Duran, E.; Isambert, A., Commercial applications of microalgae. *Journal of Bioscience and Bioengineering* **2006,** *101* (2), 87-96.

6.	Borowitzka, M. A., Commercial production of microalgae: ponds, tanks, and fermenters. In *Progress in Industrial Microbiology*, Osinga, R.; Tramper, J.; Burgess, J. G.; Wijffels, R. H., Eds. Elsevier: 1999; Vol. 35, pp 313-321.

7.	Ball, S. G., Eukaryotic Microalgae Genomics. The Essence of Being a Plant. *Plant Physiology* **2005,** *137* (2), 397.

8.	Hamed, I., The Evolution and Versatility of Microalgal Biotechnology: A Review. *Comprehensive Reviews in Food Science and Food Safety* **2016,** *15* (6), 1104-1123.

9.	Sarwar, N.; Imran, M.; Shaheen, M. R.; Ishaque, W.; Kamran, M. A.; Matloob, A.; Rehim, A.; Hussain, S., Phytoremediation strategies for soils contaminated with heavy metals: Modifications and future perspectives. *Chemosphere* **2017,** *171*, 710-721.

10.	Topcu, S.; Kirda, C., Irrigation: Environmental Effects☆. In *Reference Module in Earth Systems and Environmental Sciences*, Elsevier: 2013.

11.	Sidemo-Holm, W.; Smith, H. G.; Brady, M. V., Improving agricultural pollution abatement through result-based payment schemes. *Land Use Policy* **2018,** *77*, 209-219.

12.   Sun, R.; Sun, P.; Zhang, J.; Esquivel-Elizondo, S.; Wu, Y., Microorganisms-based methods for harmful algal blooms control: A review. *Bioresource Technology* **2018,** *248*, 12-20.

13.   Mogollón, J. M.; Beusen, A. H. W.; van Grinsven, H. J. M.; Westhoek, H.; Bouwman, A. F., Future agricultural phosphorus demand according to the shared socioeconomic pathways. *Global Environmental Change* **2018,** *50*, 149-163.

14.   Mahugo Santana, C.; Sosa Ferrera, Z.; Esther Torres Padrón, M.; Juan Santana Rodríguez, J., Methodologies for the Extraction of Phenolic Compounds from Environmental Samples: New Approaches. *Molecules (Basel, Switzerland)* **2009,** *14* (1).

15.   Raza, W.; Lee, J.; Raza, N.; Luo, Y.; Kim, K.-H.; Yang, J., Removal of phenolic compounds from industrial waste water based on membrane-based technologies. *Journal of Industrial and Engineering Chemistry* **2019,** *71*, 1-18.

16.   Jacob, J. M.; Karthik, C.; Saratale, R. G.; Kumar, S. S.; Prabakar, D.; Kadirvelu, K.; Pugazhendhi, A., Biological approaches to tackle heavy metal pollution: A survey of literature. *Journal of Environmental Management* **2018,** *217*, 56-70.

17.   Chabukdhara, M.; Gupta, S. K.; Gogoi, M., Phycoremediation of Heavy Metals Coupled with Generation of Bioenergy. In *Algal Biofuels: Recent Advances and Future Prospects*, Gupta, S. K.; Malik, A.; Bux, F., Eds. Springer International Publishing: Cham, 2017; pp 163-188.

18.   Perales-Vela, H. V.; Peña-Castro, J. M.; Cañizares-Villanueva, R. O., Heavy metal detoxification in eukaryotic microalgae. *Chemosphere* **2006,** *64* (1), 1-10.

19.   Cobbett, C.; Goldsbrough, P., Phytochelatins and metallothioneins: roles in heavy metal detoxification and homeostasis. *Annual review of plant biology* **2002,** *53*, 159-82.

20.   Arbib, Z.; Ruiz, J.; Álvarez-Díaz, P.; Garrido-Pérez, C.; Perales, J. A., Capability of different microalgae species for phytoremediation processes: Wastewater tertiary treatment, CO2 bio-fixation and low cost biofuels production. *Water Research* **2014,** *49*, 465-474.

21.   Tsang, C. K.; Lau, P. S.; Tam, N. F. Y.; Wong, Y. S., Biodegradation capacity of tributyltin by two Chlorella species. *Environmental Pollution* **1999,** *105* (3), 289-297.

22.   Chan, S. M.; Luan, T.; Wong, M. H.; Tam, N. F., Removal and biodegradation of polycyclic aromatic hydrocarbons by Selenastrum capricornutum. *Environmental toxicology and chemistry* **2006,** *25* (7), 1772-9.

23.   Todd, S. J.; Cain, R. B.; Schmidt, S., Biotransformation of naphthalene and diaryl ethers by green microalgae. *Biodegradation* **2002,** *13* (4), 229-238.

24.   Hirooka, T.; Nagase, H.; Uchida, K.; Hiroshige, Y.; Ehara, Y.; Nishikawa, J.; Nishihara, T.; Miyamoto, K.; Hirata, Z., Biodegradation of bisphenol A and disappearance of its estrogenic activity by the green alga Chlorella fusca var. vacuolata. *Environmental toxicology and chemistry* **2005,** *24* (8), 1896-901.

25.   Subashchandrabose, S. R.; Ramakrishnan, B.; Megharaj, M.; Venkateswarlu, K.; Naidu, R., Mixotrophic cyanobacteria and microalgae as distinctive biological agents for organic pollutant degradation. *Environment International* **2013,** *51*, 59-72.

26.   Omar, W. M. W., Perspectives on the use of algae as biological indicators for monitoring and protecting aquatic environments, with special reference to malaysian freshwater ecosystems. *Tropical life sciences research* **2010,** *21* (2), 51-67.

27.   Smythers, A. L.; Garmany, A.; Perry, N. L.; Higginbotham, E. L.; Adkins, P. E.; Kolling, D. R. J., Characterizing the effect of Poast on *Chlorella vulgaris*, a non-target organism. *Chemosphere* **2019,** *219*, 704-712.

28.   McCormick, P. V.; Cairns, J., Algae as indicators of environmental change. *Journal of Applied Phycology* **1994,** *6* (5), 509-526.

29.   Duong, V. T.; Thomas-Hall, S. R.; Schenk, P. M., Growth and lipid accumulation of microalgae from fluctuating brackish and sea water locations in South East Queensland-Australia. *Frontiers in plant science* **2015,** *6*, 359-359.

30.   Priyadarshani, I. a. R., Biswajit, Commercial and industrial applications of micro algae – A review. *Journal of Algal Biomass Utilization* **2012,** *3* (4), 89-100.

31.   Lordan, S.; Ross, R. P.; Stanton, C., Marine bioactives as functional food ingredients: potential to reduce the incidence of chronic diseases. *Marine drugs* **2011,** *9* (6), 1056-1100.

32.   Specht, E.; Miyake-Stoner, S.; Mayfield, S., Micro-algae come of age as a platform for recombinant protein production. *Biotechnology letters* **2010,** *32* (10), 1373-1383.

33.   Bock, R., Plastid biotechnology: prospects for herbicide and insect resistance, metabolic engineering and molecular farming. *Curr Opin Biotechnol* **2007,** *18* (2), 100-6.

34.   Rymarquis, L. A.; Higgs, D. C.; Stern, D. B., Nuclear suppressors define three factors that participate in both 5' and 3' end processing of mRNAs in Chlamydomonas chloroplasts. *The Plant journal : for cell and molecular biology* **2006,** *46* (3), 448-61.

35.   Manuell, A. L.; Beligni, M. V.; Elder, J. H.; Siefker, D. T.; Tran, M.; Weber, A.; McDonald, T. L.; Mayfield, S. P., Robust expression of a bioactive mammalian protein in Chlamydomonas chloroplast. *Plant biotechnology journal* **2007,** *5* (3), 402-12.

36.   He, D. M.; Qian, K. X.; Shen, G. F.; Zhang, Z. F.; Li, Y. N.; Su, Z. L.; Shao, H. B., Recombination and expression of classical swine fever virus (CSFV) structural protein E2 gene in Chlamydomonas reinhardtii chroloplasts. *Colloids and surfaces. B, Biointerfaces* **2007,** *55* (1), 26-30.

37.   Wang, X.; Brandsma, M.; Tremblay, R.; Maxwell, D.; Jevnikar, A. M.; Huner, N.; Ma, S., A novel expression platform for the production of diabetes-associated autoantigen human glutamic acid decarboxylase (hGAD65). *BMC Biotechnology* **2008,** *8* (1), 87.

38.   Rasala, B. A.; Muto, M.; Lee, P. A.; Jager, M.; Cardoso, R. M.; Behnke, C. A.; Kirk, P.; Hokanson, C. A.; Crea, R.; Mendez, M.; Mayfield, S. P., Production of therapeutic proteins in algae, analysis of expression of seven human proteins in the chloroplast of Chlamydomonas reinhardtii. *Plant biotechnology journal* **2010,** *8* (6), 719-33.

39.   Markou, G.; Angelidaki, I.; Georgakakis, D., Microalgal carbohydrates: an overview of the factors influencing carbohydrates production, and of main bioconversion technologies for production of biofuels. *Applied Microbiology and Biotechnology* **2012,** *96* (3), 631-645.

40.   Martins, A. P.; Simas-Rodrigues, C.; Villela, H. D. M.; Marques, L. G.; Colepicolo, P.; Tonon, A. P., Microalgae for economic applications: advantages and perspectives for bioethanol. *Journal of Experimental Botany* **2015,** *66* (14), 4097-4108.

41.   Cardozo, K. H.; Guaratini, T.; Barros, M. P.; Falcao, V. R.; Tonon, A. P.; Lopes, N. P.; Campos, S.; Torres, M. A.; Souza, A. O.; Colepicolo, P.; Pinto, E., Metabolites from algae with economical impact. *Comparative biochemistry and physiology. Toxicology & pharmacology : CBP* **2007,** *146* (1-2), 60-78.

42.   Searchinger, T.; Heimlich, R.; Houghton, R. A.; Dong, F.; Elobeid, A.; Fabiosa, J.; Tokgoz, S.; Hayes, D.; Yu, T.-H., Use of U.S. Croplands for Biofuels Increases Greenhouse Gases Through Emissions from Land-Use Change. *Science* **2008,** *319* (5867), 1238.

43.   Dismukes, G. C.; Carrieri, D.; Bennette, N.; Ananyev, G. M.; Posewitz, M. C., Aquatic phototrophs: efficient alternatives to land-based crops for biofuels. *Current Opinion in Biotechnology* **2008,** *19* (3), 235-240.

44.   Grune, T.; Lietz, G.; Palou, A.; Ross, A. C.; Stahl, W.; Tang, G.; Thurnham, D.; Yin, S.-a.; Biesalski, H. K., Beta-carotene is an important vitamin A source for humans. *The Journal of nutrition* **2010,** *140* (12), 2268S-2285S.

45.   Bernstein, P. S.; Li, B.; Vachali, P. P.; Gorusupudi, A.; Shyam, R.; Henriksen, B. S.; Nolan, J. M., Lutein, zeaxanthin, and meso-zeaxanthin: The basic and clinical science underlying carotenoid-based nutritional interventions against ocular disease. *Progress in retinal and eye research* **2016,** *50*, 34-66.

46.   Hosikian, A.; Lim, S.; Halim, R.; Danquah, M. K., Chlorophyll Extraction from Microalgae: A Review on the Process Engineering Aspects. *International Journal of Chemical Engineering* **2010,** *2010*, 11.

47.   Chisti, Y., Biodiesel from microalgae. *Biotechnology Advances* **2007,** *25* (3), 294-306.

48.   Sun, X.-M.; Ren, L.-J.; Zhao, Q.-Y.; Ji, X.-J.; Huang, H., Enhancement of lipid accumulation in microalgae by metabolic engineering. *Biochimica et Biophysica Acta (BBA) - Molecular and Cell Biology of Lipids* **2019,** *1864* (4), 552-566.

49.   Kaye, Y.; Grundman, O.; Leu, S.; Zarka, A.; Zorin, B.; Didi-Cohen, S.; Khozin-Goldberg, I.; Boussiba, S., Metabolic engineering toward enhanced LC-PUFA biosynthesis in Nannochloropsis oceanica: Overexpression of endogenous Δ12 desaturase driven by stress-inducible promoter leads to enhanced deposition of polyunsaturated fatty acids in TAG. *Algal Research* **2015,** *11*, 387-398.

50.   Peng, K. T.; Zheng, C. N.; Xue, J.; Chen, X. Y.; Yang, W. D.; Liu, J. S.; Bai, W.; Li, H. Y., Delta 5 fatty acid desaturase upregulates the synthesis of polyunsaturated fatty acids in the marine diatom Phaeodactylum tricornutum. *J Agric Food Chem* **2014,** *62* (35), 8773-6.

51.   Shi, H.; Chen, H.; Gu, Z.; Zhang, H.; Chen, W.; Chen, Y. Q., Application of a delta-6 desaturase with alpha-linolenic acid preference on eicosapentaenoic acid production in Mortierella alpina. *Microb Cell Fact* **2016,** *15* (1), 117.

52.   Brennan, L.; Owende, P., Biofuels from microalgae—A review of technologies for production, processing, and extractions of biofuels and co-products. *Renewable and Sustainable Energy Reviews* **2010,** *14* (2), 557-577.

53.   Fernandes, P.; Cabral, J. M. S., Phytosterols: Applications and recovery methods. *Bioresource Technology* **2007,** *98* (12), 2335-2350.

54.   Yamamoto, M.; Fujishita, M.; Hirata, A.; Kawano, S., Regeneration and maturation of daughter cell walls in the autospore-forming green alga Chlorella vulgaris (Chlorophyta, Trebouxiophyceae). *Journal of Plant Research* **2004,** *117* (4), 257-264.

55.   Yamamoto, M.; Kurihara, I.; Kawano, S., Late type of daughter cell wall synthesis in one of the Chlorellaceae, Parachlorella kessleri (Chlorophyta, Trebouxiophyceae). *Planta* **2005,** *221* (6), 766-775.

56.   Guarnieri, M. T.; Levering, J.; Henard, C. A.; Boore, J. L.; Betenbaugh, M. J.; Zengler, K.; Knoshaug, E. P., Genome Sequence of the Oleaginous Green Alga, Chlorella vulgaris UTEX 395. *Frontiers in bioengineering and biotechnology* **2018,** *6*, 37-37.

57.   Wijffels, R. H.; Barbosa, M. J., An Outlook on Microalgal Biofuels. *Science* **2010,** *329* (5993), 796.

58.   Kapaun, E.; Reisser, W., A chitin-like glycan in the cell wall of a Chlorella sp. (Chlorococcales, Chlorophyceae). *Planta* **1995,** *197* (4), 577-582.

59.   Blankenship, R. E., *Molecular Mechanisms of Photosynthesis*. Wiley: 2014.

60.   Kouril, R.; Dekker, J. P.; Boekema, E. J., Supramolecular organization of photosystem II in green plants. *Biochim Biophys Acta* **2012,** *1817* (1), 2-12.

61.   Karlsson, S.; Boixel, J.; Pellegrin, Y.; Blart, E.; Becker, H.-C.; Odobel, F.; Hammarström, L., Accumulative electron transfer: Multiple charge separation in artificial photosynthesis. *Faraday Discussions* **2012,** *155* (0), 233-252.

62.   Vinyard, D. J.; Ananyev, G. M.; Charles Dismukes, G., Photosystem II: The Reaction Center of Oxygenic Photosynthesis. *Annual Review of Biochemistry* **2013,** *82* (1), 577-606.

63.   Barber, J., Photosystem II: an enzyme of global significance. *Biochemical Society Transactions* **2006,** *34* (5), 619.

64.   McEvoy, J. P.; Brudvig, G. W., Water-Splitting Chemistry of Photosystem II. *Chemical Reviews* **2006,** *106* (11), 4455-4483.

65.   Hasan, S. S.; Yamashita, E.; Baniulis, D.; Cramer, W. A., Quinone-dependent proton transfer pathways in the photosynthetic cytochrome b6f complex. *Proceedings of the National Academy of Sciences of the United States of America* **2013,** *110* (11), 4297-302.

66.   Dumas, L.; Chazaux, M.; Peltier, G.; Johnson, X.; Alric, J., Cytochrome b6f function and localization, phosphorylation state of thylakoid membrane proteins and consequences on cyclic electron flow. *Photosynthesis Research* **2016,** *129* (3), 307-320.

67.   Crofts, A. R.; Shinkarev, V. P.; Kolling, D. R. J.; Hong, S., The Modified Q-cycle Explains the Apparent Mismatch between the Kinetics of Reduction of Cytochromes c1 and bH in the bc1 Complex. *Journal of Biological Chemistry* **2003,** *278* (38), 36191-36201.

68.   Melkozernov, A. N.; Barber, J.; Blankenship, R. E., Light Harvesting in Photosystem I Supercomplexes. *Biochemistry* **2006,** *45* (2), 331-345.

69.   Sharma, K. K.; Schuhmann, H.; Schenk, P. M., High Lipid Induction in Microalgae for Biodiesel Production. *Energies* **2012,** *5* (5), 1532.

70.   Griffiths, M. J.; Harrison, S. T. L., Lipid productivity as a key characteristic for choosing algal species for biodiesel production. *Journal of Applied Phycology* **2009,** *21* (5), 493-507.

71.   Shurin, J. B.; Burkart, M. D.; Mayfield, S. P.; Smith, V. H., Recent progress and future challenges in algal biofuel production. *F1000Research* **2016,** *5*, F1000 Faculty Rev-2434.

72.   Knothe, G., Dependence of biodiesel fuel properties on the structure of fatty acid alkyl esters. *Fuel Processing Technology* **2005,** *86* (10), 1059-1070.

73.   Gimpel, J. A.; Henríquez, V.; Mayfield, S. P., In Metabolic Engineering of Eukaryotic Microalgae: Potential and Challenges Come with Great Diversity. *Frontiers in Microbiology* **2015,** *6* (1376).

74.   Dubini, A.; Ghirardi, M. L., Engineering photosynthetic organisms for the production of biohydrogen. *Photosynth Res* **2015,** *123* (3), 241-53.

75.   Safi, C.; Zebib, B.; Merah, O.; Pontalier, P.-Y.; Vaca-Garcia, C., Morphology, composition, production, processing and applications of Chlorella vulgaris: A review. *Renewable and Sustainable Energy Reviews* **2014,** *35*, 265-278.

76.   Woodworth, B. D.; Mead, R. L.; Nichols, C. N.; Kolling, D. R. J., Photosynthetic light reactions increase total lipid accumulation in carbon-supplemented batch cultures of *Chlorella vulgaris*. *Bioresource Technology* **2015,** *179*, 159-164.

77.   Lv, J.-M.; Cheng, L.-H.; Xu, X.-H.; Zhang, L.; Chen, H.-L., Enhanced lipid production of Chlorella vulgaris by adjustment of cultivation conditions. *Bioresource Technology* **2010,** *101* (17), 6797-6804.

78.   Feng, Y.; Li, C.; Zhang, D., Lipid production of Chlorella vulgaris cultured in artificial wastewater medium. *Bioresource Technology* **2011,** *102* (1), 101-105.

79.   Abreu, A. P.; Fernandes, B.; Vicente, A. A.; Teixeira, J.; Dragone, G., Mixotrophic cultivation of Chlorella vulgaris using industrial dairy waste as organic carbon source. *Bioresource Technology* **2012,** *118*, 61-66.

80.   Wang, W.; Zhou, W.; Liu, J.; Li, Y.; Zhang, Y., Biodiesel production from hydrolysate of Cyperus esculentus waste by Chlorella vulgaris. *Bioresource Technology* **2013,** *136*, 24-29.

81.   Shi, J.; Pandey, P. K.; Franz, A. K.; Deng, H.; Jeannotte, R., Chlorella vulgaris production enhancement with supplementation of synthetic medium in dairy manure wastewater. *AMB Express* **2016,** *6*, 15.

82.   Zuliani, L.; Frison, N.; Jelic, A.; Fatone, F.; Bolzonella, D.; Ballottari, M., Microalgae Cultivation on Anaerobic Digestate of Municipal Wastewater, Sewage Sludge and Agro-Waste. *International journal of molecular sciences* **2016,** *17* (10), 1692.

83.   Qin, L.; Shu, Q.; Wang, Z.; Shang, C.; Zhu, S.; Xu, J.; Li, R.; Zhu, L.; Yuan, Z., Cultivation of Chlorella vulgaris in Dairy Wastewater Pretreated by UV Irradiation and Sodium Hypochlorite. *Applied Biochemistry and Biotechnology* **2014,** *172* (2), 1121-1130.

84.   Wang, L.; Wang, Y.; Chen, P.; Ruan, R., Semi-continuous Cultivation of Chlorella vulgaris for Treating Undigested and Digested Dairy Manures. *Applied Biochemistry and Biotechnology* **2010,** *162* (8), 2324-2332.

85.   Mitra, D.; van Leeuwen, J.; Lamsal, B., Heterotrophic/mixotrophic cultivation of oleaginous Chlorella vulgaris on industrial co-products. *Algal Research* **2012,** *1* (1), 40-48.

86.   Hou, Q.; Pei, H.; Hu, W.; Jiang, L.; Yu, Z., Mutual facilitations of food waste treatment, microbial fuel cell bioelectricity generation and Chlorella vulgaris lipid production. *Bioresource Technology* **2016,** *203*, 50-55.

87.   Chew, K. W.; Chia, S. R.; Show, P. L.; Ling, T. C.; Arya, S. S.; Chang, J.-S., Food waste compost as an organic nutrient source for the cultivation of Chlorella vulgaris. *Bioresource Technology* **2018,** *267*, 356-362.

88.   Lau, K. Y.; Pleissner, D.; Lin, C. S. K., Recycling of food waste as nutrients in Chlorella vulgaris cultivation. *Bioresource Technology* **2014,** *170*, 144-151.

89.   Ma, X.; Zheng, H.; Addy, M.; Anderson, E.; Liu, Y.; Chen, P.; Ruan, R., Cultivation of Chlorella vulgaris in wastewater with waste glycerol: Strategies for improving nutrients removal and enhancing lipid production. *Bioresource Technology* **2016,** *207*, 252-261.

90.   Ji, Y.; Hu, W.; Li, X.; Ma, G.; Song, M.; Pei, H., Mixotrophic growth and biochemical analysis of Chlorella vulgaris cultivated with diluted monosodium glutamate wastewater. *Bioresource Technology* **2014,** *152*, 471-476.

91.   Ebrahimian, A.; Kariminia, H.-R.; Vosoughi, M., Lipid production in mixotrophic cultivation of Chlorella vulgaris in a mixture of primary and secondary municipal wastewater. *Renewable Energy* **2014,** *71*, 502-508.

92.   Zhou, W.; Li, Y.; Min, M.; Hu, B.; Chen, P.; Ruan, R., Local bioprospecting for high-lipid producing microalgal strains to be grown on concentrated municipal wastewater for biofuel production. *Bioresource Technology* **2011,** *102* (13), 6909-6919.

93.   Lam, M. K.; Yusoff, M. I.; Uemura, Y.; Lim, J. W.; Khoo, C. G.; Lee, K. T.; Ong, H. C., Cultivation of Chlorella vulgaris using nutrients source from domestic wastewater for biodiesel production: Growth condition and kinetic studies. *Renewable Energy* **2017,** *103*, 197-207.

94.   Fernández-Linares, L. C.; Guerrero Barajas, C.; Durán Páramo, E.; Badillo Corona, J. A., Assessment of Chlorella vulgaris and indigenous microalgae biomass with treated wastewater as growth culture medium. *Bioresource Technology* **2017,** *244*, 400-406.

95.   Evans, L.; Hennige, S. J.; Willoughby, N.; Adeloye, A. J.; Skroblin, M.; Gutierrez, T., Effect of organic carbon enrichment on the treatment efficiency of primary settled wastewater by Chlorella vulgaris. *Algal Research* **2017,** *24*, 368-377.

96.   Perez-Garcia, O.; Bashan, Y.; Esther Puente, M., Organic carbon supplementation of sterilized municipal wastewater is essential for heterotrophic growth and removing ammonium by the microalga *Chlorella vulgaris*. *Journal of Phycology* **2011,** *47* (1), 190-199.

97.   Park, W.-K.; Moon, M.; Kwak, M.-S.; Jeon, S.; Choi, G.-G.; Yang, J.-W.; Lee, B., Use of orange peel extract for mixotrophic cultivation of Chlorella vulgaris: Increased production of biomass and FAMEs. *Bioresource Technology* **2014,** *171*, 343-349.

98.   Lam, M. K.; Lee, K. T., Potential of using organic fertilizer to cultivate Chlorella vulgaris for biodiesel production. *Applied Energy* **2012,** *94*, 303-308.

99.   Ji, M. K.; Kim, H. C.; Sapireddy, V. R.; Yun, H. S.; Abou-Shanab, R. A.; Choi, J.; Lee, W.; Timmes, T. C.; Inamuddin; Jeon, B. H., Simultaneous nutrient removal and lipid production from pretreated piggery wastewater by Chlorella vulgaris YSW-04. *Appl Microbiol Biotechnol* **2013,** *97* (6), 2701-10.

100.   Deng, X.-Y.; Gao, K.; Addy, M.; Li, D.; Zhang, R.-C.; Lu, Q.; Ma, Y.-W.; Cheng, Y.-L.; Chen, P.; Liu, Y.-H.; Ruan, R., Cultivation of Chlorella vulgaris on anaerobically digested swine manure with daily recycling of the post-harvest culture broth. *Bioresource Technology* **2018,** *247*, 716-723.

101.   Deng, X.-Y.; Gao, K.; Zhang, R.-C.; Addy, M.; Lu, Q.; Ren, H.-Y.; Chen, P.; Liu, Y.-H.; Ruan, R., Growing Chlorella vulgaris on thermophilic anaerobic digestion swine manure for nutrient removal and biomass production. *Bioresource Technology* **2017,** *243*, 417-425.

102.   Luque, L.; Orr, V. C. A.; Chen, S.; Westerhof, R.; Oudenhoven, S.; Rossum, G. v.; Kersten, S.; Berruti, F.; Rehmann, L., Lipid accumulation from pinewood pyrolysates by Rhodosporidium diobovatum and Chlorella vulgaris for biodiesel production. *Bioresource Technology* **2016,** *214*, 660-669.

103.   Jain, D.; Ghonse, S. S.; Trivedi, T.; Fernandes, G. L.; Menezes, L. D.; Damare, S. R.; Mamatha, S. S.; Kumar, S.; Gupta, V., CO2 fixation and production of biodiesel by Chlorella vulgaris NIOCCV under mixotrophic cultivation. *Bioresource Technology* **2019,** *273*, 672-676.

104.   Shen, Q.-H.; Gong, Y.-P.; Fang, W.-Z.; Bi, Z.-C.; Cheng, L.-H.; Xu, X.-H.; Chen, H.-L., Saline wastewater treatment by Chlorella vulgaris with simultaneous algal lipid accumulation triggered by nitrate deficiency. *Bioresource Technology* **2015,** *193*, 68-75.

105.   Church, J.; Hwang, J.-H.; Kim, K.-T.; McLean, R.; Oh, Y.-K.; Nam, B.; Joo, J. C.; Lee, W. H., Effect of salt type and concentration on the growth and lipid content of Chlorella vulgaris

in synthetic saline wastewater for biofuel production. *Bioresource Technology* **2017,** *243*, 147-153.

106.   Cho, H. U.; Kim, Y. M.; Choi, Y.-N.; Xu, X.; Shin, D. Y.; Park, J. M., Effects of pH control and concentration on microbial oil production from Chlorella vulgaris cultivated in the effluent of a low-cost organic waste fermentation system producing volatile fatty acids. *Bioresource Technology* **2015,** *184*, 245-250.

107.   Sasaki, Y.; Nagano, Y., Plant acetyl-CoA carboxylase: structure, biosynthesis, regulation, and gene manipulation for plant breeding. *Bioscience, biotechnology, and biochemistry* **2004,** *68* (6), 1175-84.

108.   Livne, A.; Sukenik, A., Lipid Synthesis and Abundance of Acetyl CoA Carboxylase in Isochrysis galbana (Prymnesiophyceae) Following Nitrogen Starvation. *Plant and Cell Physiology* **1992,** *33* (8), 1175-1181.

109.   Abedini Najafabadi, H.; Malekzadeh, M.; Jalilian, F.; Vossoughi, M.; Pazuki, G., Effect of various carbon sources on biomass and lipid production of Chlorella vulgaris during nutrient sufficient and nitrogen starvation conditions. *Bioresource Technology* **2015,** *180*, 311-317.

110.   Gim, G. H.; Kim, J. K.; Kim, H. S.; Kathiravan, M. N.; Yang, H.; Jeong, S.-H.; Kim, S. W., Comparison of biomass production and total lipid content of freshwater green microalgae cultivated under various culture conditions. *Bioprocess and Biosystems Engineering* **2014,** *37* (2), 99-106.

111.   Raven, J. A.; Beardall, J., Carbohydrate Metabolism and Respiration in Algae. In *Photosynthesis in Algae*, Larkum, A. W. D.; Douglas, S. E.; Raven, J. A., Eds. Springer Netherlands: Dordrecht, 2003; pp 205-224.

112.   Heredia-Arroyo, T.; Wei, W.; Ruan, R.; Hu, B., Mixotrophic cultivation of Chlorella vulgaris and its potential application for the oil accumulation from non-sugar materials. *Biomass and Bioenergy* **2011,** *35* (5), 2245-2253.

113.   Yeh, K.-L.; Chen, C.-Y.; Chang, J.-S., pH-stat photoheterotrophic cultivation of indigenous Chlorella vulgaris ESP-31 for biomass and lipid production using acetic acid as the carbon source. *Biochemical Engineering Journal* **2012,** *64*, 1-7.

114.   Liang, Y.; Sarkany, N.; Cui, Y., Biomass and lipid productivities of Chlorella vulgaris under autotrophic, heterotrophic and mixotrophic growth conditions. *Biotechnology Letters* **2009,** *31* (7), 1043-1049.

115.   Kong, W.-B.; Hua, S.-F.; Cao, H.; Mu, Y.-W.; Yang, H.; Song, H.; Xia, C.-G., Optimization of mixotrophic medium components for biomass production and biochemical composition biosynthesis by Chlorella vulgaris using response surface methodology. *Journal of the Taiwan Institute of Chemical Engineers* **2012,** *43* (3), 360-367.

116.   Li, X.; Xu, H.; Wu, Q., Large-scale biodiesel production from microalga Chlorella prototothecoides through heterotrophic cultivation in bioreactors. *Biotechnology and bioengineering* **2007,** *98* (4), 764-71.

117.   Choi, H.-J.; Yu, S.-W., Influence of crude glycerol on the biomass and lipid content of microalgae. *Biotechnology & Biotechnological Equipment* **2015,** *29* (3), 506-513.

118.   Sharma, A. K.; Sahoo, P. K.; Singhal, S.; Patel, A., Impact of various media and organic carbon sources on biofuel production potential from Chlorella spp. *3 Biotech* **2016,** *6* (2), 116.

119.   Sun, Y.; Liu, J.; Xie, T.; Xiong, X.; Liu, W.; Liang, B.; Zhang, Y., Enhanced Lipid Accumulation by Chlorella vulgaris in a Two-Stage Fed-Batch Culture with Glycerol. *Energy & Fuels* **2014,** *28* (5), 3172-3177.

120.   Scheller, H. V.; Ulvskov, P., Hemicelluloses. *Annual review of plant biology* **2010,** *61* (1), 263-289.

121.   Fernandez, R.; Herrero, P.; Moreno, F., Inhibition and inactivation of glucose-phosphorylating enzymes from Saccharomyces cerevisiae by D-xylose. *Journal of general microbiology* **1985,** *131* (10), 2705-9.

122.   Leite, G. B.; Paranjape, K.; Hallenbeck, P. C., Breakfast of champions: Fast lipid accumulation by cultures of Chlorella and Scenedesmus induced by xylose. *Algal Research* **2016,** *16*, 338-348.

123.   Che, J.; Wan, J.; Huang, X.; Wu, R.; Liang, K., Pretreatment of piggery digestate wastewater by ferric-carbon micro-electrolysis under alkalescence condition. *Korean Journal of Chemical Engineering* **2017,** *34* (9), 2397-2405.

124.   Yuan, X.; Kumar, A.; Sahu, A. K.; Ergas, S. J., Impact of ammonia concentration on Spirulina platensis growth in an airlift photobioreactor. *Bioresource Technology* **2011,** *102* (3), 3234-3239.

125.   Zhu, L. D.; Li, Z. H.; Hiltunen, E., Strategies for Lipid Production Improvement in Microalgae as a Biodiesel Feedstock. *BioMed Research International* **2016,** *2016*, 8.

126.   Ikaran, Z.; Suárez-Alvarez, S.; Urreta, I.; Castañón, S., The effect of nitrogen limitation on the physiology and metabolism of chlorella vulgaris var L3. *Algal Research* **2015,** *10*, 134-144.

127.   Benavente-Valdés, J. R.; Aguilar, C.; Contreras-Esquivel, J. C.; Méndez-Zavala, A.; Montañez, J., Strategies to enhance the production of photosynthetic pigments and lipids in chlorophycae species. *Biotechnology reports (Amsterdam, Netherlands)* **2016,** *10*, 117-125.

128.   Markou, G.; Dao, L. H. T.; Muylaert, K.; Beardall, J., Influence of different degrees of N limitation on photosystem II performance and heterogeneity of Chlorella vulgaris. *Algal Research* **2017,** *26*, 84-92.

129.   Mizuno, Y.; Sato, A.; Watanabe, K.; Hirata, A.; Takeshita, T.; Ota, S.; Sato, N.; Zachleder, V.; Tsuzuki, M.; Kawano, S., Sequential accumulation of starch and lipid induced by sulfur deficiency in Chlorella and Parachlorella species. *Bioresource Technology* **2013,** *129*, 150-155.

130.   Sakarika, M.; Kornaros, M., Effect of pH on growth and lipid accumulation kinetics of the microalga Chlorella vulgaris grown heterotrophically under sulfur limitation. *Bioresource Technology* **2016,** *219*, 694-701.

131.   Shen, X.-F.; Liu, J.-J.; Chauhan, A. S.; Hu, H.; Ma, L.-L.; Lam, P. K. S.; Zeng, R. J., Combining nitrogen starvation with sufficient phosphorus supply for enhanced biodiesel productivity of Chlorella vulgaris fed on acetate. *Algal Research* **2016,** *17*, 261-267.

132.   Chu, F.-F.; Chu, P.-N.; Cai, P.-J.; Li, W.-W.; Lam, P. K. S.; Zeng, R. J., Phosphorus plays an important role in enhancing biodiesel productivity of Chlorella vulgaris under nitrogen deficiency. *Bioresource Technology* **2013,** *134*, 341-346.

133.   Yang, B.; Liu, J.; Jiang, Y.; Chen, F., Chlorella species as hosts for genetic engineering and expression of heterologous proteins: Progress, challenge and perspective. *Biotechnology Journal* **2016,** *11* (10), 1244-1261.

134.   Hiraki, M.; van Rensen, J. J.; Vredenberg, W. J.; Wakabayashi, K., Characterization of the alterations of the chlorophyll a fluorescence induction curve after addition of Photosystem II inhibiting herbicides. *Photosynth Res* **2003,** *78* (1), 35-46.

135.   Lazár, D.; Nauš, J.; Matoušková, M.; Flašarová, M., Mathematical Modeling of Changes in Chlorophyll Fluorescence Induction Caused by Herbicides. *Pesticide Biochemistry and Physiology* **1997,** *57* (3), 200-210.

136.   Lazar, D.; Tomek, P.; Ilik, P.; Naus, J., Determination of the antenna heterogeneity of Photosystem II by direct simultaneous fitting of several fluorescence rise curves measured with DCMU at different light intensities. *Photosynth Res* **2001,** *68* (3), 247-57.

137.   Behrens, R. W., The Physical and Chemical Properties of Surfactants and Their Effects on Formulated Herbicides. *Weeds* **2017,** *12* (4), 255-258.

138.   Sevilla-Moran, B.; Calvo, L.; Lopez-Goti, C.; Alonso-Prados, J. L.; Sandin-Espana, P., Photodegradation behaviour of sethoxydim and its commercial formulation Poast((R)) under environmentally-relevant conditions in aqueous media. Study of photoproducts and their toxicity. *Chemosphere* **2017,** *168*, 501-507.

139.   Feckler, A.; Rakovic, J.; Kahlert, M.; Troger, R.; Bundschuh, M., Blinded by the light: Increased chlorophyll fluorescence of herbicide-exposed periphyton masks unfavorable structural responses during exposure and recovery. *Aquatic toxicology (Amsterdam, Netherlands)* **2018,** *203*, 187-193.

140.   Belkebir, A.; Benhassaine-Kesri, G., Sethoxydim treatment inhibits lipid metabolism and enhances the accumulation of anthocyanins in rape (Brassica napus L.) leaves. *Pesticide Biochemistry and Physiology* **2013,** *107* (1), 120-126.

141.   Sevilla-Morán, B.; López-Goti, C.; Alonso-Prados, J. L.; Sandín-España, P., Aqueous photodegradation of sethoxydim herbicide: Qtof elucidation of its by-products, mechanism and degradation pathway. *Science of The Total Environment* **2014,** *472*, 842-850.

142.   Davis, A. M.; Thorburn, P. J.; Lewis, S. E.; Bainbridge, Z. T.; Attard, S. J.; Milla, R.; Brodie, J. E., Environmental impacts of irrigated sugarcane production: Herbicide run-off dynamics from farms and associated drainage systems. *Agriculture, Ecosystems & Environment* **2013,** *180*, 123-135.

143.   Zhao, F.; Li, Y.; Huang, L.; Gu, Y.; Zhang, H.; Zeng, D.; Tan, H., Individual and combined toxicity of atrazine, butachlor, halosulfuron-methyl and mesotrione on the microalga Selenastrum capricornutum. *Ecotoxicology and Environmental Safety* **2018,** *148*, 969-975.

144.   Lorente, C.; Causape, J.; Glud, R. N.; Hancke, K.; Merchan, D.; Muniz, S.; Val, J.; Navarro, E., Impacts of agricultural irrigation on nearby freshwater ecosystems: the seasonal

influence of triazine herbicides in benthic algal communities. *The Science of the total environment* **2015,** *503-504*, 151-8.

145.   Booij, P.; Sjollema, S. B.; van der Geest, H. G.; Leonards, P. E. G.; Lamoree, M. H.; de Voogt, W. P.; Admiraal, W.; Laane, R. W. P. M.; Vethaak, A. D., Toxic pressure of herbicides on microalgae in Dutch estuarine and coastal waters. *Journal of Sea Research* **2015,** *102*, 48-56.

146.   Conc., B. G. B. O.-t.-T. G. K., MSDS No 7969884. Bonide Products, Inc.: Oriskany, NY, 2011.

147.   Wellburn, A. R., The Spectral Determination of Chlorophylls a and b, as well as Total Carotenoids, Using Various Solvents with Spectrophotometers of Different Resolution. *Journal of Plant Physiology* **1994,** *144* (3), 307-313.

148.   Calomeni, A. J.; Rodgers, J. H., Evaluation of the utility of six measures for algal (Microcystis aeruginosa, Planktothrix agardhii and Pseudokirchneriella subcapitata) viability. *Ecotoxicology and Environmental Safety* **2015,** *111*, 192-198.

149.   Matyash, V.; Liebisch, G.; Kurzchalia, T. V.; Shevchenko, A.; Schwudke, D., Lipid extraction by methyl-tert-butyl ether for high-throughput lipidomics. *Journal of lipid research* **2008,** *49* (5), 1137-1146.

150.   M. Dubois, K. A. G., J.K. Hamilton, P.A. Rebers, F. Smith, Colorimetric method for determination of sugars and related substances. *Analytica Chemistry* **1956,** *28*, 350-356.

151.   Lowry, O. H.; Rosebrough, N. J.; Farr, A. L.; Randall, R. J., Protein measurement with the Folin phenol reagent. *The Journal of biological chemistry* **1951,** *193* (1), 265-75.

152.   Price, C. A., A membrane method for determination of total protein in dilute algal suspensions. *Analytical Biochemistry* **1965,** *12* (2), 213-218.

153.   Slocombe, S. P.; Ross, M.; Thomas, N.; McNeill, S.; Stanley, M. S., A rapid and general method for measurement of protein in micro-algal biomass. *Bioresource Technology* **2013,** *129*, 51-57.

154.   Stirbet, A., Chlorophyll a fluorescence induction: Can just a one-second measurement be used to quantify abiotic stress responses? *Photosynthetica* **2018,** *v. 56* (no. 1), pp. 19-104-2018 v.56 no.1.

155.   Chen, L. S.; Cheng, L., Photosystem 2 is more tolerant to high temperature in apple (Malus domestica Borkh.) leaves than in fruit peel. *Photosynthetica* **2009,** *47* (1), 112-120.

156.   R.J. Strasser, M. T.-M., A. Srivastava, Analysis of the cholorophyll a fluorescent transient In *Chlorophyll a Fluorescence: A Signature of Photosynthesis*, Govindjee, G. C. P. a., Ed. Springer Netherlands: Dordrecht, NL, 2004; pp 321-362.

157.   Stirbet, A.; Govindjee, On the relation between the Kautsky effect (chlorophyll a fluorescence induction) and Photosystem II: Basics and applications of the OJIP fluorescence transient. *Journal of Photochemistry and Photobiology B: Biology* **2011,** *104* (1), 236-257.

158.   Kalaji, H. M.; Schansker, G.; Brestic, M.; Bussotti, F.; Calatayud, A.; Ferroni, L.; Goltsev, V.; Guidi, L.; Jajoo, A.; Li, P.; Losciale, P.; Mishra, V. K.; Misra, A. N.; Nebauer, S. G.; Pancaldi, S.; Penella, C.; Pollastrini, M.; Suresh, K.; Tambussi, E.; Yanniccari, M.; Zivcak, M.; Cetner, M. D.; Samborska, I. A.; Stirbet, A.; Olsovska, K.; Kunderlikova, K.; Shelonzek, H.; Rusinowski, S.; Baba, W., Frequently asked questions about chlorophyll fluorescence, the sequel. *Photosynth Res* **2017,** *132* (1), 13-66.

159.   Kalaji, H. M.; Schansker, G.; Ladle, R. J.; Goltsev, V.; Bosa, K.; Allakhverdiev, S. I.; Brestic, M.; Bussotti, F.; Calatayud, A.; Dabrowski, P.; Elsheery, N. I.; Ferroni, L.; Guidi, L.; Hogewoning, S. W.; Jajoo, A.; Misra, A. N.; Nebauer, S. G.; Pancaldi, S.; Penella, C.; Poli, D.; Pollastrini, M.; Romanowska-Duda, Z. B.; Rutkowska, B.; Serodio, J.; Suresh, K.; Szulc, W.; Tambussi, E.; Yanniccari, M.; Zivcak, M., Frequently asked questions about in vivo chlorophyll fluorescence: practical issues. *Photosynth Res* **2014,** *122* (2), 121-58.

160.   Berthold, D. A.; Babcock, G. T.; Yocum, C. F., A highly resolved, oxygen-evolving photosystem II preparation from spinach thylakoid membranes: EPR and electron-transport properties. *FEBS Letters* **1981,** *134* (2), 231-234.

161.   Kolling, D. R.; Brown, T. S.; Ananyev, G.; Dismukes, G. C., Photosynthetic oxygen evolution is not reversed at high oxygen pressures: mechanistic consequences for the water-oxidizing complex. *Biochemistry* **2009,** *48* (6), 1381-9.

162.   Suorsa, M.; Regel, R. E.; Paakkarinen, V.; Battchikova, N.; Herrmann, R. G.; Aro, E. M., Protein assembly of photosystem II and accumulation of subcomplexes in the absence of low molecular mass subunits PsbL and PsbJ. *European journal of biochemistry* **2004,** *271* (1), 96-107.

163.   Schindelin, J.; Arganda-Carreras, I.; Frise, E.; Kaynig, V.; Longair, M.; Pietzsch, T.; Preibisch, S.; Rueden, C.; Saalfeld, S.; Schmid, B.; Tinevez, J. Y.; White, D. J.; Hartenstein, V.;

Eliceiri, K.; Tomancak, P.; Cardona, A., Fiji: an open-source platform for biological-image analysis. *Nature methods* **2012,** *9* (7), 676-82.

164.   Strasser, R. J.; Srivastava, A., Polyphasic chlorophyll *a* fluorescence transient in plants and cyanobacteria. *Photochemistry and Photobiology* **1995,** *61* (1), 32-42.

165.   Suzuki, T.; Tada, O.; Makimura, M.; Tohri, A.; Ohta, H.; Yamamoto, Y.; Enami, I., Isolation and characterization of oxygen-evolving photosystem II complexes retaining the PsbO, P and Q proteins from Euglena gracilis. *Plant & cell physiology* **2004,** *45* (9), 1168-75.

166.   Moseley, J. L.; Allinger, T.; Herzog, S.; Hoerth, P.; Wehinger, E.; Merchant, S.; Hippler, M., Adaptation to Fe-deficiency requires remodeling of the photosynthetic apparatus. *The EMBO journal* **2002,** *21* (24), 6709-6720.

167.   Zuppini, A.; Andreoli, C.; Baldan, B., Heat stress: an inducer of programmed cell death in Chlorella saccharophila. *Plant & cell physiology* **2007,** *48* (7), 1000-9.

168.   Srivastava, A.; Guissé, B.; Greppin, H.; Strasser, R. J., Regulation of antenna structure and electron transport in Photosystem II of Pisum sativum under elevated temperature probed by the fast polyphasic chlorophyll a fluorescence transient: OKJIP. *Biochimica et Biophysica Acta (BBA) - Bioenergetics* **1997,** *1320* (1), 95-106.

169.   Vredenberg, W. J., Analysis of initial chlorophyll fluorescence induction kinetics in chloroplasts in terms of rate constants of donor side quenching release and electron trapping in photosystem II. *Photosynth Res* **2008,** *96* (1), 83-97.

170.   W.S. Curran, M. D. M., R.A. Liebl, D.D. Lingenfelter Adjuvents for Enhancing Herbicide Performance. (accessed Jan. 29).

171.   Patil, D. S.; Chavan, S. M.; Oubagaranadin, J. U. K., A review of technologies for manganese removal from wastewaters. *Journal of Environmental Chemical Engineering* **2016,** *4* (1), 468-487.

172.   EPA, U., Health Effects Support Document for Manganese. *U.S. Environmental Protection Agency Office of Water, Washington, DC* **2003,** *822-R-03-0003.*

173.   Veronez, A. C. d. S.; Salla, R. V.; Baroni, V. D.; Barcarolli, I. F.; Bianchini, A.; dos Reis Martinez, C. B.; Chippari-Gomes, A. R., Genetic and biochemical effects induced by iron ore, Fe

and Mn exposure in tadpoles of the bullfrog Lithobates catesbeianus. *Aquatic Toxicology* **2016,** *174*, 101-108.

174.   Pereira, A. A.; van Hattum, B.; Brouwer, A.; van Bodegom, P. M.; Rezende, C. E.; Salomons, W., Effects of iron-ore mining and processing on metal bioavailability in a tropical coastal lagoon. *Journal of Soils and Sediments* **2008,** *8* (4), 239-252.

175.   Penland, T. N.; Grieshaber, C. A.; Kwak, T. J.; Cope, W. G.; Heise, R. J.; Sessions, F. W., Food web contaminant dynamics of a large Atlantic Slope river: Implications for common and imperiled species. *Science of The Total Environment* **2018,** *633*, 1062-1077.

176.   Parsons-White, A. B.; Spitzer, N., Environmentally relevant manganese overexposure alters neural cell morphology and differentiation in vitro. *Toxicology in Vitro* **2018,** *50*, 22-28.

177.   Dobson, A. W.; Erikson, K. M.; Aschner, M., Manganese Neurotoxicity. *Annals of the New York Academy of Sciences* **2004,** *1012* (1), 115-128.

178.   Charash, B.; Placek, E.; Sos, T. A.; Kligfield, P., Dose-related effects of manganese on the canine electrocardiogram. *Journal of Electrocardiology* **1982,** *15* (2), 149-152.

179.   Jiang, Y.; Zheng, W., Cardiovascular toxicities upon manganese exposure. *Cardiovascular toxicology* **2005,** *5* (4), 345-354.

180.   Spangler, A. H.; Spangler, J. G., Groundwater Manganese and Infant Mortality Rate by County in North Carolina: An Ecological Analysis. *EcoHealth* **2009,** *6* (4), 596-600.

181.   Hafeman, D.; Factor-Litvak, P.; Cheng, Z.; van Geen, A.; Ahsan, H., Association between manganese exposure through drinking water and infant mortality in Bangladesh. *Environmental health perspectives* **2007,** *115* (7), 1107-1112.

182.   O'Neal, S. L.; Zheng, W., Manganese Toxicity Upon Overexposure: a Decade in Review. *Current environmental health reports* **2015,** *2* (3), 315-328.

183.   Zhang, W.; Cheng, C. Y.; Pranolo, Y., Investigation of methods for removal and recovery of manganese in hydrometallurgical processes. *Hydrometallurgy* **2010,** *101* (1), 58-63.

184.   Woodard, F., *Industrial Waste Treatment Handbook*. Elsevier Science: 2001.

185.   Zhang, W.; Cheng, C. Y., Manganese metallurgy review. Part II: Manganese separation and recovery from solution. *Hydrometallurgy* **2007,** *89* (3), 160-177.

186.   Silva, A. M.; Cunha, E. C.; Silva, F. D. R.; Leão, V. A., Treatment of high-manganese mine water with limestone and sodium carbonate. *Journal of Cleaner Production* **2012,** *29-30*, 11-19.

187.   Bamforth, S. M.; Manning, D. A. C.; Singleton, I.; Younger, P. L.; Johnson, K. L., Manganese removal from mine waters – investigating the occurrence and importance of manganese carbonates. *Applied Geochemistry* **2006,** *21* (8), 1274-1287.

188.   Menard, V.; Demopoulos, G. P., Gas transfer kinetics and redox potential considerations in oxidative precipitation of manganese from an industrial zinc sulphate solution with SO2/O2. *Hydrometallurgy* **2007,** *89* (3), 357-368.

189.   Mishra, S.; Kumar, V., Co-precipitation of copper-manganese sulphide in Fe-3%Si steel. *Materials Science and Engineering: B* **1995,** *32* (3), 177-184.

190.   Polat, H.; Erdogan, D., Heavy metal removal from waste waters by ion flotation. *Journal of Hazardous Materials* **2007,** *148* (1), 267-273.

191.   Gregory, O. J.; Barnett, S. M.; Deluise, F. J., Manganese Removal from Water by a Precipitate Flotation Technique. *Separation Science and Technology* **1980,** *15* (8), 1499-1512.

192.   Stoica, L.; Dinculescu, M.; Plapcianu, C. G., Mn(II) recovery from aqueous systems by flotation. *Water Research* **1998,** *32* (10), 3021-3030.

193.   White, D. A.; Asfar-Siddique, A., Removal of Manganese and Iron from Drinking Water Using Hydrous Manganese Dioxide. *Solvent Extraction and Ion Exchange* **1997,** *15* (6), 1133-1145.

194.   Kononova, O. N.; Bryuzgina, G. L.; Apchitaeva, O. V.; Kononov, Y. S., Ion exchange recovery of chromium (VI) and manganese (II) from aqueous solutions. *Arabian Journal of Chemistry* **2015**.

195.   Roccaro, P.; Barone, C.; Mancini, G.; Vagliasindi, F. G. A., Removal of manganese from water supplies intended for human consumption: a case study. *Desalination* **2007,** *210* (1), 205-214.

196.   Ellis, D.; Bouchard, C.; Lantagne, G., Removal of iron and manganese from groundwater by oxidation and microfiltration. *Desalination* **2000,** *130* (3), 255-264.

197.   Piispanen, J. K.; Sallanko, J. T., Mn(II) removal from groundwater with manganese oxide-coated filter media. *Journal of environmental science and health. Part A, Toxic/hazardous substances & environmental engineering* **2010,** *45* (13), 1732-40.

198.   He, X.; Yang, H.; He, Y., Treatment of mine water high in Fe and Mn by modified manganese sand. *Mining Science and Technology (China)* **2010,** *20* (4), 571-575.

199.   Al-Wakeel, K. Z.; Abd El Monem, H.; Khalil, M. M. H., Removal of divalent manganese from aqueous solution using glycine modified chitosan resin. *Journal of Environmental Chemical Engineering* **2015,** *3* (1), 179-186.

200.   Reiad, N. A.; Salam, O. E. A.; Abadir, E. F.; Harraz, F. A., Adsorptive removal of iron and manganese ions from aqueous solutions with microporous chitosan/polyethylene glycol blend membrane. *Journal of Environmental Sciences* **2012,** *24* (8), 1425-1432.

201.   Yavuz, Ö.; Altunkaynak, Y.; Güzel, F., Removal of copper, nickel, cobalt and manganese from aqueous solution by kaolinite. *Water Research* **2003,** *37* (4), 948-952.

202.   Vistuba, J. P.; Nagel-Hassemer, M. E.; Lapolli, F. R.; Lobo Recio, M. Á., Simultaneous adsorption of iron and manganese from aqueous solutions employing an adsorbent coal. *Environmental Technology* **2013,** *34* (2), 275-282.

203.   Ruas, F. A. D.; Barboza, N. R.; Castro-Borges, W.; Guerra-Sá, R., Manganese alters expression of proteins involved in the oxidative stress of Meyerozyma guilliermondii. *Journal of Proteomics* **2018**.

204.   Vithanage, M.; Dabrowska, B. B.; Mukherjee, A. B.; Sandhi, A.; Bhattacharya, P., Arsenic uptake by plants and possible phytoremediation applications: a brief overview. *Environmental Chemistry Letters* **2012,** *10* (3), 217-224.

205.   Saier, M. H.; Trevors, J. T., Phytoremediation. *Water, Air, and Soil Pollution* **2010,** *205* (1), 61-63.

206.   Kawahigashi, H., Transgenic plants for phytoremediation of herbicides. *Current Opinion in Biotechnology* **2009,** *20* (2), 225-230.

207.   Odjegba, V. J.; Fasidi, I. O., Phytoremediation of heavy metals by Eichhornia crassipes. *The Environmentalist* **2007,** *27* (3), 349-355.

208.   Abhilash, P. C.; Powell, J. R.; Singh, H. B.; Singh, B. K., Plant–microbe interactions: novel applications for exploitation in multipurpose remediation technologies. *Trends in Biotechnology* **2012,** *30* (8), 416-420.

209.   Liu, Z.-Y.; Wang, G.-C.; Zhou, B.-C., Effect of iron on growth and lipid accumulation in *Chlorella vulgaris*. *Bioresource Technology* **2008,** *99* (11), 4717-4722.

210.   Liu, T.; Liu, F.; Wang, C.; Wang, Z.; Li, Y., The boosted lipid accumulation in microalga Chlorella vulgaris by a heterotrophy and nutrition-limitation transition cultivation regime. *World Journal of Microbiology and Biotechnology* **2016,** *32* (12), 202.

211.   Seyfabadi, J.; Ramezanpour, Z.; Amini Khoeyi, Z., Protein, fatty acid, and pigment content of *Chlorella vulgaris* under different light regimes. *Journal of Applied Phycology* **2011,** *23* (4), 721-726.

212.   Ben Amor-Ben Ayed, H.; Taidi, B.; Ayadi, H.; Pareau, D.; Stambouli, M., Effect of magnesium ion concentration in autotrophic cultures of Chlorella vulgaris. *Algal Research* **2015,** *9*, 291-296.

213.   Slaveykova, V. I.; Wilkinson, K. J., Physicochemical aspects of lead bioaccumulation by *Chlorella vulgaris*. *Environmental science & technology* **2002,** *36* (5), 969-75.

214.   Maeda, S.; Fukuyama, H.; Yokoyama, E.; Kuroiwa, T.; Ohki, A.; Naka, K., Bioaccumulation of Antimony by *Chlorella vulgaris* and the Association Mode of Antimony in the Cell. *Applied Organometallic Chemistry* **1997,** *11* (5), 393-396.

215.   Ruangsomboon, S.; Wongrat, L., Bioaccumulation of cadmium in an experimental aquatic food chain involving phytoplankton (*Chlorella vulgaris*), zooplankton (*Moina macrocopa*), and the predatory catfish *Clarias macrocephalus×C. gariepinus*. *Aquatic Toxicology* **2006,** *78* (1), 15-20.

216.   Vogel, M.; Günther, A.; Rossberg, A.; Li, B.; Bernhard, G.; Raff, J., Biosorption of U(VI) by the green algae *Chlorella vulgaris* in dependence of pH value and cell activity. *Science of The Total Environment* **2010,** *409* (2), 384-395.

217.   Muñoz, M. J.; Ramos, C.; Tarazona, J., Bioaccumulation and toxicity of hexachlorobenzene in *Chlorella vulgaris* and *Daphnia magna*. *Aquatic Toxicology* **1996,** *35* (3), 211-220.

218.   Bajguz, A., Suppression of *Chlorella vulgaris* growth by cadmium, lead, and copper stress and its restoration by endogenous brassinolide. *Archives of environmental contamination and toxicology* **2011,** *60* (3), 406-416.

219.   Baranov, S. V.; Tyryshkin, A. M.; Katz, D.; Dismukes, G. C.; Ananyev, G. M.; Klimov, V. V., Bicarbonate Is a Native Cofactor for Assembly of the Manganese Cluster of the Photosynthetic Water Oxidizing Complex. Kinetics of Reconstitution of O2 Evolution by Photoactivation. *Biochemistry* **2004,** *43* (7), 2070-2079.

220.   Blaby-Haas, C. E.; Merchant, S. S., The ins and outs of algal metal transport. *Biochimica et biophysica acta* **2012,** *1823* (9), 1531-1552.

221.   Knauer, K.; Jabusch, T.; Sigg, L., Manganese uptake and Mn(II) oxidation by the alga Scenedesmus subspicatus. *Aquatic Sciences* **1999,** *61* (1), 44-58.

222.   Stirbet, A.; Lazár, D.; Kromdijk, J.; Govindjee, Chlorophyll a fluorescence induction: Can just a one-second measurement be used to quantify abiotic stress responses? *Photosynthetica* **2018,** *56* (1), 86-104.

223.   Ouyang, H.; Kong, X.; He, W.; Qin, N.; He, Q.; Wang, Y.; Wang, R.; Xu, F., Effects of five heavy metals at sub-lethal concentrations on the growth and photosynthesis of *Chlorella vulgaris*. *Chinese Science Bulletin* **2012,** *57* (25), 3363-3370.

224.   Bao, H.; Burnap, R. L., Photoactivation: The Light-Driven Assembly of the Water Oxidation Complex of Photosystem II. *Frontiers in plant science* **2016,** *7*, 578-578.

225.   Administration, U. S. E. I., International Energy Outlook 2016. *https://www.eia.gov/outlooks/ieo/world.cfm* **2016**.

226.   Juergens, M. T.; Deshpande, R. R.; Lucker, B. F.; Park, J.-J.; Wang, H.; Gargouri, M.; Holguin, F. O.; Disbrow, B.; Schaub, T.; Skepper, J. N.; Kramer, D. M.; Gang, D. R.; Hicks, L. M.; Shachar-Hill, Y., The regulation of photosynthetic structure and function during nitrogen deprivation in Chlamydomonas reinhardtii. *Plant physiology* **2015,** *167* (2), 558-573.

227.   Lam, M. K.; Lee, K. T., Effect of carbon source towards the growth of Chlorella vulgaris for CO2 bio-mitigation and biodiesel production. *International Journal of Greenhouse Gas Control* **2013,** *14*, 169-176.

228.   Mokashi, K.; Shetty, V.; George, S. A.; Sibi, G., Sodium Bicarbonate as Inorganic Carbon Source for Higher Biomass and Lipid Production Integrated Carbon Capture in Chlorella vulgaris. *Achievements in the Life Sciences* **2016,** *10* (1), 111-117.

229.   Lohman, E. J.; Gardner, R. D.; Pedersen, T.; Peyton, B. M.; Cooksey, K. E.; Gerlach, R., Optimized inorganic carbon regime for enhanced growth and lipid accumulation in Chlorella vulgaris. *Biotechnology for Biofuels* **2015,** *8* (1), 82.

230.   Hu, Q.; Sommerfeld, M.; Jarvis, E.; Ghirardi, M.; Posewitz, M.; Seibert, M.; Darzins, A., Microalgal triacylglycerols as feedstocks for biofuel production: perspectives and advances. *The Plant Journal* **2008,** *54* (4), 621-639.

231.   Daroch, M.; Geng, S.; Wang, G., Recent advances in liquid biofuel production from algal feedstocks. *Applied Energy* **2013,** *102*, 1371-1381.

232.   Yang, F.; Hanna, M. A.; Sun, R., Value-added uses for crude glycerol--a byproduct of biodiesel production. *Biotechnology for Biofuels* **2012,** *5* (1), 13.

233.   Agren, J. J.; Julkunen, A.; Penttilä, I., Rapid separation of serum lipids for fatty acid analysis by a single aminopropyl column. *Journal of Lipid Research* **1992,** *33* (12), 1871-6.

234.   Christie, W. W., A simple procedure for rapid transmethylation of glycerolipids and cholesteryl esters. *Journal of Lipid Research* **1982,** *23* (7), 1072-5.

235.   Siler, S. Q.; Neese, R. A.; Parks, E. J.; Hellerstein, M. K., VLDL-triglyceride production after alcohol ingestion, studied using [2-13C1] glycerol. *Journal of Lipid Research* **1998,** *39* (12), 2319-2328.

236.   Yao, L.; Gerde, J. A.; Lee, S.-L.; Wang, T.; Harrata, K. A., Microalgae Lipid Characterization. *Journal of Agricultural and Food Chemistry* **2015,** *63* (6), 1773-1787.

237.   Kong, W.; Yang, H.; Cao, Y.; Song, H.; Hua, S.; Xia, C., Effect of glycerol and glucose on the enhancement of biomass, lipid and soluble carbohydrate production by Chlorella vulgaris in mixotrophic culture. *Food Technology and Biotechnology* **2013,** *51* (1), 62-69.

238.   Anderca, M. I.; Suga, S.; Furuichi, T.; Shimogawara, K.; Maeshima, M.; Muto, S., Functional identification of the glycerol transport activity of Chlamydomonas reinhardtii CrMIP1. *Plant & cell physiology* **2004,** *45* (9), 1313-9.

239.   Perez-Garcia, O.; Escalante, F. M. E.; de-Bashan, L. E.; Bashan, Y., Heterotrophic cultures of microalgae: Metabolism and potential products. *Water Research* **2011,** *45* (1), 11-36.

240.   Dao, L. H. T.; Beardall, J., Effects of lead on two green microalgae Chlorella and Scenedesmus: photosystem II activity and heterogeneity. *Algal Research* **2016,** *16*, 150-159.

241.   Park, J. J.; Wang, H.; Gargouri, M.; Deshpande, R. R.; Skepper, J. N.; Holguin, F. O.; Juergens, M. T.; Shachar-Hill, Y.; Hicks, L. M.; Gang, D. R., The response of Chlamydomonas reinhardtii to nitrogen deprivation: a systems biology analysis. *The Plant journal : for cell and molecular biology* **2015,** *81* (4), 611-24.

242.   Liu, M.; Lu, S., Plastoquinone and Ubiquinone in Plants: Biosynthesis, Physiological Function and Metabolic Engineering. *Frontiers in Plant Science* **2016,** *7* (1898).

243.   Catalanotti, C.; Yang, W.; Posewitz, M.; Grossman, A., Fermentation metabolism and its evolution in algae. *Frontiers in Plant Science* **2013,** *4* (150).

244.   Planavsky, N. J.; Asael, D.; Hofmann, A.; Reinhard, C. T.; Lalonde, S. V.; Knudsen, A.; Wang, X.; Ossa Ossa, F.; Pecoits, E.; Smith, A. J. B.; Beukes, N. J.; Bekker, A.; Johnson, T. M.; Konhauser, K. O.; Lyons, T. W.; Rouxel, O. J., Evidence for oxygenic photosynthesis half a billion years before the Great Oxidation Event. *Nature Geoscience* **2014,** *7*, 283.

245.   Raven, J. A.; Evans, M. C. W.; Korb, R. E., The role of trace metals in photosynthetic electron transport in O2-evolving organisms. *Photosynthesis Research* **1999,** *60* (2), 111-150.

246.   Nishiyama, Y.; Murata, N., Revised scheme for the mechanism of photoinhibition and its application to enhance the abiotic stress tolerance of the photosynthetic machinery. *Appl Microbiol Biotechnol* **2014,** *98* (21), 8777-96.

247.   Takahashi, S.; Badger, M. R., Photoprotection in plants: a new light on photosystem II damage. *Trends in plant science* **2011,** *16* (1), 53-60.

248.   Gururani, Mayank A.; Venkatesh, J.; Tran, L. S. P., Regulation of Photosynthesis during Abiotic Stress-Induced Photoinhibition. *Molecular Plant* **2015,** *8* (9), 1304-1320.

249.	Allakhverdiev, S. I.; Murata, N., Environmental stress inhibits the synthesis de novo of proteins involved in the photodamage-repair cycle of Photosystem II in Synechocystis sp. PCC 6803. *Biochim Biophys Acta* **2004,** *1657* (1), 23-32.

250.	Nishiyama, Y.; Allakhverdiev, S. I.; Murata, N., A new paradigm for the action of reactive oxygen species in the photoinhibition of photosystem II. *Biochim Biophys Acta* **2006,** *1757* (7), 742-9.

251.	Schmitt, F.-J.; Renger, G.; Friedrich, T.; Kreslavski, V. D.; Zharmukhamedov, S. K.; Los, D. A.; Kuznetsov, V. V.; Allakhverdiev, S. I., Reactive oxygen species: Re-evaluation of generation, monitoring and role in stress-signaling in phototrophic organisms. *Biochimica et Biophysica Acta (BBA) - Bioenergetics* **2014,** *1837* (6), 835-848.

252.	Bajguz, A., An enhancing effect of exogenous brassinolide on the growth and antioxidant activity in Chlorella vulgaris cultures under heavy metals stress. *Environmental and Experimental Botany* **2010,** *68* (2), 175-179.

253.	Guenther, J. E.; Melis, A., The physiological significance of photosystem II heterogeneity in chloroplasts. *Photosynthesis Research* **1990,** *23* (1), 105-109.

254.	de Marchin, T.; Ghysels, B.; Nicolay, S.; Franck, F., Analysis of PSII antenna size heterogeneity of Chlamydomonas reinhardtii during state transitions. *Biochimica et Biophysica Acta (BBA) - Bioenergetics* **2014,** *1837* (1), 121-130.

255.	Cao, J.; Govindjee, Chlorophyll a fluorescence transient as an indicator of active and inactive Photosystem II in thylakoid membranes. *Biochim Biophys Acta* **1990,** *1015* (2), 180-8.

256.	Tomek, P. L., Dusan; Ilik, Petr; Naus, Jan On the intermediate steps between the O and P steps in chlorophyll *a* fluorescence rise measured at different intensities of exciting light. *Australian Journal of Plant Physiology* **2001,** *28*, 1151-1160.

257.	Lambreva, M. D.; Russo, D.; Polticelli, F.; Scognamiglio, V.; Antonacci, A.; Zobnina, V.; Campi, G.; Rea, G., Structure/function/dynamics of photosystem II plastoquinone binding sites. *Current protein & peptide science* **2014,** *15* (4), 285-295.

258.	Bennoun, P.; Li, Y.-s., New results on the mode of action of 3,-(3,4-dichlorophenyl)-1,1-dimethylurea in spinach chloroplasts. *Biochimica et Biophysica Acta (BBA) - Bioenergetics* **1973,** *292* (1), 162-168.

259.   Belatik, A.; Hotchandani, S.; Carpentier, R., Inhibition of the Water Oxidizing Complex of Photosystem II and the Reoxidation of the Quinone Acceptor QA− by Pb2+. *PLOS ONE* **2013,** *8* (7), e68142.

260.   *Chlorophyll a Fluorescence in Aquatic Sciences: Methods and Applications*. Springer: Dordrecht, 2010; Vol. 4.

261.   Shinkarev, V. P., Oxygen evolution in photosynthesis: simple analytical solution for the Kok model. *Biophysical journal* **2003,** *85* (1), 435-441.

262.   Kolling, D. R.; Cox, N.; Ananyev, G. M.; Pace, R. J.; Dismukes, G. C., What are the oxidation states of manganese required to catalyze photosynthetic water oxidation? *Biophysical journal* **2012,** *103* (2), 313-22.

263.   Kaftan, D.; Meszaros, T.; Whitmarsh, J.; Nedbal, L., Characterization of Photosystem II Activity and Heterogeneity during the Cell Cycle of the Green Alga *Scenedesmus quadricauda*. *Plant Physiology* **1999,** *120* (2), 433.

264.   Lavergne, J.; Leci, E., Properties of inactive Photosystem II centers. *Photosynthesis Research* **1993,** *35* (3), 323-343.

265.   Müller, P.; Li, X.-P.; Niyogi, K. K., Non-Photochemical Quenching. A Response to Excess Light Energy. *Plant Physiology* **2001,** *125* (4), 1558.

266.   Schansker, G.; Toth, S. Z.; Strasser, R. J., Dark recovery of the Chl a fluorescence transient (OJIP) after light adaptation: the qT-component of non-photochemical quenching is related to an activated photosystem I acceptor side. *Biochim Biophys Acta* **2006,** *1757* (7), 787-97.

APPENDIX A. APPROVAL LETTER

MARSHALL UNIVERSITY®
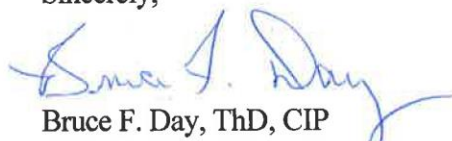www.marshall.edu

Office of Research Integrity

January 2, 2018

Amanda L. Smythers
Gradate Assistant – Kolling Lab
Department of Chemistry
Marshall University

Dear Ms. Smythers:

This letter is in response to the submitted thesis abstract entitled *"Characterizing the Effects of Environmental Stressors on the Photosynthetic Capacity of Chlorella Vulgaris"*. After assessing the abstract, it has been deemed not to be human subject research and therefore exempt from oversight of the Marshall University Institutional Review Board (IRB). The Code of Federal Regulations (45CFR46) has set forth the criteria utilized in making this determination. Since the information in this study does not involve human subjects as defined in the above referenced instruction, it is not considered human subject research. If there are any changes to the abstract you provided then you would need to resubmit that information to the Office of Research Integrity for review and a determination.

I appreciate your willingness to submit the abstract for determination. Please feel free to contact the Office of Research Integrity if you have any questions regarding future protocols that may require IRB review.

Sincerely,

Bruce F. Day, ThD, CIP
Director